BROADBAND DESIGN OF DUAL AND CIRCULARLY POLARIZED ANTENNAS FOR WIRELESS COMMUNICATION SYSTEMS

KHOO KAH WEE JONATHAN
(B.Eng. (Hons), NUS)

A THESIS SUBMITTED

FOR THE DEGREE OF MASTER OF ENGINEERING

DEPARTMENT OF ELECTRICAL AND COMPUTER ENGINEERING

NATIONAL UNIVERSITY OF SINGAPORE

2007

ABSTRACT

The broadband design of dual and circularly polarized antennas demands precise wideband control of individual orthogonal radiated polarizations. The quality of polarization is related to the inherent isolation between the two orthogonal modes. This isolation is in turn dependent on the antenna Q and excitation geometry. Dual linear polarization involves two orthogonal linearly polarized modes, while circular polarization involves two or more orthogonal linearly polarized modes with equal amplitude excitation and quadrature phasing. Lowering the antenna Q allows for wider impedance bandwidth but at the expense of higher order modes generation that causes poor isolation between the orthogonal modes. For linear and circular polarization, this shows up as increased cross-polarization and axial ratio levels, respectively; resulting in diminished polarization (or axial-ratio) bandwidth. Therefore, the excitation geometry has to be properly designed for a given antenna Q in order to enhance the polarization performance of the antenna within a broad impedance bandwidth.

The two or four point sequential feed structure provides wider impedance and polarization (or axial ratio) bandwidths compared to a single feed point structure, since the amplitude and phase of the linearly polarized field components can be controlled by a relatively broadband power divider circuit. The use of a balanced feed network supplies impedance matching, balanced power splitting, and appropriate phasing, to each feed point. However, the conventional balanced feed networks used in prior arts only provide a very narrowband operation. This severely restricts the allowable impedance, polarization and isolation bandwidths

of the dual linearly polarized antenna, and the allowable impedance and axial ratio bandwidths of the circularly polarized antenna. The use of a novel 180^o broadband balun (~45%), and novel 90^o broadband baluns (Type I) (~57.5%) and (Type II) (~72.46%), with wide operating bandwidths, are compared with the conventional 180^o narrowband balun (~10%) and conventional 90^o hybrid coupler (~14%), for various two and four point sequential feed structures. For circular polarization, the symmetrical four point sequential feed structure, is also shown to afford further improved impedance and axial ratio bandwidths.

A dual linearly polarized quadruple L-probe square patch antenna utilizing the proposed 180^o broadband balun pair is shown to deliver good impedance matching (SWR < 2), low cross-polarization levels (< -15 dB), high input port isolation (S_{21} < -33 dB), and high gain (> 6 dBi), across a wide measured operating bandwidth of ~25%, from 1.7 to 2.2 GHz. A circularly polarized quadruple L-probe circular patch antenna utilizing the proposed 90^o broadband balun pair (Type I) is shown to deliver good impedance matching (SWR < 2), low axial ratio (AR < 2 dB), and sufficiently high gain (> 4 dBic), across a wide measured operating bandwidth of 59.1%, from 1.24 to 2.28 GHz. A circularly polarized dual L-probe 2x2 circular patch elements sequential array utilizing six of the proposed 90^o broadband balun (Type II) is shown to deliver good impedance matching (SWR < 2), low axial ratio (AR < 2 dB), and sufficiently high gain (> 4 dBic), across a wide measured operating bandwidth of 53.11%, from 1.3 to 2.24 GHz. A quadruple stripline cylindrical dielectric resonator antenna utilizing a 90^o hybrid coupler pair is shown to deliver good impedance matching (SWR < 2) and low axial ratio (AR < 3 dB), across a wide measured operating bandwidth of 20.1%, from 1.75 to 2.14 GHz.

ACKNOWLEDGMENTS

I would like to express my sincere appreciation to my academic advisors, Dr Guo Yong-Xin and Dr Ong Ling-Chuen, for their guidance and continual support throughout my M.Eng. studies. And I extend special thanks to my department manager, Dr Chen Zhi-Ning, for his caring attitude and concern for my academic pursuit and personal development. I have gained a lot from their continuous inspiration and in-depth expertise in the field of antennas.

I would like to acknowledge my friends and colleagues in the RF and Optical Department, Institute for Infocomm Research, James Chung, Terence See, Toh Wee-Kian, and Qing Xian-Ming, and previously with this laboratory, Bian Lei and Zhang Zhen-Yu, for their helpful suggestions, insights, expert opinions, and frequent encouragement throughout the course of my M.Eng. research. It has been a joy and privilege to work with such wonderful people and I have benefited greatly from their willingness to share their resources and wealth of knowledge and experience. I also thank Hee Kian-Poh and Chiam Tat-Meng for assisting me in the fabrication of some of the antenna prototypes.

I express my heartfelt gratitude to my parents, and my girlfriend, Su Lin, for their daily prayers and emotional support. Their continual love and relentless belief were absolutely essential in helping me go the distance in fulfilling this endeavor.

Most of all, thanks be to God for making it possible for me to engage in this M.Eng. research, and for being ever so faithful, always with me, guiding me each and every step of the way. Indeed, the Lord is good and His love endures forever.

CONTENTS

ABSTRACT i

ACKNOWLEDGMENTS iii

LIST OF FIGURES viii

LIST OF TABLES xvi

LIST OF SYMBOLS AND ABBREVIATIONS xvii

CHAPTER 1 INTRODUCTION 1

1.1 Background 1

1.2 Bandwidth Definitions 3

1.3 Polarization Control 6

1.4 Research Motivation 7

1.5 Thesis Overview 12

CHAPTER 2 BROADBAND DUAL LINEARLY POLARIZED MICROSTRIP ANTENNAS 14

2.1 Research Direction 14

2.2 Broadband Linearly Polarized Dual L-Probe Patch Antenna with a 180^{o} Broadband Balun 17

2.2.1 Antenna Design and Geometry 17

2.2.2 Feed Network Configurations 18

2.2.3 Fabrication and Experimental Setup 23

2.2.4 Impedance and Radiation Performances 24

2.2.5 Discussions 33

2.3 Broadband Dual Linearly Polarized Quadruple L-Probe Patch Antenna with 180^{o} Broadband Baluns 34

2.3.1 Antenna Design and Geometry 34

2.3.2 Feed Network Configurations 35

2.3.3 Fabrication and Experimental Setup 37

2.3.4 Impedance and Radiation Performances 38
2.3.5 Discussions 43
2.4 Concluding Remarks 44
CHAPTER 3 BROADBAND CIRCULARLY POLARIZED MICROSTRIP ANTENNAS 45
3.1 Research Direction 45
3.2 Broadband Circularly Polarized Dual L-Probe Patch Antenna with a 90^o Broadband Balun (Type I) 48
3.2.1 Antenna Design and Geometry 48
3.2.2 Feed Network Configurations 49
3.2.3 Fabrication and Experimental Setup 54
3.2.4 Impedance and Radiation Performances 57
3.2.5 Discussions 60
3.3 Broadband Circularly Polarized Quadruple L-Probe Patch Antenna with 90^o Broadband Baluns (Type I) 61
3.3.1 Antenna Design and Geometry 61
3.3.2 Feed Network Configuration 62
3.3.3 Fabrication and Experimental Setup 63
3.3.4 Impedance and Radiation Performances 64
3.3.5 Discussions 68
3.4 Concluding Remarks 69
CHAPTER 4 BROADBAND CIRCULARLY POLARIZED MICROSTRIP ANTENNAS AND ARRAYS 70
4.1 Research Direction 70
4.2 Broadband Circularly Polarized Dual L-Probe Patch Antenna with a 90^o Broadband Balun (Type II) 72
4.2.1 Antenna Design and Geometry 72
4.2.2 Feed Network Configurations 74
4.2.3 Fabrication and Experimental Setup 78

4.2.4 Impedance and Radiation Performances 80
4.2.5 Discussions 83
4.3 Broadband Circularly Polarized Dual Capacitive-Feed Patch Antenna with a 90^o Broadband Balun (Type II) 84
4.3.1 Antenna Design and Geometry 84
4.3.2 Feed Network Configuration 85
4.3.3 Fabrication and Experimental Setup 86
4.3.4 Impedance and Radiation Performances 87
4.3.5 Discussions 92
4.4 Broadband Circularly Polarized Dual L-Probe Patch Array with 90^o Broadband Baluns (Type II) 93
4.4.1 Antenna Array Configuration 93
4.4.2 Feed Network Configuration 94
4.4.3 Fabrication and Experimental Setup 95
4.4.4 Impedance and Radiation Performances 96
4.4.5 Discussions 101
4.5 Concluding Remarks 102
CHAPTER 5 BROADBAND CIRCULARY POLARIZED DIELECTRIC RESONATOR ANTENNAS 103
5.1 Research Direction 103
5.2 Broadband Circularly Polarized Dual Stripline Dielectric Resonator Antenna with a 90^o Hybrid Coupler 105
5.2.1 Antenna Design and Geometry 105
5.2.2 Feed Network Configuration 106
5.2.3 Impedance and Radiation Performances 106
5.2.4 Discussions 108
5.3 Broadband Circularly Polarized Quadruple Stripline Dielectric Resonator Antenna with 90^o Hybrid Couplers 109
5.3.1 Antenna Design and Geometry 109

5.3.2 Feed Network Configuration 110
5.3.3 Fabrication and Experimental Setup 111
5.3.4 Impedance and Radiation Performances 112
5.3.5 Discussions 116
5.4 Concluding Remarks 117
CHAPTER 6 CONCLUSION 118
6.1 Summary of Important Results 118
6.2 Suggestions for Future Works 119
6.3 Concluding Remarks 120
REFERENCES 125
LIST OF PUBLICATIONS 136

LIST OF FIGURES

Fig. 1. Co-ordinate system for antenna analysis. 3

Fig. 2. Geometry of the dual L-probe square patch antenna. 17

Fig. 3. Schematics of the conventional 180^{o} narrowband balun. 18

Fig. 4. Schematics of the proposed 180^{o} broadband balun. 19

Fig. 5. Simulated and measured input port return loss comparison between the 180^{o} narrowband and broadband baluns. 19

Fig. 6. Simulated and measured output ports amplitude response comparison between the 180^{o} narrowband and broadband baluns. 20

Fig. 7. Simulated and measured output ports phase difference comparison between the 180^{o} narrowband and broadband baluns. 21

Fig. 8. Prototype of the dual L-probe square patch antenna utilizing the 180^{o} narrowband balun. 23

Fig. 9. Prototype of the dual L-probe square patch antenna utilizing the 180^{o} broadband balun. 23

Fig. 10. Simulated and measured SWR for the dual L-probe square patch antenna utilizing the 180^{o} narrowband or broadband balun. 24

Fig. 11. Simulated and measured gain for the dual L-probe square patch antenna utilizing the 180^{o} narrowband or broadband balun. 25

Fig. 12. Simulated radiation patterns for the single L-probe square patch antenna. 26

Fig. 13. Simulated radiation patterns for the dual L-probe square patch antenna utilizing the 180^{o} narrowband balun. 27

Fig. 14. Simulated radiation patterns for the dual L-probe square patch antenna utilizing the 180^{o} broadband balun. 27

Fig. 15. Measured normalized radiation patterns for the dual L-probe square patch antenna utilizing the 180^{o} narrowband balun. 28

Fig. 16. Measured normalized radiation patterns for the dual L-probe square patch antenna utilizing the 180^{o} broadband balun. 29

Fig. 17. Simulated normalized current distribution for the radiating element of the single L-probe square patch antenna. 31

Fig. 18. Simulated normalized current distribution for the radiating element of the dual L-probe square patch antenna utilizing the 180^{o} narrowband balun. 31

Fig. 19. Simulated normalized current distribution for the radiating element of the dual L-probe square patch antenna utilizing the 180^{o} broadband balun. 31

Fig. 20. Geometry of the dual polarized quadruple L-probe square patch antenna 34

Fig. 21. Feed network layout of the 180^{o} narrowband balun pair. 35

Fig. 22. Feed network layout of the 180^{o} broadband balun pair. 36

Fig. 23. Prototype of the dual polarized quadruple L-probe square patch antenna utilizing the 180^{o} narrowband balun pair. 37

Fig. 24. Prototype of the dual polarized quadruple L-probe square patch antenna utilizing the 180^{o} broadband balun pair. 37

Fig. 25. Simulated return loss for the dual polarized quadruple L-probe square patch antenna utilizing the 180^{o} narrowband or broadband balun pair. 38

Fig. 26. Simulated input port isolation for the dual polarized quadruple L-probe square patch antenna utilizing the 180^{o} narrowband or broadband balun pair. 39

Fig. 27. Measured SWR for the dual polarized quadruple L-probe square patch antenna utilizing the 180^{o} narrowband or broadband balun pair. 40

Fig. 28. Measured input port isolation for the dual polarized quadruple L-probe square patch antenna utilizing the 180^{o} narrowband or broadband balun pair. 40

Fig. 29. Measured gain for the dual polarized quadruple L-probe square patch antenna utilizing the 180^{o} broadband balun pair. 41

Fig. 30. Measured normalized radiation patterns (port 1) for the dual polarized quadruple L-probe square patch antenna utilizing the 180^{o} broadband balun pair. 42

Fig. 31. Measured normalized radiation patterns (port 2) for the dual polarized quadruple L-probe square patch antenna utilizing the 180^{o} broadband balun pair. 42

Fig. 32. Geometry of the circularly polarized dual L-probe circular patch antenna utilizing the 90^{o} broadband balun (Type I). 48

Fig. 33. Schematics of the conventional 90^{o} hybrid coupler. 49

Fig. 34. Schematics of the proposed 90^{o} broadband balun (Type I). 50

Fig. 35. Layout of the C-section coupled lines. 50

Fig. 36. Simulated input port return loss comparison between the 90^{o} hybrid coupler and 90^{o} broadband balun (Type I). 51

Fig. 37. Simulated output ports amplitude response comparison between the 90^{o} hybrid coupler and 90^{o} broadband balun (Type I). 52

Fig. 38. Simulated output ports phase difference comparison between the 90^{o} hybrid coupler and 90^{o} broadband balun (Type I). 52

Fig. 39. Prototype of the circularly polarized dual L-probe circular patch antenna utilizing the 90^{o} narrowband balun (Type I). 54

Fig. 40. Simulated and measured SWR for the circularly polarized dual L-probe circular patch antenna utilizing the 90^{o} broadband balun (Type I). 57

Fig. 41. Simulated and measured axial ratio for the circularly polarized dual L-probe circular patch antenna utilizing the 90^o broadband balun (Type I). 57

Fig. 42. Simulated and measured gain for the circularly polarized dual L-probe circular patch antenna utilizing the 90^o broadband balun (Type I). 58

Fig. 43. Measured normalized x-z plane ($\phi = 0^o$) radiation patterns for the circularly polarized dual L-probe circular patch antenna utilizing the 90^o broadband balun (Type I). 59

Fig. 44. Measured normalized y-z plane ($\phi = 90^o$) radiation patterns for the circularly polarized dual L-probe circular patch antenna utilizing the 90^o broadband balun (Type I). 59

Fig. 45. Geometry of the circularly polarized quadruple L-probe circular patch antenna utilizing the 90^o broadband balun (Type I) pair. 61

Fig. 46. Schematics of the proposed 90^o broadband balun (Type I) pair. 62

Fig. 47. Prototype of the circularly polarized quadruple L-probe circular patch antenna utilizing the 90^o narrowband balun (Type I) pair. 63

Fig. 48. Simulated and measured SWR for the circularly polarized quadruple L-probe circular patch antenna utilizing the 90^o broadband balun (Type I) pair. 64

Fig. 49. Simulated and measured axial ratio for the circularly polarized quadruple L-probe circular patch antenna utilizing the 90^o broadband balun (Type I) pair. 65

Fig. 50. Simulated and measured gain for the circularly polarized quadruple L-probe circular patch antenna utilizing the 90^o broadband balun (Type I) pair. 66

Fig. 51. Measured normalized x-z plane ($\phi = 0^o$) radiation patterns for the circularly polarized quadruple L-probe circular patch antenna utilizing the 90^o broadband balun (Type I) pair. 67

Fig. 52. Measured normalized y-z plane ($\phi = 90^o$) radiation patterns for the circularly polarized quadruple L-probe circular patch antenna utilizing the 90^o broadband balun (Type I) pair. 67

Fig. 53. Geometry of the circularly polarized dual L-probe circular patch antenna utilizing the 90^o broadband balun (Type II). 72

Fig. 54. Schematics of the proposed 90^o broadband balun (Type II). 74

Fig. 55. Simulated input port return loss comparison between the 90^o hybrid coupler and 90^o broadband balun (Type II). 75

Fig. 56. Simulated output ports amplitude response comparison between the 90^o hybrid coupler and 90^o broadband balun (Type II). 76

Fig. 57. Simulated output ports phase difference comparison between the 90^o hybrid coupler and 90^o broadband balun (Type II). 76

Fig. 58. Prototype of the circularly polarized dual L-probe circular patch antenna utilizing the 90^o broadband balun (Type II). 78

Fig. 59. Simulated and measured SWR for the circularly polarized dual L-probe circular patch antenna utilizing the 90^o broadband balun (Type II). 80

Fig. 60. Simulated and measured axial ratio for the circularly polarized dual L-probe circular patch antenna utilizing the 90^o broadband balun (Type II). 80

Fig. 61. Simulated and measured gain for the circularly polarized dual L-probe circular patch antenna utilizing the 90^o broadband balun (Type II). 81

Fig. 62. Measured normalized spinning linear radiation patterns for the circularly polarized dual L-probe circular patch antenna utilizing the 90^o broadband balun (Type II). 82

Fig. 63 Geometry of the circularly polarized dual capacitive-feed circular patch antenna utilizing the 90^o broadband balun (Type II). 84

Fig. 64. Prototype of the circularly polarized dual capacitive-feed circular patch antenna utilizing the 90^{o} broadband balun (Type II). 86

Fig. 65. Simulated and measured SWR for the circularly polarized dual capacitive-feed circular patch antenna utilizing the 90^{o} broadband balun (Type II). 87

Fig. 66. Simulated and measured axial ratio for the circularly polarized dual capacitive-feed circular patch antenna utilizing the 90^{o} broadband balun (Type II). 88

Fig. 67. Simulated and measured gain for the circularly polarized dual capacitive-feed circular patch antenna utilizing the 90^{o} broadband balun (Type II). 89

Fig. 68. Measured normalized spinning linear radiation patterns for the circularly polarized dual capacitive-feed circular patch antenna utilizing the 90^{o} broadband balun (Type II). 90

Fig. 69. Geometry of the circularly polarized 2x2 sequential-rotated L-probe circular patch array utilizing six 90^{o} broadband baluns (Type II). 93

Fig. 70. Schematics of the proposed 90^{o} broadband balun (Type II) pair. 94

Fig. 71. Prototype of the circularly polarized 2x2 sequential-rotated L-probe circular patch array utilizing six 90^{o} broadband baluns (Type II). 95

Fig. 72. Simulated and measured SWR for the circularly polarized 2x2 sequential-rotated L-probe circular patch array utilizing six 90^{o} broadband baluns (Type II). 96

Fig. 73. Simulated and measured axial ratio for the circularly polarized 2x2 sequential-rotated L-probe circular patch array utilizing six 90^{o} broadband baluns (Type II). 97

Fig. 74. Simulated and measured gain for the circularly polarized 2x2 sequential-rotated L-probe circular patch array utilizing six 90^o broadband baluns (Type II). 97

Fig. 75. Measured normalized spinning linear radiation patterns for the circularly polarized 2x2 sequential-rotated L-probe circular patch array utilizing six 90^o broadband baluns (Type II). 98

Fig. 76. Geometry of the circularly polarized dual stripline cylindrical dielectric resonator antenna utilizing the 90^o hybrid coupler. 105

Fig. 77. Simulated SWR comparison between the single stripline cylindrical DRA and the circularly polarized dual stripline cylindrical DRA utilizing the 90^o hybrid coupler. 106

Fig. 78. Simulated axial ratio and gain comparison between the single stripline cylindrical DRA and the circularly polarized dual stripline cylindrical DRA utilizing the 90^o hybrid coupler. 107

Fig. 79. Geometry of the circularly polarized quadruple stripline cylindrical dielectric resonator antenna utilizing the 90^o hybrid coupler pair. 109

Fig. 80. Schematics of the proposed 90^o hybrid coupler pair. 110

Fig. 81. Prototype of the circularly polarized quadruple stripline cylindrical dielectric resonator antenna utilizing the 90^o hybrid coupler pair. 111

Fig. 82. Simulated and measured SWR for the circularly polarized quadruple stripline cylindrical DRA utilizing the 90^o hybrid coupler pair. 112

Fig. 83. Simulated and measured axial ratio for the circularly polarized quadruple stripline cylindrical DRA utilizing the 90^o hybrid coupler pair. 113

Fig. 84. Simulated and measured peak gain for the circularly polarized quadruple stripline cylindrical DRA utilizing the 90^o hybrid coupler pair. 114

Fig. 85. Simulated radiation efficiency for the circularly polarized quadruple stripline cylindrical DRA utilizing the 90^o hybrid coupler pair. 114

Fig. 86. Measured normalized spinning linear radiation patterns for the circularly polarized quadruple stripline cylindrical dielectric resonator antenna utilizing the 90^o hybrid coupler pair. 115

LIST OF TABLES

Table 1 Simulated and Measured H-plane Cross-Polarization Levels for the Dual L-Probe Square Patch Antenna with the 180^{o} Narrowband or Broadband Balun 30

Table 2 Simulated Return Loss, Output Ports Power Distribution and Output Ports Phase Difference for Various Feed Networks 118

Table 3 Measured SWR, Cross-Polarization Levels, Input Port Isolation and Gain for Single and Dual Linearly Polarized Square Patch Antennas Utilizing Various Feed Configurations within Bandwidth of Interest (1.7 to 2.2 GHz) 118

Table 4 Measured SWR, Axial Ratio and Gain Bandwidths for Circularly Polarized Circular Patch Antennas Utilizing Various Feed Configurations 119

LIST OF SYMBOLS AND ABBREVIATIONS

AR	Axial-Ratio
AUT	Antenna under Test
BW	Bandwidth
Co-Pol	Co-polarization
CP	Circular Polarization
dBi	Decibels (isotropic)
dBic	Decibels (isotropic; circularly polarized)
DRA	Dielectric Resonator Antenna
FDTD	Finite Difference Time Domain
FEM	Finite Element Method
GPS	Global Positioning Satellite
GSM	Global System for Mobile Communications
LHCP	Left Hand Circular Polarization
MoM	Method of Moments
PCB	Printed Circuit Board
PCS	Personal Communications Service
Q	Quality factor
RFID	Radio Frequency Identification
RHCP	Right Hand Circular Polarization
SWR	Standing Wave Ratio
UMTS	Universal Mobile Telecommunications System
UWB	Ultra-Wideband
VSWR	Voltage Standing Wave Ratio
X-Pol	Cross-polarization

CHAPTER 1

INTRODUCTION

1.1 Background

The antenna, a transducer for radiating or receiving electromagnetic waves, is a critical component in wireless communication systems. The history of antennas date back to 1886 when Professor Heinrich Rudolph Hertz demonstrated, in his laboratory, that when sparks were produced at a gap of a half-wave dipole, sparks also occurred at a gap of a resonant square loop [1]. Subsequently, from 1887 to 1891, Hertz went on to perform a series of radiation experiments which completely validated Maxwell's theory of electromagnetic waves, formulated in 1873. These findings remained a laboratory curiosity until Guglielmo Marconi, who repeated Hertz's experiments, developed a radio system that could signal over large distances. Marconi performed, in 1901, the first transatlantic transmission from Poldhu in Cornwall, England, to St. John's, Newfoundland [2]. This marked the dawn of an antenna era and many wire related radiating elements (such as long wires, dipoles, helices, rhombuses, and fans) proliferated. In the 1940's, during and after World War II, new radiating elements (such as waveguide apertures, horns, and reflectors) were developed. This coincided with the invention of microwave sources (such as klystron and magnetron). In the 1960's to 1980's, advances in computer architecture led to numerical methods that allowed complex antenna system configurations to be analyzed and designed accurately. Asymptotic methods like the Method of Moments (MoM), the Finite Difference Time Domain (FDTD) and the Finite Element Method (FEM), were

introduced. In the early 1970's, the microstrip antenna, a radiating element with very attractive mechanical and fabricational features, started to receive widespread attention. In the early 1980's, some research attention began to be diverted towards the study of the dielectric resonator antenna as a viable alternative to conventional metallic antennas.

Today, microstrip antennas form one of the most innovative areas of current antenna work. Numerous variations in patch shape, feeding techniques, substrate configurations, and array geometries have resulted from a large volume of research and development around the world. The variety in design that is possible with microstrip antennas probably exceeds that of any other antenna elements [3]. Microstrip antennas are low-profile, conformable to planar and non-planar surfaces, simple and inexpensive to manufacture using modern printed circuit technology, mechanically robust when mounted on rigid surfaces and compatible with integrated circuit designs [4]. Microstrip antennas, however, suffer from inherent limitations like narrow bandwidth, spurious feed radiation and poor polarization purity. For this reason, much of the research work on microstrip antennas has been targeted at improving these electrical characteristics. Bandwidth enhancement has been a dominant topic in the microstrip antenna literature. Unfortunately, there are at times confusing and misleading conclusions presented due to lack of clear bandwidth definitions, and the failure to consider all the relevant electrical characteristics [5]. The gain, for example, has been often omitted in many published works claiming broad operating bandwidth. This thesis presents the broadband design of dual and circularly polarized antennas, and the bandwidth definitions are first established.

1.2 Bandwidth Definitions

The bandwidth of an antenna can be defined for impedance, radiation pattern and polarization [5], [6]; and also isolation (in the case of dual polarization). The most basic consideration for all antenna designs is a satisfactory impedance bandwidth which allows for most of the energy to be transmitted to an antenna from a feed or transmission system at a transmitter, and from an antenna to its load at a receiver, in a wireless communication system. The impedance variation with frequency of the antenna element limits the frequency range over which the element can be matched to its feed line. In general, an input return loss of $S_{11} < -10$ dB (better still, < -14 dB) or an input voltage standing wave ratio of SWR < 2 (better still, < 1.5), are considered acceptable levels for impedance matching.

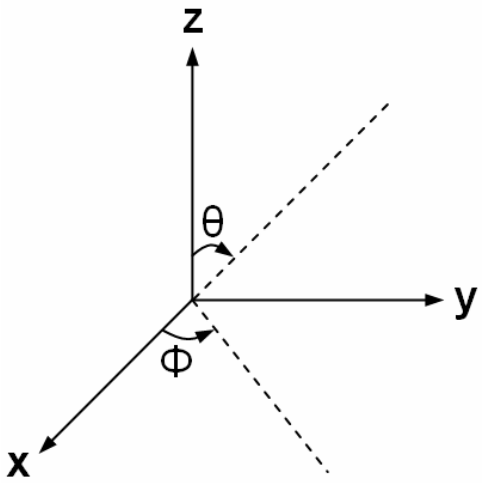

Fig. 1. Co-ordinate system for antenna analysis.

Pattern (or gain) bandwidth is a second important consideration for all antenna designs. A designated radiation pattern ensures that the desired extend of energy is radiated in a specific direction. The pattern symmetry, half-power beamwidth, side-, back-, and grating-lobe levels, front-to-back ratio, and gain, which all can vary with frequency, are some of the parameters commonly used to describe the

radiation performances of an antenna. If any of these quantities are specified as a minimum or maximum, the operating frequency range can be determined. Fig. 1 shows the co-ordinate system for antenna analysis. Radiation pattern plots in the x-z ($\phi = 0^o$) and y-z ($\phi = 90^o$) planes have been provided, across a bandwidth of interest, for all measured antenna radiation performances presented in this thesis. The pattern symmetry, half-power beamwidth, side-, back-, and grating-lobe levels, and front-to-back ratio can all be inferred from the normalized radiation pattern versus elevation angle (θ), in both principle planes. Gain plots, across a bandwidth of interest, have also been given for all measured antenna radiation performances presented in this thesis. Gain is a very important figure of merit used to gauge the amount of power radiated from the antenna relative to the incident power received. In general, a gain that is > 3 dB below the highest gain within a bandwidth of interest is considered an acceptable gain level. This is commonly referred to as the 3-dB gain bandwidth. To compare the measured gain bandwidths between the circularly polarized patch antennas and arrays presented in this thesis, a boresight gain of > 4 dBic has been specified as the minimum gain level. A typical circularly polarized L-probe fed circular patch element is capable of providing an average gain of 7 dBic, so a 4 dBic gain (3 dB below 7 dBic) was deemed a reasonable minimum gain level.

Polarization (or axial ratio) bandwidth is a third important consideration for all antenna designs. Polarization is a property of single-frequency electromagnetic radiation describing the shape and orientation of the locus of the extremity of the field vectors (usually the E-field vector) as a function of time [7], [8]. Waves in general are elliptically polarized and are defined by their axial ratio, tilt angle and

sense [9]. For an infinite or zero axial ratio (AR = ± ∞ dB), linear polarization results and the tilt angle defines the orientation of the electric vector; sense is not applicable. The quality of slightly off linearly polarized waves is specified by the cross-polarization levels. Ludwig's third definition of cross-polarization is assumed [10], and the cross-polarization level ($|E_{co-pol}|/|E_{x-pol}|$) is defined as the ratio of the maximum value of $|E_{co-pol}|$ to the maximum value of $|E_{x-pol}|$ in a specified plane [11]. For unity axial ratio (AR = 0 dB), circular polarization results; tilt angle is not applicable. The quality of slightly off circularly polarized waves is specified by the axial ratio. The lower the axial ratio, the better the quality level of circular polarization (ie. the radiated waves are more circularly rotated rather than elliptically rotated). The polarization properties of a linearly or circularly polarized antenna should be specified in order to avoid possible losses due to polarization mismatch within its operating bandwidth. The polarization bandwidth can be defined by specifying a maximum cross-polarization or axial ratio level. In general, a cross-polarization level of < -15 dB (better still, < -20 dB) is considered an acceptable quality level for linear polarization, while an axial ratio level of AR < 3 dB (better still, < 2 dB) is considered an acceptable quality level for circular polarization.

Isolation bandwidth is an important consideration for dual polarized antenna designs. For dual polarization systems, the isolation between the two input ports represents that part of the signal to be transmitted on polarization 1 that is coupled into port 2, assuming both polarizations are being transmitted simultaneously. In general, an input port isolation of S_{21} < -25 dB (better still, < -30 dB) is considered an acceptable level of input port decoupling by industry standards.

1.3 Polarization Control

Many wireless communication systems require a high degree of polarization control in order to optimize system performance. For antennas to be fully exploited in such systems, high polarization purity and isolation between orthogonal polarizations, be they linearly or circularly polarized, are needed [9]. The quality of polarization in either linear or circular systems is linked to how well the two orthogonal modes in the antenna are excited and how well they can be controlled. This to some extent is related to the inherent isolation between them. This isolation, which determines the cross-polarization or axial ratio level, is in turn dependent on the antenna Q (radiating element geometry, substrate thickness or permittivity) and the excitation geometry (feed size, feed point positioning). In general, a low antenna Q provides for wide impedance bandwidth but at the expense higher order modes generation that causes poorer isolation between the orthogonal modes. This translates to higher cross-polarization levels for linearly polarized systems, or higher axial ratio levels for circularly polarized systems. It is therefore difficult to improve both impedance bandwidth and polarization purity by adjusting only the antenna Q. Instead, the excitation geometry has to be properly designed for a given antenna Q in order to enhance the polarization performance of the antenna within a broad impedance bandwidth.

The broadband design of dual and circularly polarized antennas demands precise wideband control of individual orthogonal radiated polarizations. Dual linear polarization is attained by the superposition of two orthogonal linearly polarized modes, while circular polarization is attained by the superposition of two orthogonal linearly polarized modes with equal amplitude excitation and

quadrature phasing. Even for single linear polarization, higher order orthogonal modes may be generated, showing up as increased cross-polarization levels.

1.4 Research Motivation

Microstrip antennas, or patch antennas, are typically constrained by their narrow impedance bandwidth, especially when the radiating elements are printed on thin dielectric substrates. The use of a thick low permittivity dielectric substrate that allows for loosely bound electromagnetic fields is an established method for overcoming this limitation [12]. A probe feed, which couples well to a radiating patch positioned above the antenna substrate, has been commonly used in this bandwidth-widening approach. The probe feed, however, introduces the problems of probe inductance, probe leakage radiation and probe coupling.

Probe inductance has direct implications on impedance matching and limits the achievable impedance bandwidth of a patch antenna to less than 10% [13]. Several probe inductance compensation techniques have been demonstrated [14]-[16]. The L-probe proximity-feed approach, first introduced in [16], extends the achievable impedance bandwidth for probe-fed patch antennas on thick (~0.1 λ_o) low-permittivity dielectric substrates. The proximity-feed feature allows for the radiating patch element to exist on a relatively thicker antenna substrate without having to correspondingly lengthen the vertical probe arm responsible for added probe inductance. Moreover, the horizontal probe arm responsible for probe capacitance can be lengthened to compensate the probe inductance. The L-probe fed patch antenna is capable of providing a ~30% impedance bandwidth (SWR $\leq$ 2) with an average gain of 7.0 dBi [16]-[18]. Hence, the L-probe feed technique is

adopted in the broadband design of dual and circularly polarized patch antennas and arrays presented in this thesis.

Probe leakage radiation leads to increased cross-polarization levels due to higher order modes. The probe feed primarily excites the dominant mode of the radiating patch element. However, the asymmetrical positioning of the probe feed point and the use of a thick low permittivity antenna substrate tends to encourage the generation of higher order modes that give rise to more cross-polarized components. The L-probe feed, though effective in widening impedance bandwidth, has a vertical component emitting probe leakage radiation that produces monopole-like H-plane cross-polarization patterns and asymmetrical E-plane co-polarization patterns. This increase in cross-polarization levels due to higher order modes leads to a diminished polarization (or axial ratio) bandwidth.

Probe coupling leads to increased cross-polarization levels due to mutual coupling effects. This mutual coupling between probe feeds is prevalent in multi-point fed patch elements with closely spaced probe feeds. The L-probe feed has a vertical component capable of emitting probe leakage radiation that can couple strongly with the leakage radiation emitted from an adjacent L-probe feed in close proximity. This increase in cross-polarization levels due to mutual coupling effects leads to a diminished polarization (or axial ratio) bandwidth, and in the case of dual polarization, the resulting worsened isolation between the two co-polarized components also leads to a reduced isolation bandwidth.

For a single linearly polarized square patch element, a second L-probe feed, supplied an equal amplitude and 180^{o} out-of-phase excitation, can be added at the opposite side of the patch in order to cancel out probe leakage radiation [17], [19]. This balanced and symmetrical two point feeding structure can help suppress cross-polarization due to higher order modes. Substantial research efforts have been devoted towards combating the high cross-polarization levels prominent in probe-fed patch antennas [20]-[26]. In prior arts [17], [19]-[21], balanced feed networks have been used to excite the probe feed pair. However, the conventional balanced feed networks used only provide a consistent 180^{o} (±10^{o}) phase shift over a very narrow band (~10%), severely limiting the frequency range across which proper cancellation of probe leakage radiation can take place. The use of a novel 180^{o} broadband balun is proposed in this thesis. The proposed 180^{o} broadband balun delivers good impedance matching, equal amplitude power splitting and consistent 180^{o} (±10^{o}) phase shifting, across a wide band (~45%). A single linearly polarized quadruple L-probe square patch antenna utilizing the proposed 180^{o} broadband balun is shown, in Chapter 2, to deliver good impedance matching (SWR < 2), low cross-polarization levels (< -21 dB), and high gain (> 6 dBi), across a wide measured operating bandwidth of ~30%, from 1.7 to 2.3 GHz.

For a dual linearly polarized square patch element, a second pair of L-probe feeds, with each pair supplied equal amplitude and 180^{o} out-of-phase excitations, can be added to cancel out probe leakage radiation and probe coupling [19]. Probe leakage radiation cancellation in turn leads to probe coupling cancellation since the probe feeds no longer emit leakage radiation that couples to that of adjacent probe feeds. This balanced and symmetrical four point feeding structure allows

for the suppression of cross-polarization due to higher order modes and due to mutual coupling effects, and also improved input port isolation. However, the conventional balanced feed network used only provides a consistent 180^{o} ($\pm 10^{o}$) phase shift over a very narrow band (~10%), severely limiting the frequency range across which proper cancellation of probe leakage radiation and probe coupling can take place. A dual linearly polarized quadruple L-probe square patch antenna utilizing the proposed 180^{o} broadband balun pair is shown, in Chapter 2, to deliver good impedance matching (SWR < 2), low cross-polarization levels (< -15 dB), high input port isolation (S_{21} < -33 dB), and high gain (> 6 dBi), across a wide measured operating bandwidth of ~25%, from 1.7 to 2.2 GHz.

For a circularly polarized circular patch element, two or four L-probe feeds can be sequentially rotated and supplied equal amplitude power with appropriate phasing. The technique of sequential rotation enables errors in the radiated polarization of each probe feed to be cancelled by the adjacent probe feed. Similarly, reflections from the mismatched feed points off resonance can add destructively at the corporate feed input terminal. This allows for better impedance matching and the suppression of cross-polarization due to multiple reflections and due to feed phase errors off resonance; resulting in improved impedance and axial ratio bandwidths. The balanced and symmetrical four point feeding structure has the added advantage of enforcing the cancellation of probe leakage radiation and probe coupling. This allows for better impedance matching and the suppression of cross-polarization due to higher order modes and due to mutual coupling effects; resulting in further improved impedance and axial ratio bandwidths. However, the conventional 90^{o} hybrid coupler used in prior arts only provides a narrowband

operation (~14%). Therefore, the use of a novel 90^o broadband balun (Type I) is proposed in this thesis. The proposed 90^o broadband balun (Type I) delivers good impedance matching, equal amplitude power splitting and consistent 90^o ($\pm 5^o$) phase shifting, across a wide band (~57.5%). A circularly polarized quadruple L-probe circular patch antenna utilizing the proposed 90^o broadband balun pair (Type I) is shown, in Chapter 3, to deliver good impedance matching (SWR < 2), low axial ratio (AR < 2 dB), and sufficiently high gain (> 4 dBic), across a wide measured operating bandwidth of 59.1%, from 1.24 to 2.28 GHz. The four point sequential feed structure is conceptually extended to a four element sequential array. The use of a novel 90^o broadband balun (Type II) is also proposed in this thesis. The proposed 90^o broadband balun (Type II) delivers good impedance matching, equal amplitude power splitting and consistent 90^o ($\pm 5^o$) phase shifting, across a wide band (~72.5%). A circularly polarized dual L-probe 2x2 circular patch elements sequential array utilizing six of the proposed 90^o broadband balun (Type II) is shown, in Chapter 4, to deliver good impedance matching (SWR < 2), low axial ratio (AR < 2 dB), and sufficiently high gain (> 4 dBic), across a wide measured operating bandwidth of 53.11%, from 1.3 to 2.24 GHz. The four point sequential feed structure is also investigated for the dielectric resonator antenna. A quadruple stripline cylindrical dielectric resonator antenna utilizing a 90^o hybrid coupler pair is shown, in Chapter 5, to deliver good impedance matching (SWR < 2) and low axial ratio (AR < 3 dB), across a wide measured operating bandwidth of 20.1%, from 1.75 to 2.14 GHz.

1.5 Thesis Overview

This thesis is divided into six chapters. The bandwidth definitions are clarified in Chapter 1 and the research motivation for wideband polarization control in the broadband design of dual and circular polarized antennas is explained.

Chapter 2 presents the broadband design of dual linearly polarized patch antennas. The use of a novel 180^{o} broadband balun is introduced. Wideband cross-polarization suppression is demonstrated for a linearly polarized two point L-probe fed square patch element. This work has been published in the Oct. 2007 issue of Radio Science. Wideband cross-polarization suppression and input port decoupling is demonstrated for a dual linearly polarized four point L-probe fed square patch element. This work was presented in the Oct. 2006 IEEE International Conference on Communication Systems (ICCS2006), held in Singapore, and a full paper was published in the Jan. 2007 issue of IEEE Transactions on Antennas and Propagation.

Chapter 3 presents the broadband design of circularly polarized patch antennas. The use of a novel 90^{o} broadband balun (Type I) is introduced. Wideband circular polarization operation is demonstrated for a two point L-probe fed circular patch element. Improved wideband circular polarization operation is demonstrated for a four point L-probe fed circular patch element. This work was presented in the Dec. 2006 Asia Pacific Microwave Conference (APMC2006), held in Yokohama, Japan, and a full paper has been published in the Feb. 2008 issue of IEEE Transactions on Antennas and Propagation.

Chapter 4 presents the broadband design of circularly polarized patch antennas and arrays using sequential rotation. The use of a novel 90^{o} broadband balun (Type II) is introduced. Wideband circular polarization operation is demonstrated for a two point L-probe fed circular patch element. Improved wideband circular polarization operation is demonstrated for a two point capacitive-fed circular patch element. Further improved wideband circular polarization operation is demonstrated for a sequential patch array composed of four sets of two point L-probe fed circular patch elements.

Chapter 5 presents the broadband design of circularly polarized dielectric resonator antennas. Wideband circular polarization operation is demonstrated for a two point stripline feed cylindrical dielectric resonator antenna. Improved wideband circular polarization operation is demonstrated for a four point stripline fed cylindrical dielectric resonator antenna. This work was presented in the Nov. 2006 IEICE International Symposium on Antennas and Propagation (ISAP2006), held in Singapore, and a full paper was published in the Jul. 2007 issue of IEEE Transactions on Antennas and Propagation.

The important results presented in this thesis are summarized and some suggestions for future work are given in Chapter 6.

CHAPTER 2

BROADBAND DUAL LINEARLY POLARIZED MICROSTRIP ANTENNAS

2.1 Research Direction

Dual linearly polarized microstrip antennas are widely adopted in wireless communication systems, most notably in cellular-phone base stations, deploying frequency reuse or polarization diversity schemes. Polarization diversity supports increased channel capacity and allows for two orthogonal dominant modes operating in the same frequency band to be collocated in a single antenna element. This scheme has been preferred over space diversity because it occupies significantly lesser real estate and incurs lower installation costs. The diversity gain from polarization diversity is maximized when both the input ports of the dual-polarized antenna receive radiation in an orthogonal manner, with equal field strengths, over the desired coverage area. The input port coupling S_{21} represents the part of the signal to be transmitted on a given polarization (polarization 1) that is coupled to the input port (port 2) producing the other polarization, assuming both polarizations are being transmitted simultaneously. Input port coupling refers to the undesired interaction between the orthogonal dominant modes that perturbs the impedance matching and polarization purity control at each input port. The cross-polarization of the radiated waves represents the amount of signal that was to be transmitted on a given polarization (polarization 1) but appears instead as the other polarization (polarization 2). Cross-polarization refers to the spurious polarization orthogonal to the reference co-polarization produced at a given input

port that interferes with the orthogonal co-polarization produced at the other input port; resulting in diminished gain and co-to-cross-polarization ratios attributed to each input port. It is not easy to suppress both input port coupling and cross-polarization levels, especially across a wide impedance bandwidth.

For dual polarized radiation, traditionally, a square patch is coupled to a pair of microstrip lines through two offset orthogonal slots cut in the ground plane [27]. The input port isolation was of the order of 18 dB, which is unacceptable for most wireless communication applications. Several other aperture-coupled dual polarization solutions have since been presented for single-element patch configurations [28]-[34]. Positioning the two orthogonal slots further apart may help enhance the input port isolation but at the expense of reduced coupling with the radiating element. The use of an aperture-feed at one port and an L-probe feed [35] or capacitive-feed [36] at the second port, affords good input port isolation between the closely spaced orthogonal feeds. However, the high back radiation inherent in aperture-coupling can lead to increased levels of interference for sectored mobile communication systems. Typical base stations provide sectoral coverage area to increase system capacity, and the back radiation from each antenna has to be kept low to ensure minimal interference from adjoining subcells.

Dual polarized dual and quadruple L-probe patch antennas in [19] were shown to deliver improved front-to-back ratio and impedance bandwidths (~30%). The L-probe proximity feed approach allows for the use of a thick low permittivity antenna substrate that can help broaden the impedance bandwidth. Unfortunately, a lower patch Q encourages higher order modes generation that give rise to more

cross-polarized components and stronger mode coupling. To cancel out the strong probe leakage radiation and probe coupling, the L-probe feeds were supplied equal amplitude out-of-phase excitations. This accounts for the particularly good input port decoupling and cross-polarization suppression, especially at the center operating frequency. However, the conventional 180^o narrowband baluns used only provide a consistent 180^o ($\pm 10^o$) phase shift over a narrow band (~10%), and proper cancellation of probe leakage radiation and probe coupling cannot take place throughout the wide impedance passband (~30%) of the antenna.

In this chapter, the broadband design of dual linearly polarized L-probe fed patch antennas is presented. The L-probe patch antenna affords low back radiation and wide impedance bandwidth (~30%). For the pattern bandwidth (minimum beamwidth) and polarization bandwidth (maximum cross-polarization level) to match up to the wide impedance bandwidth afforded, the high probe leakage radiation (due to the thick low permittivity antenna substrate) and strong probe coupling (due to the closely spaced multipoint probe feeds) have to be cancelled out across the 30% impedance passband. The use of a novel 180^o broadband balun [37] is proposed. The proposed 180^o broadband balun delivers good impedance matching, equal amplitude power splitting and consistent 180^o ($\pm 10^o$) phase shifting, across a wide band (~45%). In Section 2.2, wideband H-plane cross-polarization suppression is demonstrated for a linearly polarized dual L-probe patch antenna utilizing the proposed 180^o broadband balun. In Section 2.3, wideband H-plane cross-polarization suppression and input port decoupling is demonstrated for a dual linearly polarized quadruple L-probe patch antenna utilizing a pair of the proposed 180^o broadband baluns.

2.2 Broadband Linearly Polarized Dual L-Probe Patch Antenna with a 180° Broadband Balun

2.2.1 Antenna Design and Geometry

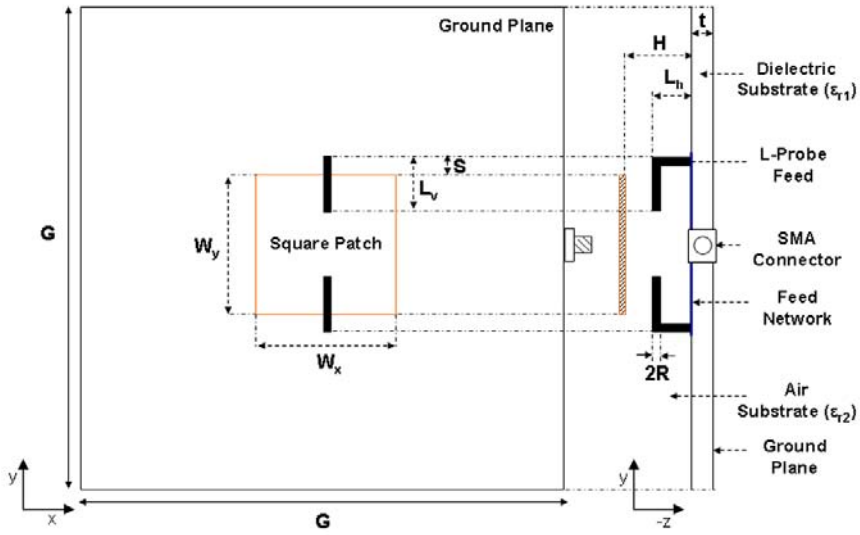

Fig. 2. Geometry of the dual L-probe square patch antenna.

The single L-probe rectangular patch antenna has been found to deliver a wide impedance bandwidth (SWR < 2) of ~30% [16]-[18]. However, the use of a thick (~$0.1\lambda_o$) low permittivity (ε_{r2} = 1) air substrate encourages the generation of unwanted higher order modes and causes the L-probe feed to emit probe leakage radiation that gives rise to increased cross-polarization levels in the H-plane and asymmetrical co-polarization patterns in the E-plane. The cross-polarization level ($|E_{co-pol}|/|E_{x-pol}|$), defined as the ratio of the maximum value of $|E_{co-pol}|$ to the maximum value of $|E_{x-pol}|$ in a specified plane, is dependent on the aspect ratio of the rectangular patch element [11], and varies with feed position, substrate thickness and substrate permittivity [38]. A rectangular patch with a high aspect ratio can give a relatively pure linearly polarized wave and a slightly wider impedance bandwidth, but a square or circular patch is required for a dual

polarized patch configuration where the two orthogonal polarizations must have equal field strengths for maximum diversity gain. The dual L-probe square patch antenna, shown in Fig. 2, is designed for low cross-polarization across a wide impedance passband (~30%) centered at 2.0 GHz. A second L-probe feed is symmetrically positioned at the opposite radiating edge (W_x) of the patch element. At this location and with an equal amplitude power and 180^o phase shift, the second L-probe feed couples into the same dominant mode of the patch element; and the probe leakage radiation from the two L-probe feeds cancels out. The use of a feed network with wideband 180^o phase shifting capabilities is required in order for the probe leakage radiation to cancel out across the wide impedance passband (~30%) afforded by the L-probe patch antenna.

2.2.2 Feed Network Configurations

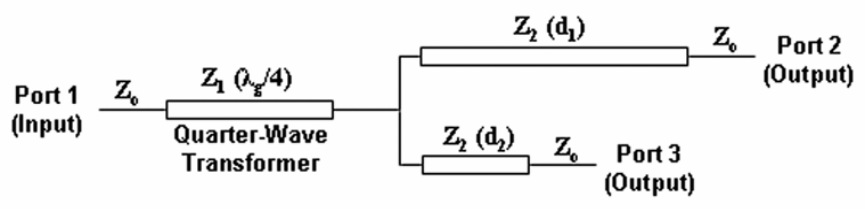

Fig. 3. Schematics of the conventional 180^o narrowband balun.

The conventional 180^o narrowband balun, shown in Fig. 3, is commonly used as a balanced phase shifting feed network in antenna designs. To provide a 180^o phase shift, the lengths of the microstrip branches, d_1 and d_2, must be such that $d_1 - d_2 = \lambda_g / 2$, where λ_g refers to the guide wavelength at a center operating frequency of 2.0 GHz. The characteristic impedances of the microstrip branches are given by $Z_o = 50\ \Omega$, $Z_1 = 35.36\ \Omega$, and $Z_2 = 50\ \Omega$.

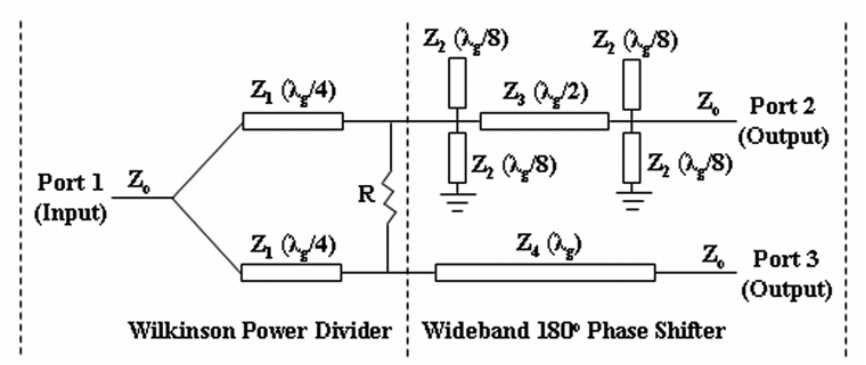

Fig. 4. Schematics of the proposed 180° broadband balun.

The proposed 180° broadband balun [37], shown in Fig. 4, delivers balanced power splitting and consistent 180° (±10°) phase shifting across a wide band. This broadband balun comprises of a 3-dB Wilkinson power divider [39], for wideband balanced power splitting, cascaded with a broadband 180° phase shifter [40], for wideband 180° phase shifting. λ_g refers to the guide wavelength at a center operating frequency of 2.0 GHz. The characteristic impedances of the microstrip branches are given by Z_1 = 70.71 Ω, Z_2 = 63.5 Ω, Z_3 = 80.5 Ω, and Z_4 = 50 Ω.

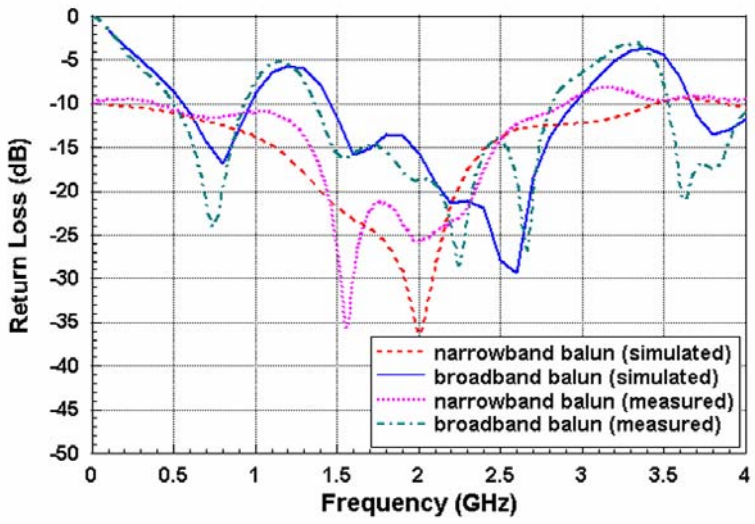

Fig. 5. Simulated and measured input port return loss comparison between the 180° narrowband and broadband baluns.

All simulations presented in this chapter were performed using IE3D, a commercially available electromagnetic field solver based on the Method of Moments (MoM). The feed networks were modeled on a Rogers RO4003 laminate of thickness t = 0.8 mm, dielectric constant ε_{r1} = 3.38, and an assumed loss tangent of tan δ = 0.0027. For convenient analysis, the input and output ports of the feed networks were all set to 50 Ω.

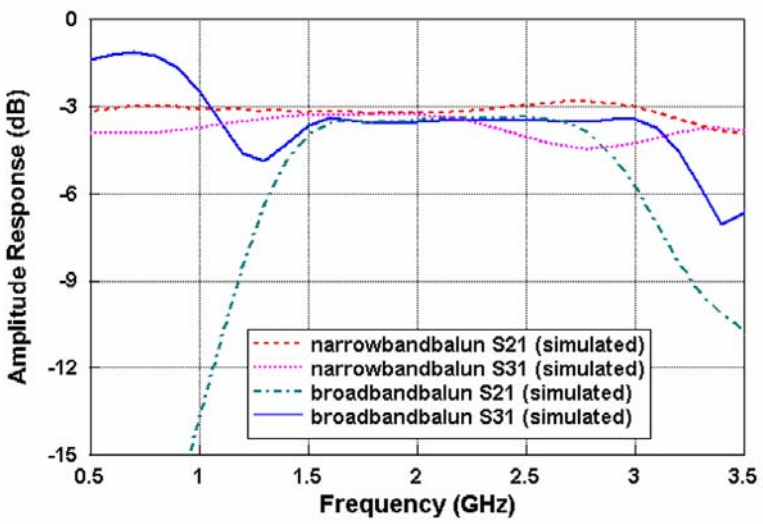

(a) Simulated

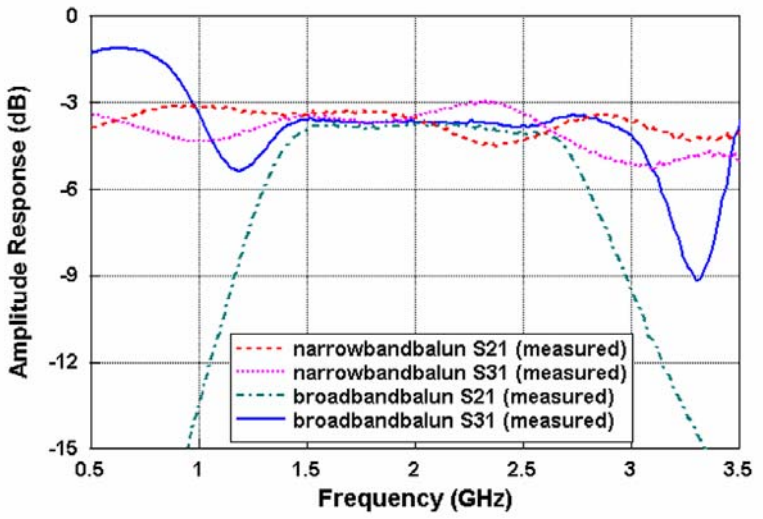

(b) Measured

Fig. 6. Simulated and measured output ports amplitude response comparison between the 180° narrowband and broadband baluns.

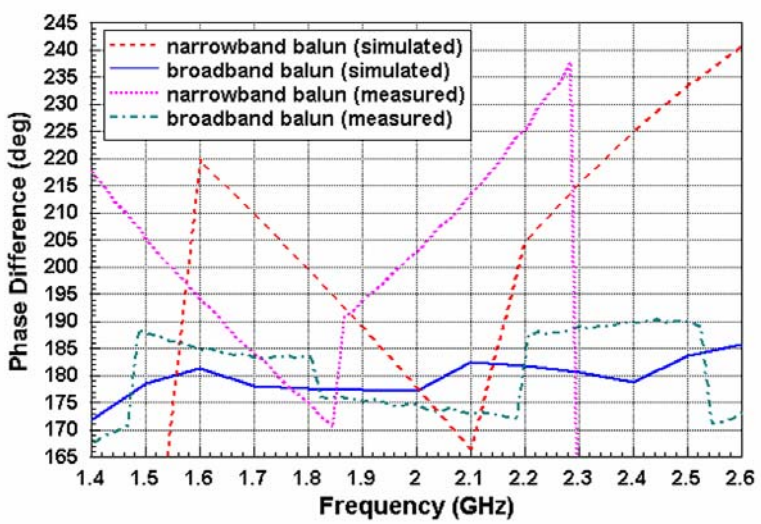

Fig. 7. Simulated and measured output ports phase difference comparison between the 180° narrowband and broadband baluns.

Fig. 5 shows the simulated and measured return loss comparison between the two baluns. The 180° broadband balun exhibits wide simulated and measured impedance bandwidths (S_{11} < -10 dB) of 67.57%, from 1.46 to 2.95 GHz, and 67.3%, from 1.39 to 2.8 GHz, respectively. The 180° narrowband balun exhibits relatively wider simulated and measured impedance bandwidths (S_{11} < -10 dB) of 188.76%, from 0.1 to 3.46 GHz, and 150.15%, from 0.41 to 2.88 GHz, respectively. Fig. 6 shows the simulated and measured output port amplitude response comparison between the two baluns. The 180° broadband balun exhibits wide simulated and measured balanced output ports power distribution bandwidths (S_{21} = S_{31} = -3 dB (±1.0 dB)) of 60.79%, from 1.5 to 2.81 GHz, and 44.73%, from 1.51 to 2.38 GHz, respectively. The 180° narrowband balun exhibits relatively wider simulated and measured balanced output ports power distribution bandwidths (S_{21} = S_{31} = -3 dB (±1.0 dB)) of 114.2%, from 0.68 to 2.49 GHz, and 55.29%, from 1.23 to 2.17 GHz, respectively. Fig. 7 shows the simulated and measured output ports phase difference comparison between the two baluns. The 180° broadband balun exhibits a wide simulated 180° (±5°) output

ports phase difference bandwidth of 55.72%, from 1.45 to 2.57 GHz, and a wide measured 180^o ($\pm 10^o$) output ports phase difference bandwidth of 48.84%, from 1.47 to 2.42 GHz. The measured output port phase differences at 1.7, 2.0 and 2.3 GHz are 184, 175 and 189^o, respectively. The 180^o narrowband balun exhibits a narrow simulated 180^o ($\pm 5^o$) output ports phase difference bandwidth of 4.53%, from 1.94 to 2.03 GHz, and a narrow measured 180^o ($\pm 10^o$) output ports phase difference bandwidth of 11.43%, from 1.65 to 1.85 GHz. The measured output port phase differences at 1.7, 2.0 and 2.3 GHz are 184, 202.5 and 165^o, respectively. The simulated and measured results are in rather good agreement. For the narrowband balun, however, the 180^o phase shift predicted by the simulator at 2.0 GHz is detected at 1.75 GHz in measurement. This is due to the tolerance errors in fabricating the narrowband balun in house.

Combining the measured results in Fig. 5 to 7, it is observed that the proposed 180^o broadband balun delivered low input port return loss (S_{11} < -10 dB), balanced output ports power distribution (S_{21} = S_{31} = -3 dB (±1.0 dB)), and consistent 180^o ($\pm 10^o$) output ports phase difference over a wide band of 44.73%, from 1.51 to 2.38 GHz; hence it is termed a "broadband" balun. The conventional 180^o narrowband balun delivered both low input port return loss and balanced output ports power distribution over a relatively wider band. However, its overall performance was inherently limited by its narrowband 180^o ($\pm 10^o$) phase shifting capability (~11.5%); hence it is termed a "narrowband" balun.

2.2.3 Fabrication and Experimental Setup

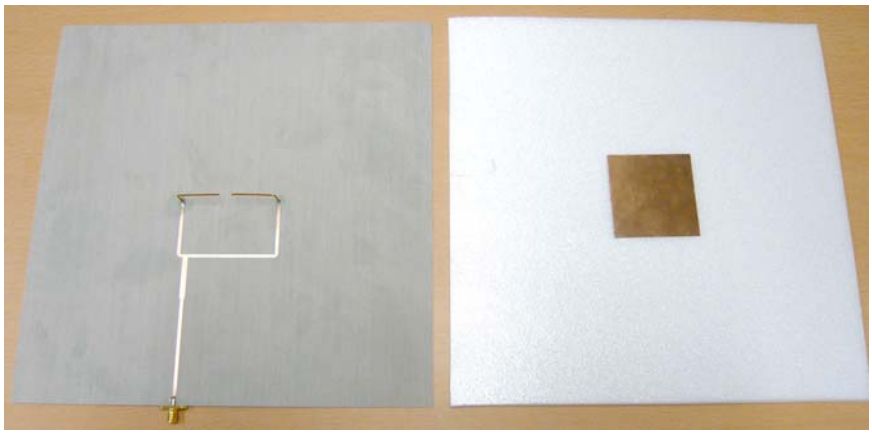

Fig. 8. Prototype of the dual L-probe square patch antenna utilizing the 180^{o} narrowband balun.

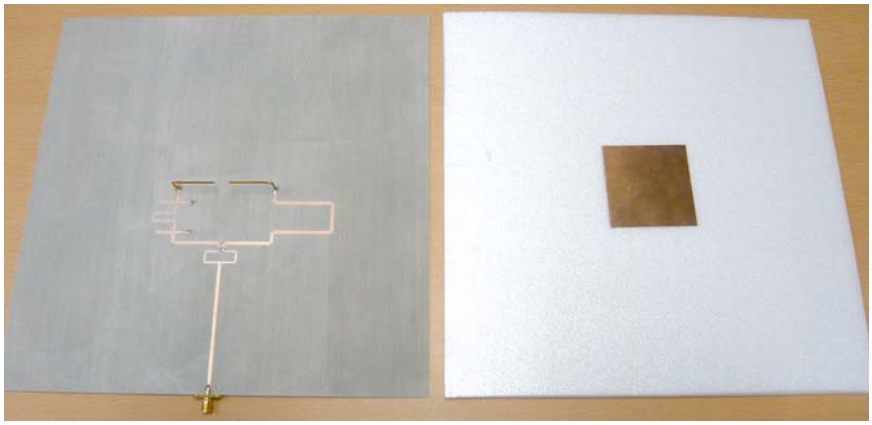

Fig. 9. Prototype of the dual L-probe square patch antenna utilizing the 180^{o} broadband balun.

Fig. 8 and 9 show the prototype of the dual L-probe square patch antenna utilizing the 180^{o} narrowband and broadband baluns, respectively. The antenna and feed network parameters were optimized for a wide impedance bandwidth centering 2.0 GHz. The square copper patch, of dimensions $W_x = W_y = 53.5$ mm (0.357 λ_o), was positioned at a height above the dielectric substrate to create an air substrate of thickness H = 23.5 mm (0.157 λ_o). The feed network and square copper ground plane of length G = 250 mm (1.67 λ_o), were respectively printed on the top and

bottom of the dielectric substrate. The two L-probe feeds, of diameter 2R = 1 mm, with vertical length L_h = 12 mm (0.08 λ_o) and horizontal length L_v = 26.5 mm (0.177 λ_o), were positioned S = 4 mm away from the edge of the patch, and respectively soldered at the output ports of the feed network. The impedance measurements were taken using the Agilent E8364B network analyzer, while the far-field radiation measurements were taken using the Hewlett Packard 8510C vector network analyzer and the Orbit-MiDAS far-field measurement system in an anechoic chamber. With a reference linearly polarized standard horn antenna, the comparison method (gain-transfer method) was used to determine the measured gain (see Section 3.2.3).

2.2.4 Impedance and Radiation Performances

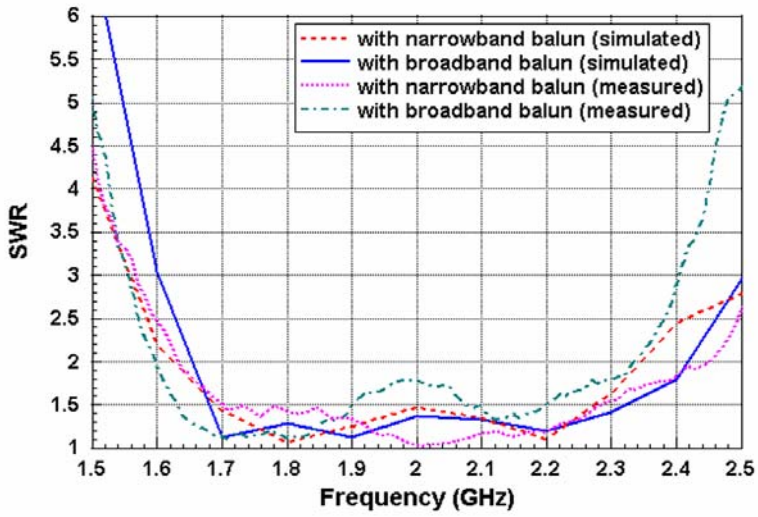

Fig. 10. Simulated and measured SWR for the dual L-probe square patch antenna utilizing the 180° narrowband or broadband balun.

Fig. 10 shows the simulated and measured SWR for the dual L-probe square patch antenna utilizing either balun. The antenna with the broadband balun exhibits wide simulated and measured impedance bandwidths (SWR < 2) of 37.84%, from

1.65 to 2.42 GHz, and 37.15%, from 1.6 to 2.33 GHz, respectively. The same antenna with the narrowband balun exhibits roughly similar simulated and measured impedance bandwidths (SWR < 2) of 35.77%, from 1.63 to 2.34 GHz, and 39.22%, from 1.64 to 2.44 GHz, respectively. The simulated and measured SWR results are in reasonably good agreement. From 1.7 to 2.3 GHz (30%), good simulated and measured impedance matching (SWR < 2) is observed for the antenna utilizing either balun. This common impedance passband, sufficient to cover the GSM1800 (1710-1880 MHz), GSM1900 (1850-1990 MHz) and UMTS2000 (1920-2170 MHz) bands, will be the designated bandwidth of interest in comparing the radiation performances of the antenna utilizing either balun.

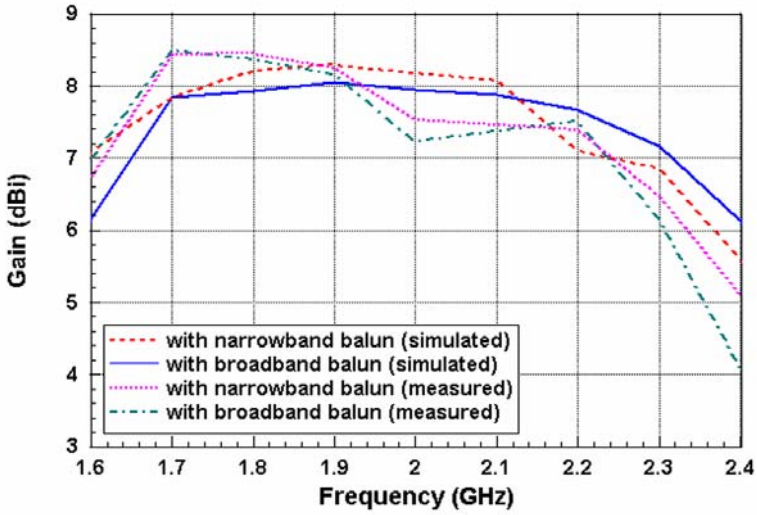

Fig. 11. Simulated and measured gain for the dual L-probe square patch antenna utilizing the 180^{o} narrowband or broadband balun.

Fig. 11 shows the simulated and measured boresight gain for the dual L-probe square patch antenna utilizing either balun. Within the bandwidth of interest (1.7 to 2.3 GHz), the measured boresight gain of the antenna with the broadband balun ranges from 6.16 to 8.5 dBi, while that of the same antenna with the narrowband balun ranges from 6.49 to 8.46 dBi. It is observed that the use of the broadband

balun in place of the narrowband balun does not greatly affect the boresight gain profile of the antenna. This suggests that the proposed broadband balun, compared to the narrowband balun, does not incur significantly higher insertion losses that translate to lower antenna gain. The simulated and measured boresight gain results are in reasonably good agreement.

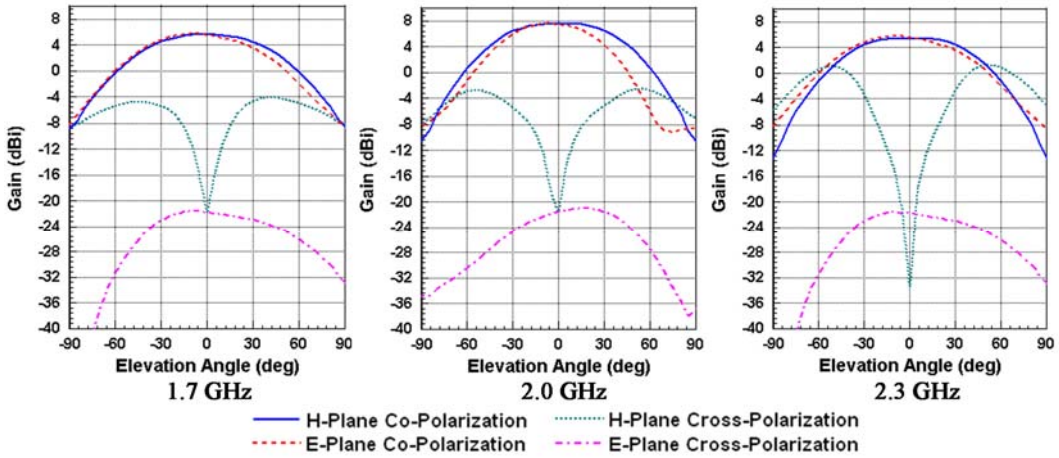

Fig. 12. Simulated radiation patterns for the single L-probe square patch antenna.

Fig. 12 shows the simulated radiation patterns for the single L-probe square patch antenna, at the lower frequency edge (1.7 GHz), center operating frequency (2.0 GHz), and upper frequency edge (2.3 GHz), of the bandwidth of interest. The second L-probe feed of the dual L-probe square patch antenna shown in Fig. 2 has been removed, keeping all other antenna parameters the same. The single L-probe feed was excited using a 50 Ω microstrip feed line. The antenna geometry has been optimized for a dual L-probe feed configuration. Hence, in adopting the same antenna parameters, the single L-probe case does not provide the expected 30% impedance passband and the gain dips sharply off resonance. Nevertheless, the simulated radiation patterns give insight to the effect of this asymmetrical feeding structure on the co- and cross-polarization. Across this passband, the antenna exhibits slightly asymmetrical E-plane co-polarization patterns (especially

at 2.0 GHz) and symmetrical H-plane co-polarization patterns. The antenna also exhibits consistently low E-plane cross-polarization levels (< -27 dB) but consistently high H-plane cross-polarization levels (up to -4.5 dB). Consistently low H-plane cross-polarization levels (< -27.5 dB) are observed at the boresight, but can be seen to increase drastically off the boresight observation angles.

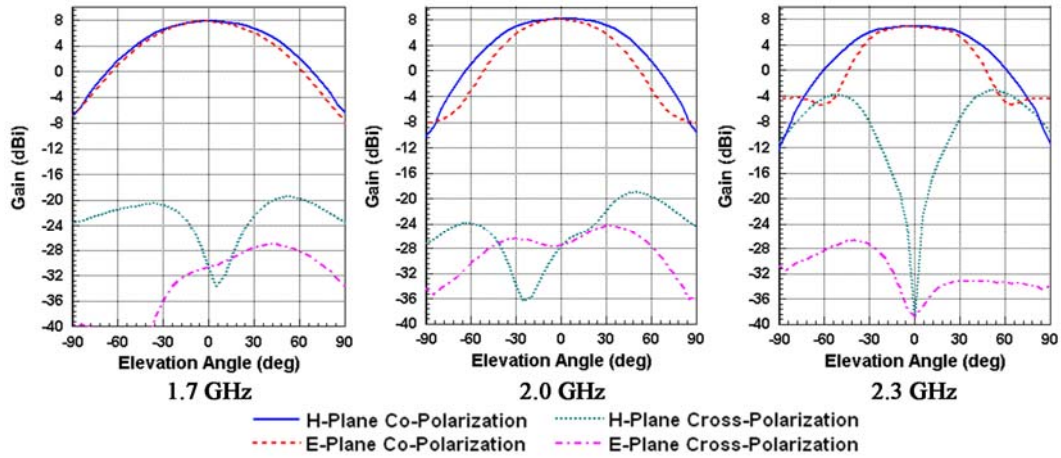

Fig. 13. Simulated radiation patterns for the dual L-probe square patch antenna utilizing the 180^{o} narrowband balun.

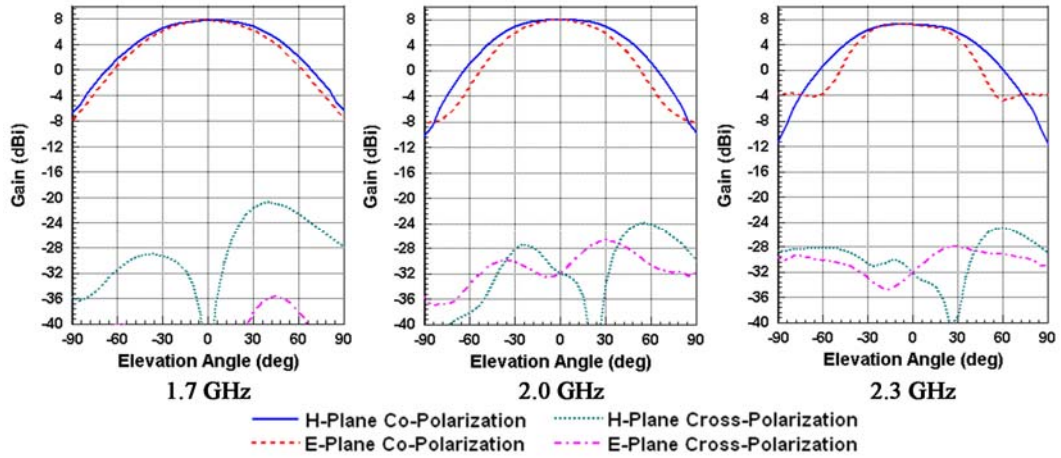

Fig. 14. Simulated radiation patterns for the dual L-probe square patch antenna utilizing the 180^{o} broadband balun.

Fig. 13 and 14 show the simulated radiation patterns for the dual L-probe square patch antenna utilizing the 180^{o} narrowband and broadband baluns, respectively,

at the lower frequency edge (1.7 GHz), center operating frequency (2.0 GHz), and upper frequency edge (2.3 GHz), of the bandwidth of interest. Across this passband, the antenna utilizing either balun exhibits symmetrical E- and H-plane co-polarization patterns and consistently low E-plane cross-polarization levels (< -32 dB). The E-plane beamwidths are narrower at the upper frequency point. Nonetheless, consistently wide E- and H-plane half-power beamwidths, no less than 60^{o} ($\pm$ 30^{o}), are maintained. Consistently low H-plane cross-polarization levels (< -36 dB) are observed at the boresight, but seen to increase off the boresight observation angles. The antenna utilizing the narrowband balun exhibits high H-plane cross-polarization levels (up to -11 dB) at the upper frequency point. The same antenna utilizing the broadband balun exhibits consistently low H-plane cross-polarization (< -28 dB), across the passband. Compared to the simulated results in Fig. 12, it is evident that the balanced and symmetrical dual L-probe feeding structure delivers lower E- and H-plane cross-polarization levels. In particular, significant H-plane cross-polarization suppression is observed at the lower and center frequency points, with the narrowband balun, and across the passband, with the broadband balun.

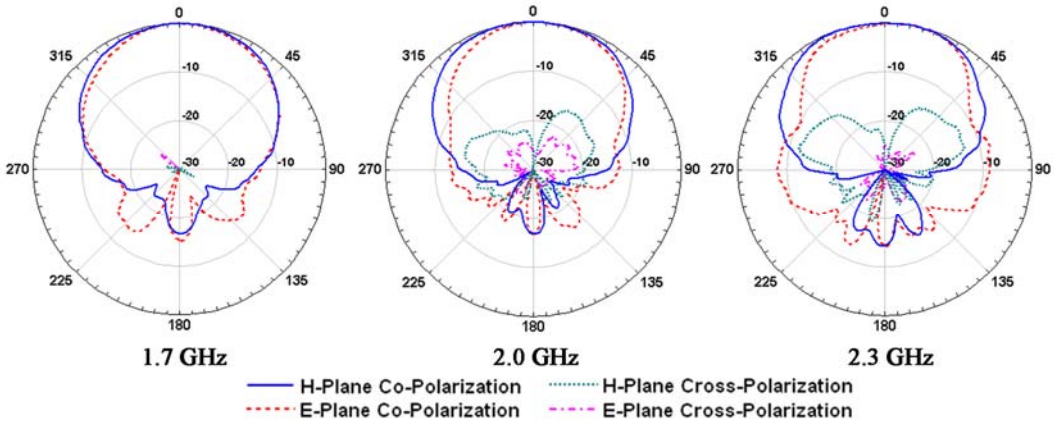

Fig. 15. Measured normalized radiation patterns for the dual L-probe square patch antenna utilizing the 180^{o} narrowband balun.

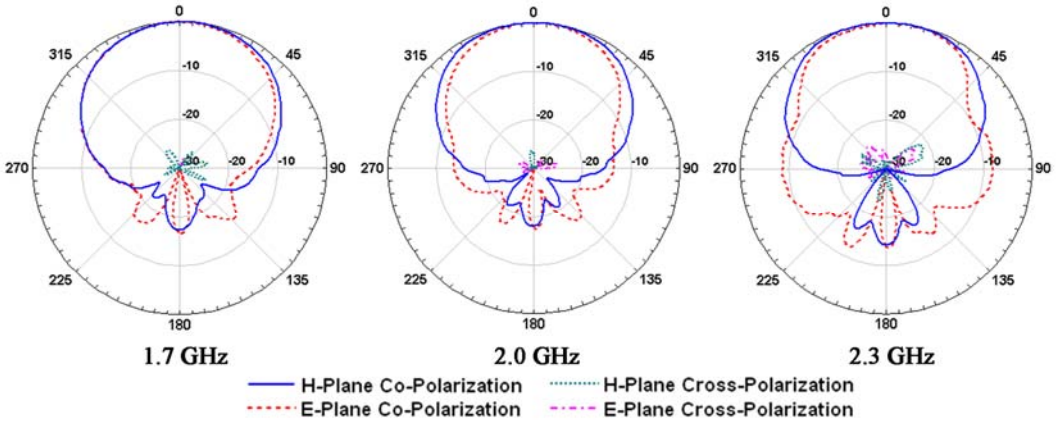

Fig. 16. Measured normalized radiation patterns for the dual L-probe square patch antenna utilizing the 180° broadband balun.

Fig. 15 and 16 show the measured normalized radiation patterns for the dual L-probe square patch antenna utilizing the 180° narrowband and broadband baluns, respectively, at the lower frequency edge (1.7 GHz), center operating frequency (2.0 GHz), and upper frequency edge (2.3 GHz), of the bandwidth of interest. Across this passband, the antenna utilizing the narrowband balun exhibits symmetrical E- and H-plane co-polarization patterns and consistently low E-plane cross-polarization levels (< -22 dB). At the boresight, the H-plane cross-polarization levels (< -30 dB) are low. Off the axis, the H-plane cross-polarization levels are low (< -26 dB) at the lower frequency point, but appreciate considerably (up to -12 dB) at the center and upper frequency points. Across this passband, the antenna utilizing the broadband balun exhibits symmetrical E- and H-plane co-polarization patterns and consistently low E- and H-plane cross-polarization levels (< -21 dB). It is evident that the use of the broadband balun provides improved cross-polarization suppression, especially in the H-plane, across the bandwidth of interest. As shown in Fig. 7, the measured output port phase differences of the narrowband balun at 1.7, 2.0 and 2.3 GHz are 184, 175 and 189°, respectively, while that of the broadband balun are 184, 202.5 and 165°, respectively. These

measured results indicate that when the output port phase difference delivered by the balun is kept within 180^o ($\pm 10^o$), the measured H-plane cross-polarization levels of the antenna do not exceed -20 dB. It is also observed from the E- and H-plane co-polarization patterns that the use of the L-probe feeding structure has allowed for the back radiation levels to be kept in check. Across this passband, the antenna utilizing either balun exhibits E- and H-plane front-to-back ratios no less than 15 dB. Consistently wide E- and H-plane half-power beamwidths, better than 60^o ($\pm 30^o$), can also be observed from the co-polarization patterns.

Table 1 Simulated and Measured H-plane Cross-Polarization Levels for the Dual L-Probe Square Patch Antenna with the 180^o Narrowband or Broadband Balun

Freq (GHz)	**with 180^o Narrowband Balun**		**with 180^o Broadband Balun**	
	Simulated X-Pol (dB)	**Measured X-Pol (dB)**	**Simulated X-Pol (dB)**	**Measured X-Pol (dB)**
1.7	-27.2	-26.7	-28.6	-24.1
1.8	-27.0	-24.9	-28.3	-27.2
1.9	-27.9	-22.9	-28.6	-22.8
2.0	-27.2	-15.6	-31.9	-26.3
2.1	-20.6	-12.9	-31.0	-24.4
2.2	-6.4	-8.3	-27.5	-22.1
2.3	-10.1	-12.1	-32.1	-21.1

Table 1 provides a summary of the simulated and measured H-plane cross-polarization levels for the dual L-probe square patch antenna utilizing either balun, across the bandwidth of interest. The antenna with the narrowband balun exhibits low H-plane cross-polarization levels (< -21 dB) from 1.7 to 2.1 GHz, in simulation, and from 1.7 to 1.9 GHz, in measurement. In contrast, the antenna with the broadband balun exhibits consistently low H-plane cross-polarization levels (< -21 dB) from 1.7 to 2.3 GHz, in both simulation and measurement. The higher measured cross-polarization levels can be attributed to the fabrication tolerance, and L-probe and patch alignment errors not accounted for in simulation.

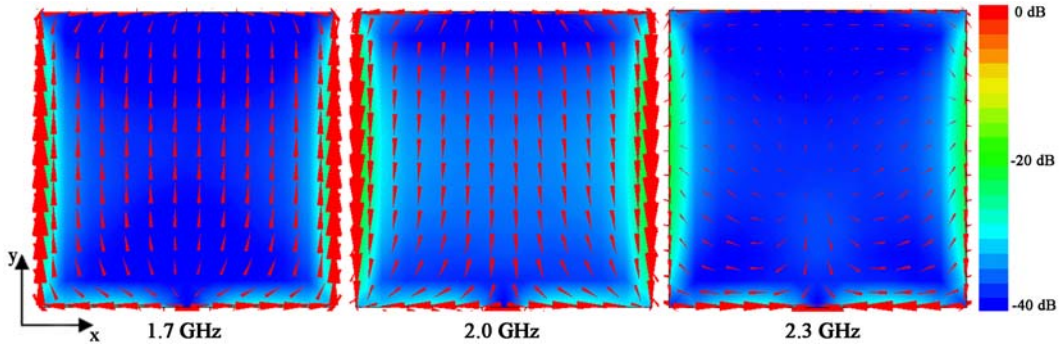

Fig. 17. Simulated normalized current distribution for the radiating element of the single L-probe square patch antenna.

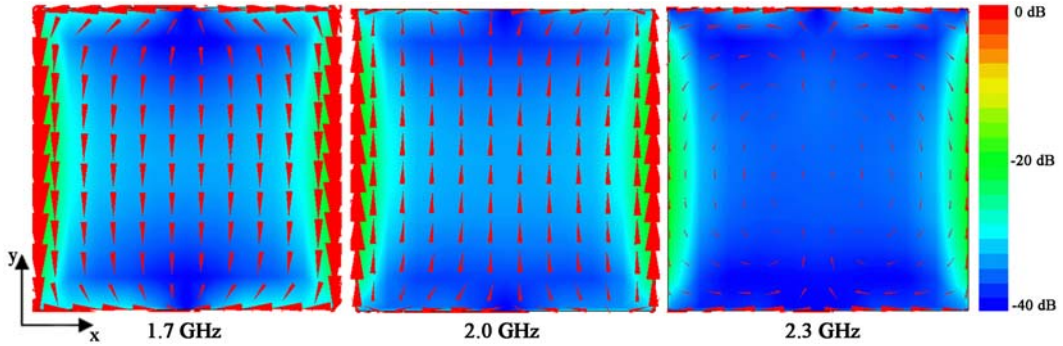

Fig. 18. Simulated normalized current distribution for the radiating element of the dual L-probe square patch antenna utilizing the 180^{o} narrowband balun.

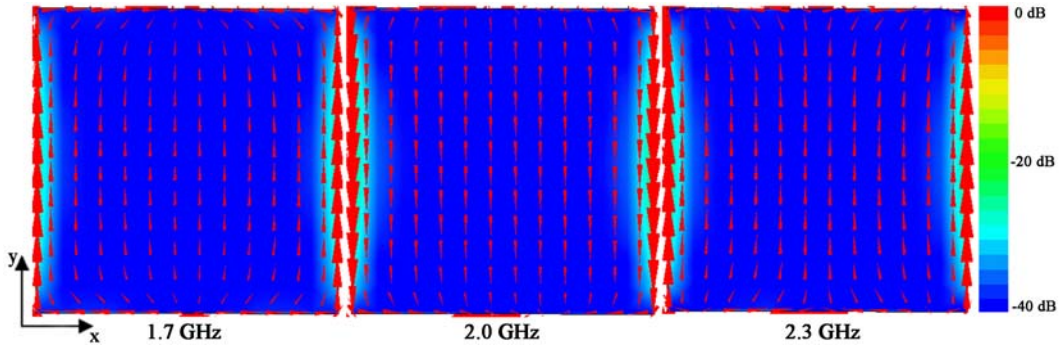

Fig. 19. Simulated normalized current distribution for the radiating element of the dual L-probe square patch antenna utilizing the 180^{o} broadband balun.

Fig. 17 to 19 show the simulated normalized current distribution for the radiating element of the single L-probe square patch antenna, and the dual L-probe square patch antenna utilizing the 180^{o} narrowband and broadband baluns, respectively,

at the lower frequency edge (1.7 GHz), center operating frequency (2.0 GHz), and upper frequency edge (2.3 GHz), of the bandwidth of interest. The current distribution has been normalized to the respective electric current maxima at each frequency point. The L-probe feed has been positioned such that it primarily excites the TM_{010} mode of the patch element, as seen in Fig. 17 to 19, with the co-polarized electric current components along the y-axis and the cross-polarized electric current components along the x-axis.

The single L-probe antenna, as seen in Fig. 17, has an asymmetrical feeding structure and an unbalanced current distribution. The co-polarized electric currents are symmetrical with respect to the E-plane ($\phi = 90^o$) but slightly asymmetrical with respect to the H-plane ($\phi = 0^o$). This explains the symmetrical H-plane co-polarization patterns and the slightly asymmetrical E-plane co-polarization patterns, seen in Fig. 12, across the passband. The cross polarized electric currents are stronger near the feed point and asymmetrical with respect to the H-plane. At the upper frequency point, more cross-polarized electric current components are detected as the effect of the competing higher order modes set in. This accounts for high H-plane cross-polarization levels, seen in Fig. 12, across the passband; and higher H-plane cross-polarization levels (up to -4.5 dB) observed at 2.3 GHz. The dual L-probe antenna, as seen in Fig. 18 and 19, has a symmetrical feeding structure and a balanced current distribution. The co- and cross-polarized electric currents are symmetrical with respect to the E- and H-planes. This explains the symmetrical E- and H-plane co-polarization patterns, seen in Fig. 13 and 14, across the passband. It is noteworthy that the dual L-probe feeding structure, compared to the single L-probe feeding structure, allows for

relatively more symmetrical E-plane co-polarization patterns, across the passband. Due to symmetry about the E- and H-plane, the cross-polarized electric currents can cancel out when provided the necessary anti-phase excitations. At the upper frequency point, more cross-polarized electric current components are detected for the dual L-probe antenna with the narrowband balun, as seen in Fig. 18, as the effect of the competing higher order modes set in. In contrast, consistently less cross-polarized electric current components are detected for the dual L-probe antenna with the broadband balun, as seen in Fig. 19, across the passband; with the effect of the higher order modes kept in check even at the upper frequency point. This accounts for the consistently better H-plane cross-polarization suppression for the dual L-probe antenna with the broadband balun, seen in Fig. 13 and 14, across the passband. The H-plane cross-polarized levels are significantly reduced, as detailed in Table 1, from 2.2 to 2.3 GHz. These simulated results highlight the importance of deploying a feed network with wideband 180^o phase shifting capabilities. The E-plane cross-polarization levels are consistently low for all three cases, as seen in Fig. 12 to 14, due to the mutual cancellation of the cross-polarized electric current components on axis ($\phi = 90^o$), as seen in Fig. 17 to 19.

2.2.5 Discussions

In this section, the broadband design of a low cross-polarization dual L-probe square patch antenna utilizing a novel 180^o broadband balun has been presented. The broadband balun provides good impedance matching, equal amplitude power splitting and consistent 180^o phase shifting, over a wide band (~45%). The proposed antenna delivers good impedance matching (SWR < 2), high gain (> 6

dBi), symmetrical E- and H-plane co-polarization patterns, and consistently low E- and H-plane cross-polarizations levels (< -21 dB), across the across the bandwidth of interest from 1.7 to 2.3 GHz (~30%). The antenna in study lends itself to emerging broadband mobile base station applications covering three bands, i.e. PCS1800 (1710-1880 MHz), GSM1900 (1850-1990 MHz) and UMTS2000 (1920-2170 MHz).

2.3 Broadband Dual Linearly Polarized Quadruple L-Probe Patch Antenna with 180° Broadband Baluns

2.3.1 Antenna Design and Geometry

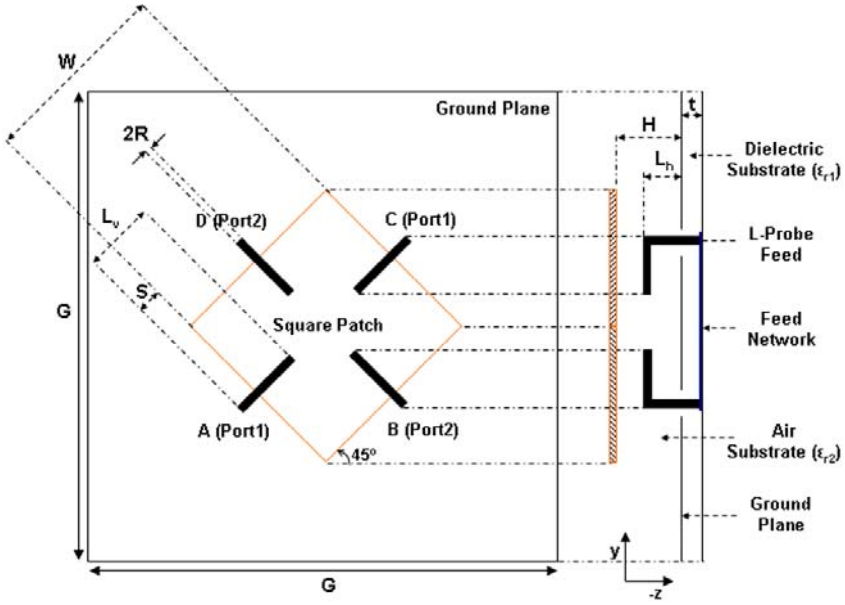

Fig. 20. Geometry of the dual polarized quadruple L-probe square patch antenna

The dual polarized quadruple L-probe square patch antenna, shown in Fig. 20, is designed for low cross-polarization and high input port isolation across a wide impedance passband (~30%) centered at 2.0 GHz. Building upon the dual L-probe square antenna design shown in Fig. 2, a second pair of L-probe feeds are

positioned at the orthogonal radiating edges of the square patch element. L-probe A and C are supplied balanced and anti-phase excitations at port 1, allowing for their probe leakage radiation to mutually cancel out. Similarly, L-probe B and D are supplied balanced and anti-phase excitations at port 2, allowing for their probe leakage radiation to mutually cancel out. Vertical probe feeds are not commonly adopted in dual polarized antenna designs because the strong coupling between the probe feeds leads to poor input port isolation. For the L-probe feed, the vertical arm is capable of emitting undesired monopole-like leakage radiation that strongly couples with the leakage radiation produced by the vertical arm of an adjacent L-probe feed in close proximity. The cancellation of the probe leakage radiation produced by each of the four L-probe feeds confers significant reduction in the probe coupling between adjacent L-probe feeds. In the absence of probe leakage radiation emitted from each of the four L-probe feeds, say, L-probe A will then couple less strongly with L-probe B and with L-probe D. The use of a feed network with wideband 180^{o} phase shifting capabilities is required in order for the probe leakage radiation and probe coupling to cancel out across the wide impedance passband (~30%) afforded by the L-probe patch antenna.

2.3.2 Feed Network Configurations

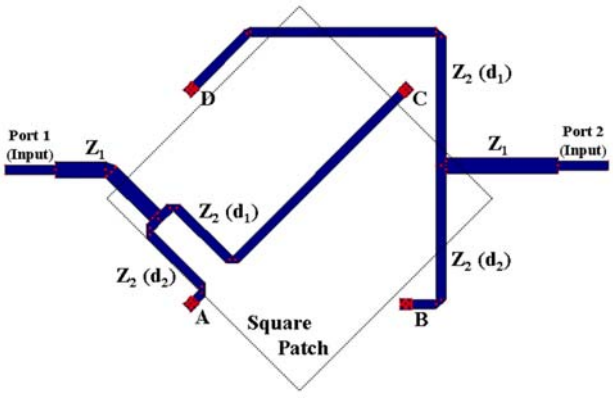

Fig. 21. Feed network layout of the 180^{o} narrowband balun pair.

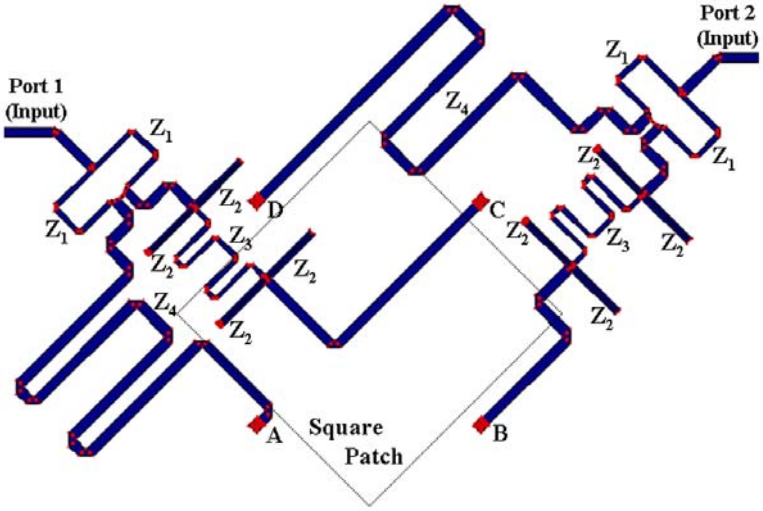

Fig. 22. Feed network layout of the 180° broadband balun pair.

Fig. 21 and 22 show the feed network layout of 180° narrowband and broadband balun pairs, respectively. The narrowband balun, as shown in Fig. 3, and broadband balun, as shown in Fig. 4, are used in this dual-feed mechanism. For both feed networks, the port 1 balun is designed to have a slightly different layout compared to that of the port 2 balun. This is because the microstrip branches will intersect if the layouts for both baluns are to be the same. The feed line may be allowed to cross by using an air bridge [28], similar to the concept of wire bonding, but this complicates the manufacturing process and give rise to spurious radiation that lead to higher insertion losses. Instead, the feed lines are meandered so as to ensure no overlap and to provide a more compact overall feed layout. Special attention was also paid to make sure the folded feed lines were sufficiently spaced out (at least 0.1 λ_o apart) so that they do not interact and act as coupled transmission lines. Since the port 1 balun and port 2 balun have a different layout arrangement, each balun had to be individually optimized to provide the dual linearly polarized antenna with the widest possible common impedance bandwidth centering 2.0 GHz, at input port 1 and 2.

2.3.3 Fabrication and Experimental Setup

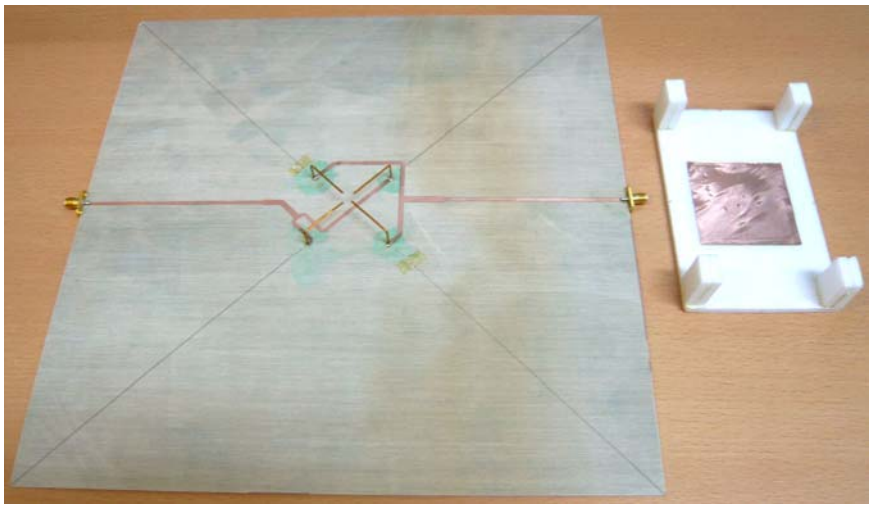

Fig. 23. Prototype of the dual polarized quadruple L-probe square patch antenna utilizing the 180^o narrowband balun pair.

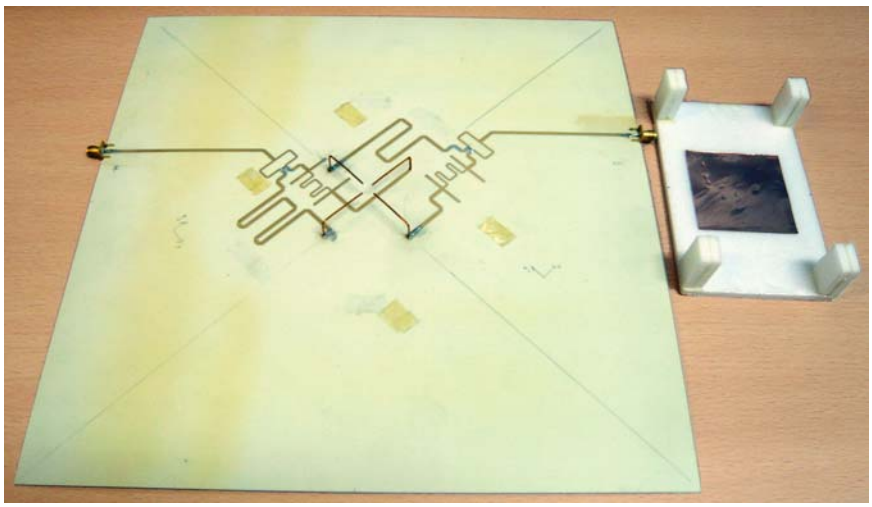

Fig. 24. Prototype of the dual polarized quadruple L-probe square patch antenna utilizing the 180^o broadband balun pair.

Fig. 23 and 24 show the prototype of the dual polarized quadruple L-probe square patch antenna utilizing the 180^o narrowband and broadband balun pairs, respectively. The antenna and feed network parameters were optimized for a wide impedance bandwidth centering 2.0 GHz. The square copper patch, of length W_x = 53.5 mm (0.357 λ_o), was positioned at a height above the dielectric substrate to

create an air substrate of thickness H = 22.4 mm (0.15 λ_o). The feed network and square copper ground plane of length G = 300 mm (1.5 λ_o), were respectively printed on the top and bottom of the dielectric substrate. The four L-probe feeds, of diameter 2R = 1 mm, with vertical length L_h = 12.4 mm (0.827 λ_o) and horizontal length L_v = 26.5 mm (0.177 λ_o), were positioned S = 4 mm away from the edge of the patch, and soldered at the respective output ports of the feed network. The impedance measurements were taken using the Agilent E8364B network analyzer, while the far-field radiation measurements were taken using the Hewlett Packard 8510C vector network analyzer and the Orbit-MiDAS far-field measurement system in an anechoic chamber. With a reference linearly polarized standard horn antenna, the comparison method (gain-transfer method) was used to determine the measured gain (see Section 3.2.3). A 50 Ω load was connected to port 2 when measuring the port 1 radiation performances, and vice versa.

2.3.4 Impedance and Radiation Performances

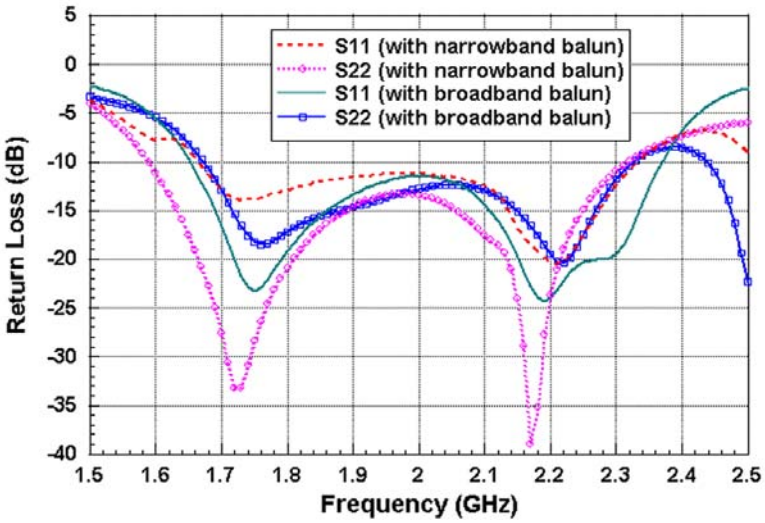

Fig. 25. Simulated return loss for the dual polarized quadruple L-probe square patch antenna utilizing the 180° narrowband or broadband balun pair.

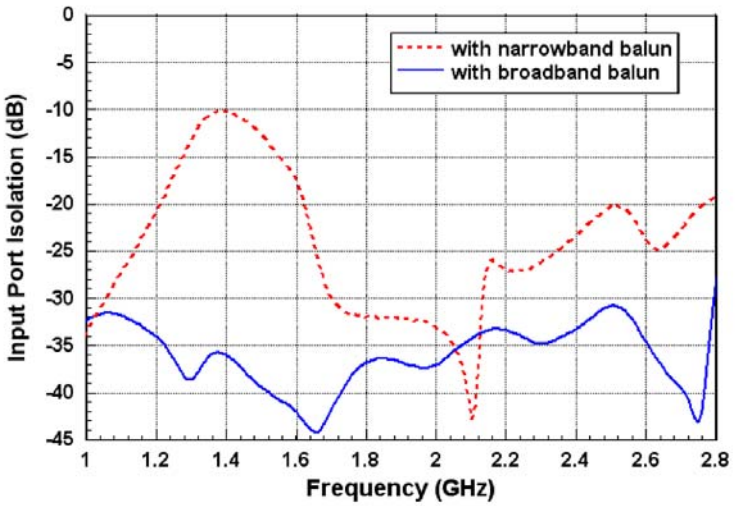

Fig. 26. Simulated input port isolation for the dual polarized quadruple L-probe square patch antenna utilizing the 180^{o} narrowband or broadband balun pair.

Fig. 25 shows the simulated return loss for the dual polarized quadruple L-probe square patch antenna utilizing either balun pair. The antenna with the broadband balun pair exhibits simulated impedance bandwidths of 34.8% (S_{11} < -10 dB), from 1.66 to 2.36 GHz, and 32% (S_{22} < -10 dB), from 1.68 to 2.32 GHz, while the same antenna with the narrowband balun pair exhibits simulated impedance bandwidths of 33% (S_{11} < -10 dB), from 1.67 to 2.33 GHz, and 36.9% (S_{22} < -10 dB), from 1.59 to 2.31 GHz. The simulated results indicate that the use of the broadband balun in place of the narrowband balun do not significantly affect the impedance bandwidth of the dual polarized antenna, at either port.

Fig. 26 shows the simulated input port isolation for the dual polarized quadruple square patch antenna utilizing either balun pair. The antenna with the broadband balun pair exhibits good simulated input port isolation (S_{21} < -30 dB), from 1 to 2.8 GHz (~95%). The same antenna with the narrowband balun pair exhibits good simulated input port isolation (S_{21} < -30 dB), from 1.71 to 2.12 GHz (21.4%).

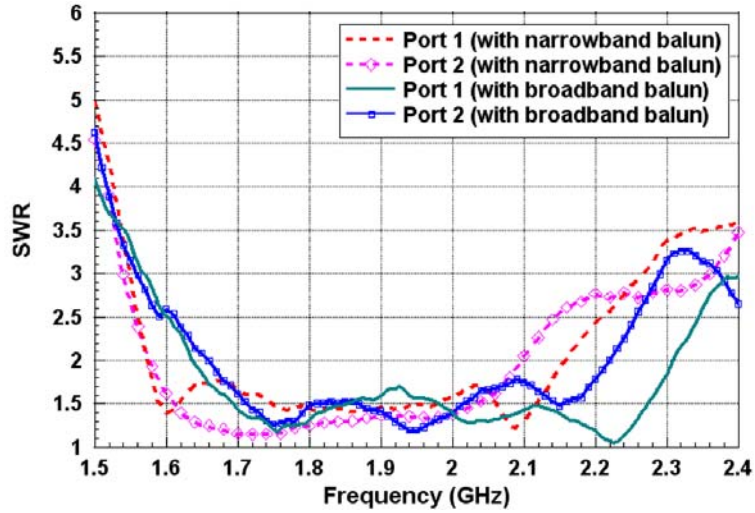

Fig. 27. Measured SWR for the dual polarized quadruple L-probe square patch antenna utilizing the 180^{o} narrowband or broadband balun pair.

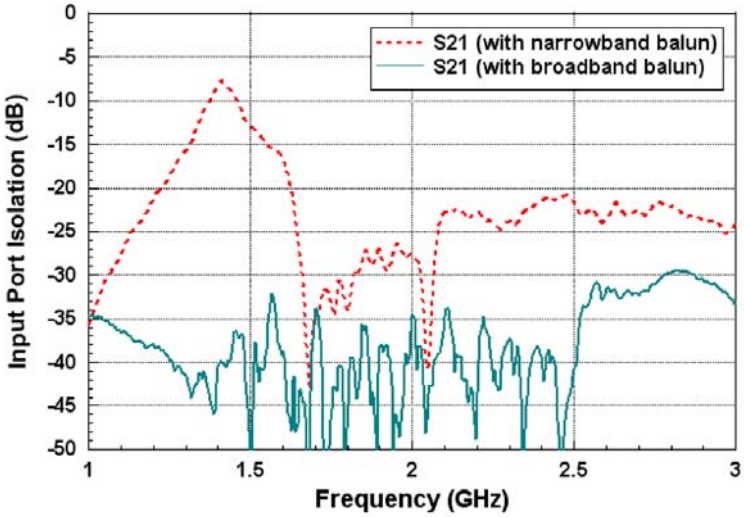

Fig. 28. Measured input port isolation for the dual polarized quadruple L-probe square patch antenna utilizing the 180^{o} narrowband or broadband balun pair.

Fig. 27 shows the measured SWR for the dual polarized quadruple L-probe square patch antenna utilizing either balun pair. The antenna with the broadband balun pair exhibits, for SWR < 2, a measured port 1 impedance bandwidth of 34%, from 1.64 to 2.31 GHz, and a measured port 2 impedance bandwidth of 29%, from 1.66 to 2.22 GHz. The common impedance passband (SWR < 2) ranges from 1.66 to 2.22 GHz (29%). Hence, the designated bandwidth of interest ranges from 1.7 to

2.2 GHz (25.64%). The same antenna with the narrowband balun pair exhibits, for SWR < 2, a measured port 1 impedance bandwidth of 30.6%, from 1.58 to 2.15 GHz, and a measured port 2 impedance bandwidth of 27.8%, from 1.58 to 2.09 GHz. The common impedance passband (SWR < 2) ranges from 1.58 to 2.09 GHz (27.8%). The measured results indicate that the use of the broadband balun in place of the narrowband balun do not significantly affect the impedance bandwidth of the dual polarized antenna, at either port.

Fig. 28 shows the measured input port isolation for the dual polarized quadruple L-probe square patch antenna utilizing either balun pair. The antenna with the broadband balun pair exhibits good measured input port isolation (S_{21} < -30 dB), from below 1 GHz to 2.8 GHz (> 95%). Within the bandwidth of interest (1.7 to 2.2 GHz), the input port isolation ranges from 33 to above 50 dB. It is observed that the use of the broadband balun pair, in place of the narrowband balun pair, provides the dual polarized antenna with consistently better input port isolation, across a very wide frequency range, from 1.0 GHz to beyond 3.0 GHz (> 100%).

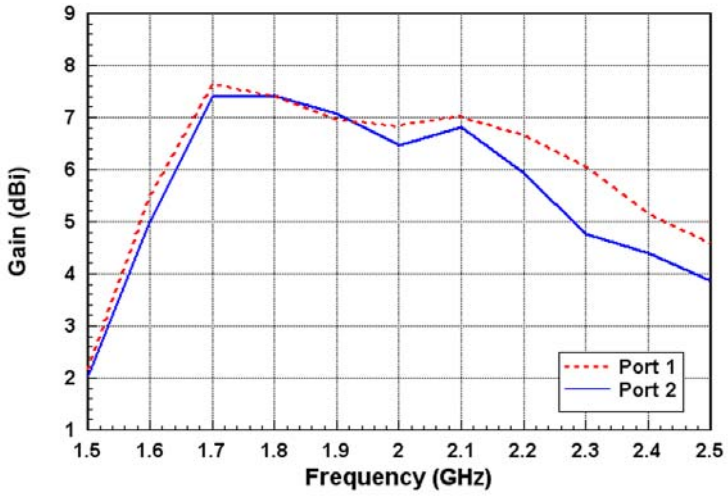

Fig. 29. Measured gain for the dual polarized quadruple L-probe square patch antenna utilizing the 180° broadband balun pair.

Fig. 29 shows the measured boresight gain for the dual-polarized quadruple L-probe square patch antenna utilizing the broadband balun pair. Within the bandwidth of interest (1.7 to 2.2 GHz), the measured boresight gain of the antenna with the broadband balun pair ranges from 6.6 to 7.6 dBi, for port 1, and from 6 to 7.4 dBi, for port 2. The measured gain profiles for both ports are similar.

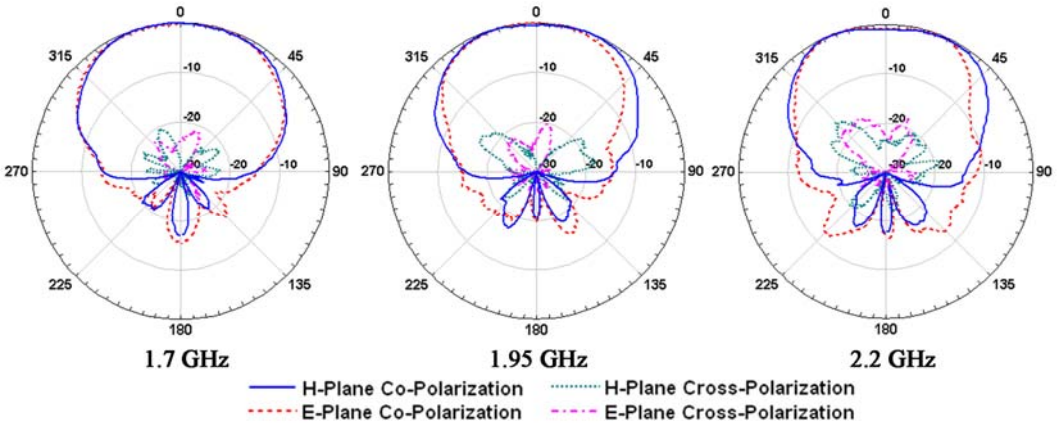

Fig. 30. Measured normalized radiation patterns (port 1) for the dual polarized quadruple L-probe square patch antenna utilizing the 180^{o} broadband balun pair.

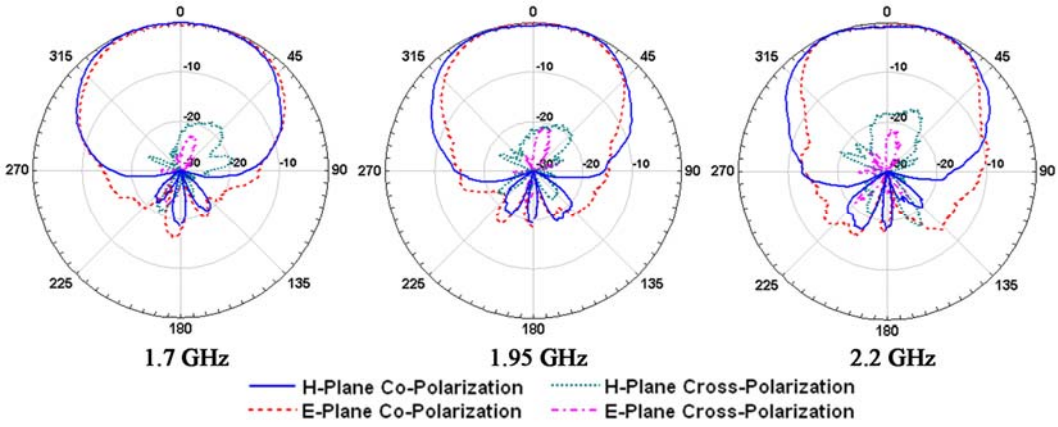

Fig. 31. Measured normalized radiation patterns (port 2) for the dual polarized quadruple L-probe square patch antenna utilizing the 180^{o} broadband balun pair.

Fig. 30 and 31 show the measured radiation patterns at port 1 and port 2, respectively, for the dual polarized quadruple L-probe square patch antenna utilizing the broadband balun pair, at the lower frequency edge (1.7 GHz), center

operating frequency (1.95 GHz), and upper frequency edge (2.2 GHz), of the bandwidth of interest. Across this passband, the antenna with the broadband balun pair exhibits at both ports symmetrical E- and H-plane co-polarization patterns and consistently low E- and H-plane cross-polarization levels (< -15 dB). It is evident that the use of the broadband balun pair provides wideband cross-polarization suppression, particularly needed in the H-plane. For both principle cuts, the front-to-back ratios are consistently better than 16 dB and the half-power beamwidths are consistently better than 60^{o} ($\pm 30^{o}$).

2.3.5 Discussions

In this section, the broadband design of a dual linearly polarized quadruple L-probe square patch antenna utilizing the proposed 180^{o} broadband balun pair has been presented. Each broadband balun provides good impedance matching, equal amplitude power splitting and consistent 180^{o} phase shifting, over a wide band (~45%). The use of the proposed broadband balun pair, in place of the conventional narrowband balun pair, has been shown to provide significantly improved input port isolation across the wide impedance bandwidth (~30%) intended for the quadruple L-probe antenna. The proposed dual polarized antenna delivers good impedance matching (SWR < 2), improved input port isolation (> 33 dB), high gain (> 6 dBi), symmetrical E- and H-plane co-polarization patterns, and consistently low E- and H-plane cross-polarizations levels (< -15 dB), across the bandwidth of interest from 1.7 to 2.2 GHz (~25%). The antenna in study lends itself to emerging broadband mobile base station applications demanding input port isolation in excess of 25 dB and broadband coverage encompassing three

bands, i.e. PCS1800 (1710-1880 MHz), GSM1900 (1850-1990 MHz) and UMTS2000 (1920-2170 MHz).

2.4 Concluding Remarks

The wideband impedance matching, balanced power splitting, and 180^{o} phasing afforded by the 180^{o} broadband balun leads to enhanced impedance bandwidth and the wideband suppression of cross-polarization due to multiple reflections and due to feed phase errors. Moreover, the balanced and symmetrical two or four point feeding structure, with the feed points supplied wideband equal amplitude anti-phase excitations, allows for enhanced impedance bandwidth and the wideband cancellation of the probe leakage radiation and probe coupling, which will in turn lead to the suppression of cross-polarization due to higher order modes and due to mutual coupling effects. The cross-polarization suppression shows up as improved polarization (maximum cross-polarization level) and pattern (minimum beamwidth) bandwidths. The cancellation of probe coupling also results in improved isolation bandwidth in the case of dual polarization.

For the broadband low cross-polarization patch antenna presented in Section 2.2, a full paper has been published in the Oct. 2007 issue of Radio Science [41]. For the broadband dual linearly polarized patch antenna presented in Section 2.3, an oral presentation was given in the Oct. 2006 IEEE International Conference on Communication Systems (ICCS2006) [42], held in Singapore, and a full paper has been published in the Jan. 2007 issue of IEEE Transactions on Antennas and Propagation [43].

CHAPTER 3

BROADBAND CIRCULARLY POLARIZED MICROSTRIP ANTENNAS

3.1 Research Direction

Circularly polarized microstrip antennas are widely employed in radar, navigation, satellite and mobile communication systems. Circular polarization, compared to linear polarization, allows for greater flexibility in orientation angle between transmitter and receiver, better mobility and weather penetration, and reduction in multipath reflections and other kinds of interference. Microstrip antennas are low profile and light weight, easy to fabricate, conformable to mounting structures, and compatible with integrated circuit technology. However, inherent limitations include the achievable impedance and axial-ratio bandwidths.

Circularly polarized waves are produced when two or more orthogonal linearly polarized modes, with equal amplitude and quadrature phasing, are independently excited to generate a rotating field. The sign of the relative phase determines the polarization sense (left- or right-hand). Circularly polarized patch antenna designs, differing primarily in how the linearly polarized modes are excited, can be broadly categorized into two main types: those using a single feed point, and those using two feed points in phase quadrature. For microstrip antennas of the single-fed type [44]-[48] circular polarization can be generated without the need of an external polarizer. The patch asymmetry excites the orthogonal mode. However, while the impedance bandwidth remains acceptable, the axial ratio degrades rapidly with

frequency off resonance. The allowable 3-dB axial ratio bandwidth is typically less than 10%. Notable exceptions involve the additional use of an L-shaped ground plane [47], or a parasitic patch element [48]. For microstrip antennas of the dual-fed type [49]-[55], circular polarization can be generated with the use of an external polarizer. Compared to the single-fed type, much wider impedance and axial-ratio bandwidths can be achieved since the amplitude and phase of the orthogonal linearly polarized field components can be controlled by a relatively broadband power divider circuit. Such designs are also more robust in terms of degradation due to manufacturing and material tolerances, but have the drawback of requiring a separate feed network, which adds complexity, takes up space and increases loss. Feed network configurations comprising Wilkinson power dividers [49]-[52], a log periodic balun [53], a two-stub 90^o hybrid coupler [54], and a three-stub 90^o hybrid coupler [55], have been explored. The two-stub 90^o hybrid coupler, in particular, has been the most commonly used external polarizer in circularly polarized patch antenna designs.

Circularly polarized dual and quadruple L-probe patch antennas utilizing two-stub 90^o hybrid couplers were shown in [56] to deliver wide impedance bandwidths (SWR < 2) of 42% and 45%, respectively, and wide 3-dB axial ratio bandwidths of 27.23% and 45%, respectively. The four-point balanced L-probe feeding structure in [56] presents one of the best combinations of impedance (45%) and axial-ratio (45%) bandwidths yet reported in open literature. The L-probe proximity feed approach allows for the use of a thick low permittivity antenna substrate that can help broaden the impedance bandwidth. Unfortunately, a lower patch Q encourages higher order modes generation that give rise to more cross-

polarized components and stronger mode coupling; hence diminishing the level of circular polarization purity that can be obtained. A symmetrical four point feeding structure allows for the cross-circularly polarized components to mutually cancel out as long as the four feed points are supplied equal amplitude power with relative excitation phases of 0^o, 90^o, 180^o and 270^o. This explains the lower axial ratio and wider axial ratio bandwidths afforded by the four point feeding structure over the two point feeding structure. However, the pair of conventional 90^o hybrid couplers used in [56] each have inherently narrow impedance matching (~30%), quadrature phase shifting (~32%), and equal power splitting (~14%) bandwidths; thereby constricting the achievable impedance and axial ratio bandwidths of the L-probe patch antenna. Recently developed in this laboratory, a circularly polarized quadruple L-probe patch antenna utilizing a 90^o broadband balun pair [57] was found to deliver a wide impedance bandwidth (SWR < 2) of 79.4% and 3- and 2- dB axial ratio bandwidths of 82% and 57%, respectively. This 90^o broadband balun (Type II) will be featured in the following chapter.

In this chapter, the broadband design of circularly polarized L-probe fed patch antennas is presented. The L-probe patch antenna allows for wider impedance bandwidth. However, to maintain good circular polarization purity, the high probe leakage radiation, due to the thick low permittivity antenna substrate, and strong probe coupling, due to the closely spaced multipoint probe feeds, have to be cancelled out across the wide allowable impedance passband. The use of a novel 90^o broadband balun (Type I) is proposed. The proposed 90^o broadband balun delivers good impedance matching, equal amplitude power splitting and consistent 90^o ($\pm 5^o$) phase shifting, across a wide band (~57.5%). In Section 3.2,

wideband circular polarization operation is demonstrated for a circularly polarized dual L-probe patch antenna utilizing the proposed 90° broadband balun (Type I). In Section 3.3, wideband circular polarization operation is demonstrated for a circularly polarized quadruple L-probe patch antenna utilizing a pair of the proposed 90° broadband baluns (Type I).

3.2 Broadband Circularly Polarized Dual L-Probe Patch Antenna with a 90° Broadband Balun (Type I)

3.2.1 Antenna Design and Geometry

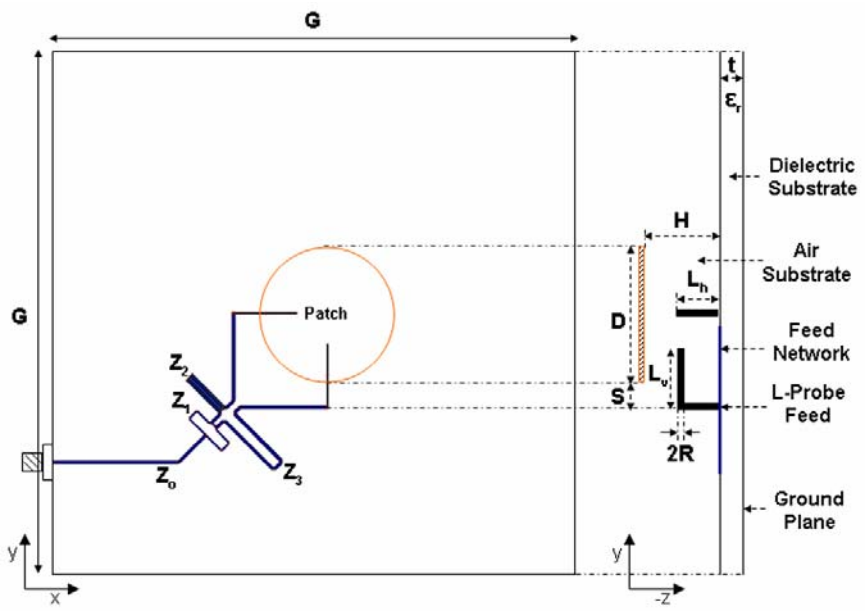

Fig. 32. Geometry of the circularly polarized dual L-probe circular patch antenna utilizing the 90° broadband balun (Type I).

The L-probe proximity feed technique extends the allowable impedance bandwidth of patch antennas. However, the use of a thick (~0.1λ_o) low permittivity (ε_r = 1) air substrate encourages the generation of higher order modes along with the wanted one. The unwanted modes cause the L-probe feed to emit leakage radiation that perturb the radiation pattern and, in the case of multiple L-

probe feeds, lead to probe coupling between the feeds. The inherent asymmetry in a two point feeding structure implies that the cross-circularly polarized components due to higher order modes do not cancel out, thereby diminishing the overall circularly polarization purity. The dual L-probe circular patch antenna, shown in Fig. 32, is designed for wideband circular polarization operation. The circular symmetry of the circular patch element gives no azimuthal variation and is well-suited for radiating circular polarized waves. The two L-probe feeds are orthogonally positioned and supplied equal amplitude power with relative excitation phases of 0^o and 90^o. The use of a 90^o broadband balun (Type I) with wideband impedance matching, equal power splitting and 90^o phase shifting capabilities is studied in order to properly control the amplitude and phase of the linearly polarized field components, so as to reduce the cross-polarization due to multiple reflections and feed phase errors; thus providing the patch antenna with wider impedance and axial ratio bandwidths.

3.2.2 Feed Network Configurations

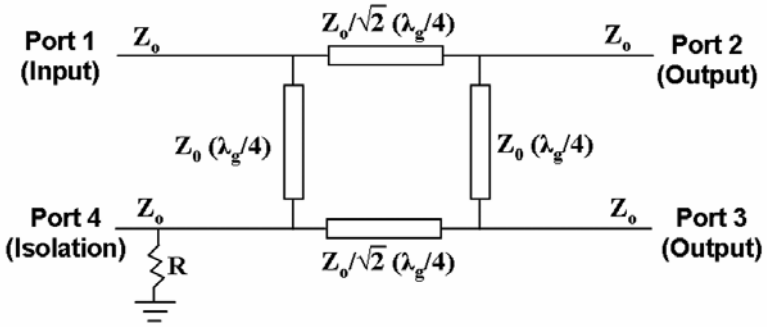

Fig. 33. Schematics of the conventional 90^o hybrid coupler.

The conventional 90^o hybrid coupler [58], shown in Fig. 33, is commonly used as an external polarizer for dual-fed type circularly polarized antennas. This symmetrical 3-dB directional coupler provides balanced power splitting and 90^o

phase shifting between its output ports. The two output ports are isolated when the power reflected from a mismatched antenna on these ports is transferred to an impedance-matched absorbing load at the isolation port. λ_g refers to the guide wavelength at a center operating frequency. The isolation port was terminated to a 50 Ω resistor. The characteristic impedances of the microstrip branches are given by $Z_o = 50\ \Omega$ and $Z_o / \sqrt{2} = 35.36\ \Omega$.

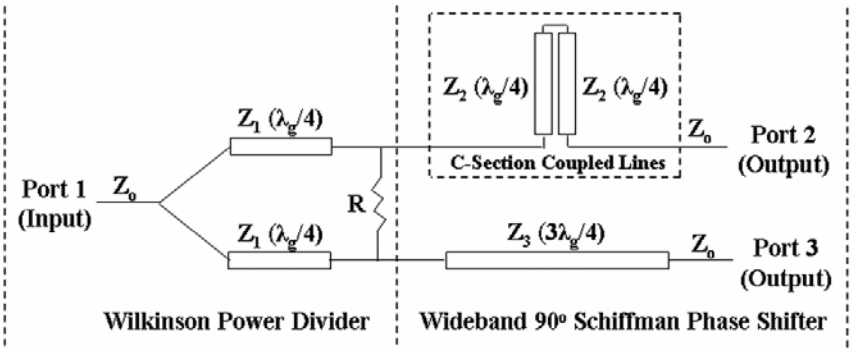

Fig. 34. Schematics of the proposed 90° broadband balun (Type I).

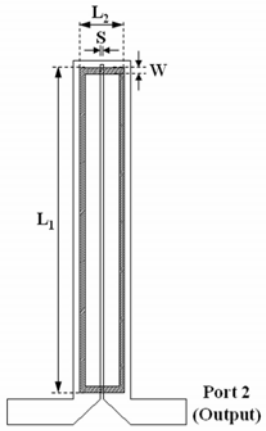

Fig. 35. Layout of the C-section coupled lines.

The proposed 90° broadband balun (Type I), shown in Fig. 34, delivers good impedance matching, balanced power splitting and regular 90° phase shifting, across a wide band. This broadband balun comprises of a 3-dB Wilkinson power divider [39], for wideband impedance matching and balanced power splitting, cascaded with a novel broadband 90° Schiffman phase shifter [58], for wideband

90^o phase shifting. λ_g refers to the guide wavelength at a center operating frequency. The characteristic impedances of the microstrip branches are given by $Z_o = 50\ \Omega$, $Z_1 = 70.71\ \Omega$, $Z_2 = 50\ \Omega$, and $Z_3 = 50\ \Omega$.

Fig. 35 shows the layout of the C-section coupled lines used in the 90^o broadband balun (Type I). The coupled lines are separated by a small distance of S = 0.3 mm. The gray-shaded rectangular slot, of dimensions $L_1 = 24.4$ mm, $L_2 = 4.0$ mm, and W = 0.5 mm, was cut out on the ground plane, beneath the C-section coupled lines, to allow for the odd-mode capacitance to decrease and the even-mode capacitance to decrease even faster. The 23.4 mm by 3.05 mm rectangle patch, encapsulated by the rectangular slot, functions as a capacitor which compensates the odd-mode capacitance. This patterned ground plane approach provides for wideband regular 90^o phase shifting with minimal insertion losses. The feed line layer and patterned ground plane layer are respectively printed on each side of a double-sided single-laminate PCB. No vias are required.

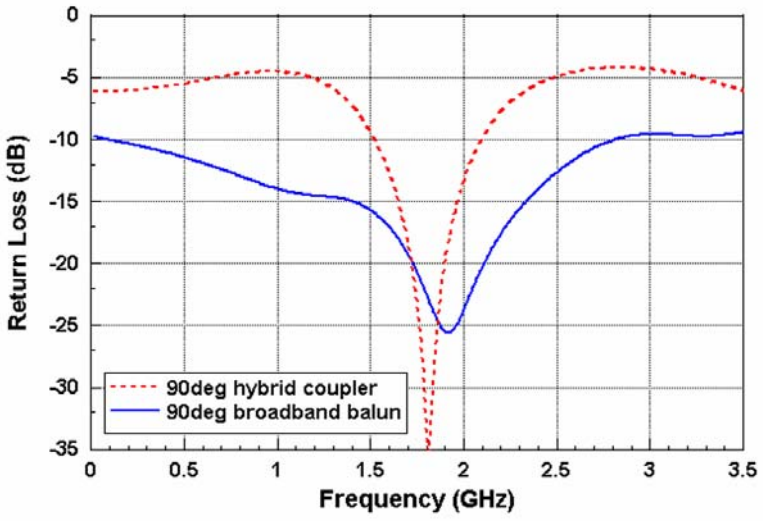

Fig. 36. Simulated input port return loss comparison between the 90^o hybrid coupler and 90^o broadband balun (Type I).

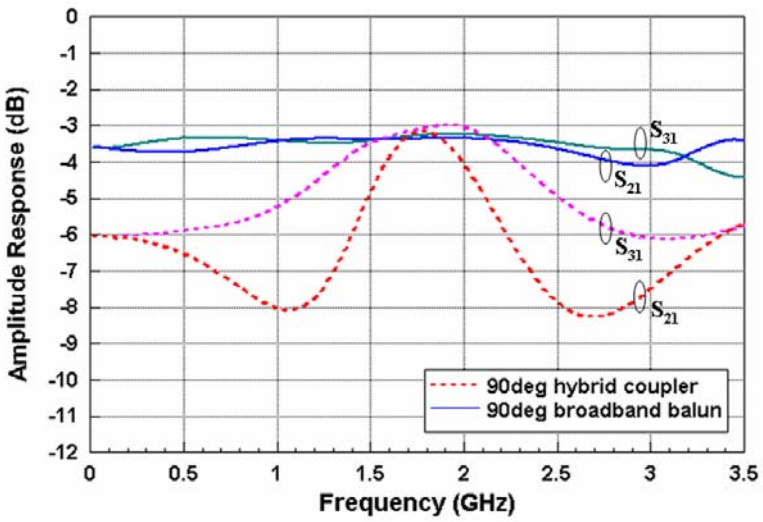

Fig. 37. Simulated output ports amplitude response comparison between the 90° hybrid coupler and 90° broadband balun (Type I).

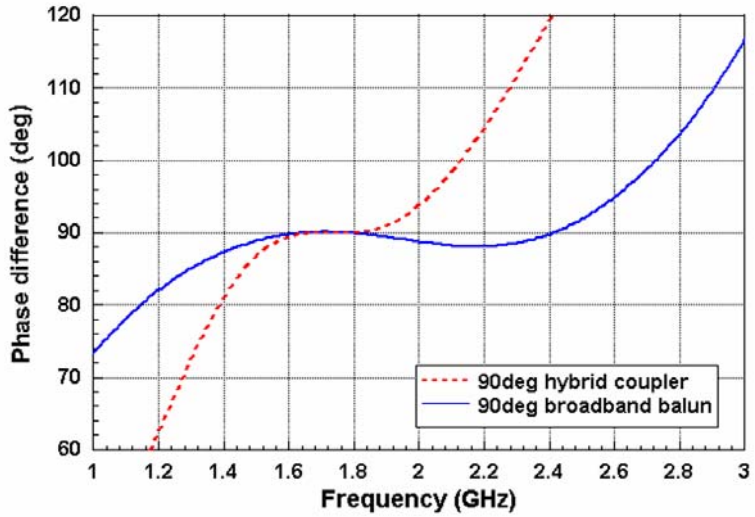

Fig. 38. Simulated output ports phase difference comparison between the 90° hybrid coupler and 90° broadband balun (Type I).

All simulations presented in this chapter were performed using IE3D. The feed networks were modeled on a Rogers RO4003 laminate of thickness t = 0.8 mm, dielectric constant ε_{r1} = 3.38, and an assumed loss tangent of tan δ = 0.0027. The feed line widths of the 50 and 70.71 Ω branches were 1.85 and 1.02 mm, respectively. For convenient analysis, the input and output ports of the feed networks were all set to 50 Ω.

Fig. 36 shows the simulated return loss comparison between the two feeders. The 90^o broadband balun (Type I) exhibits a wide impedance bandwidth (S_{11} < -10 dB) of 187.6%, from 0.09 to 2.81 GHz, while the 90^o hybrid coupler exhibits a much narrower impedance bandwidth (S_{11} < -10 dB) of 30.9%, from 1.53 to 2.09 GHz. Fig. 37 shows the simulated output ports amplitude response comparison between the two feeders. The 90^o broadband balun (Type I) exhibits balanced output ports power distribution (S_{21} = S_{31} = -3 dB (±0.5 dB)) over a wide band of 91.9%, from 0.87 to 2.35 GHz, while the 90^o hybrid coupler exhibits balanced output ports power distribution (S_{21} = S_{31} = -3 dB (±0.5 dB)) over a much narrower band of 14%, from 1.66 to 1.91 GHz. Fig. 38 shows the simulated output ports phase difference comparison between the two feeders. The 90^o broadband balun (Type I) exhibits consistent 90^o ($\pm5^o$) output ports phase difference over a considerably wide band of 66.7%, from 1.3 to 2.6 GHz, while the 90^o hybrid coupler exhibits consistent 90^o ($\pm5^o$) output ports phase difference over a much narrower band of 32%, from 1.47 to 2.03 GHz.

Combining the simulated results in Fig. 36 to 38, it is observed that the proposed 90^o broadband balun (Type I) delivered low input port return loss (S_{11} < -10 dB), balanced output ports power distribution (S_{21} = S_{31} = -3 dB (±0.5 dB)), and consistent 90^o ($\pm5^o$) output ports phase difference, over a significantly wide band of 57.5%, from 1.3 to 2.35 GHz; hence it is termed a “broadband” balun. The conventional 90^o hybrid coupler delivered low input port return loss (S11 < -10 dB), balanced output ports power distribution (S_{21} = S_{31} = -3 dB (±0.5 dB)), and consistent 90^o ($\pm5^o$) output ports phase difference over a much narrower band of

14%, from 1.66 to 1.91 GHz; inherently limited by its balanced output port power distribution bandwidth.

3.2.3 Fabrication and Experimental Setup

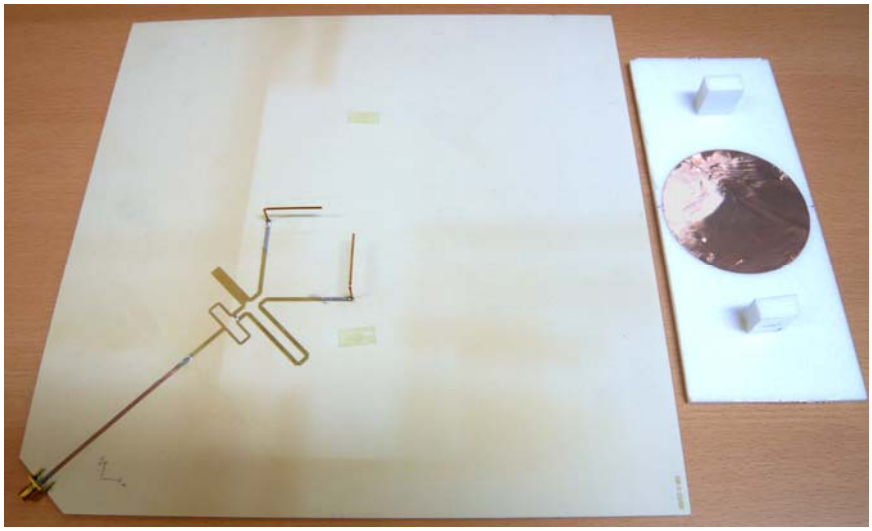

Fig. 39. Prototype of the circularly polarized dual L-probe circular patch antenna utilizing the 90^{o} narrowband balun (Type I).

Fig. 39 shows the prototype of the circularly polarized dual L-probe circular patch antenna utilizing the 90^{o} broadband balun (Type I). The antenna and feed network parameters were optimized for a wide impedance bandwidth. The circular copper patch, of diameter D = 76.5 mm, was positioned at an air substrate height of H = 20 mm above the feed substrate. The two L-probe feeds, each of diameter 2R = 1 mm, vertical length L_h = 11 mm, and horizontal length L_v = 35 mm, were orthogonally oriented and positioned a distance S = 8.5 mm away from the circumference of the patch, and soldered to the respective output ports of the feed network. The square ground plane is of length G = 300 mm. The impedance measurements were taken using the Agilent E8364B network analyzer, while the far-field radiation measurements were taken using the Hewlett Packard 8510C

vector network analyzer and the Orbit-MiDAS far-field measurement system in an anechoic chamber. With a reference linearly polarized standard horn antenna, the comparison method (gain-transfer method) was used to determine the measured gain and the polarization-pattern method was used to estimate the measured axial ratio [8], [60]. The standard horn antenna is commonly used as a reference antenna because it has a predictable gain and pure polarization. In the comparison method, the powers received with the AUT and with the reference horn antenna are compared by mounting each antenna, one at a time, at the exact same location. The power gain of the reference horn antenna is determined by some other means like the absolute method based on Friis transmission formula [60].

In the comparison method, the gain of the AUT (in dBi) is given by

$$G_{AUT} = \frac{P_{AUT}}{P_{ref}} G_{ref} \tag{1}$$

$$(G_{AUT})_{dBi} = (P_{AUT})_{dB} - (P_{ref})_{dB} + (G_{ref})_{dBi}$$

where

P_{AUT} = power received with the AUT

P_{ref} = power received with the reference antenna (standard horn)

G_{ref} = power gain of the reference antenna (standard horn)

The gain of a linearly polarized AUT (in dBi) is given by

$$(G_{AUT})_{dBi} = 10\log_{10}\sqrt{(P_{E_\theta})^2 + (P_{E_\phi})^2} - (P_{ref})_{dB} + (G_{ref})_{dBi} \tag{2}$$

where

P_{E_θ} = power received with the AUT at the E_θ polarization

P_{E_ϕ} = power received with the AUT at the E_ϕ polarization

The gain of a circularly polarized AUT (in dBic) is given by

$$(G_{AUT})_{dBic} = 10\log_{10}[G_H + G_V] \quad (3)$$

where

G_H = partial power gain of the AUT at the horizontal polarization

G_V = partial power gain of the AUT at the vertical polarization

The total power of the wave radiated by an antenna can be separated into two orthogonal linearly polarized components. Hence, the gain of the circularly polarized AUT was determined by measuring the partial gains for two orthogonal linear polarizations. The linearly polarized reference horn antenna was rotated 90^o to achieve the two orthogonal linear polarizations. The powers received with the AUT at the horizontal and vertical polarizations were measured. The partial gains for the two orthorgonal polarization, G_H and G_V, were computed using Eqn (1). The gain of the circularly polarized AUT was then determined using Eqn (3).

In the polarization-pattern method, the angle of polarization of the linearly polarized reference horn (source) antenna is rotated to produce a polarization pattern that showcase the measured field amplitude versus the tilt angle of the source antenna in polar form. The axial ratio can be determined by taking the ratio between the major and minor axes of the polarization ellipse. Tapping on the gain-transfer measured data, only the powers received with the AUT at the horizontal and vertical polarizations of the reference horn antenna were considered. The axial ratio can be estimated by taking the ratio between the horizontal and vertical axes of the polarization ellipse. This approach is reasonably accurate for small tilt angles. A more precise method is described in Section 4.2.3.

3.2.4 Impedance and Radiation Performances

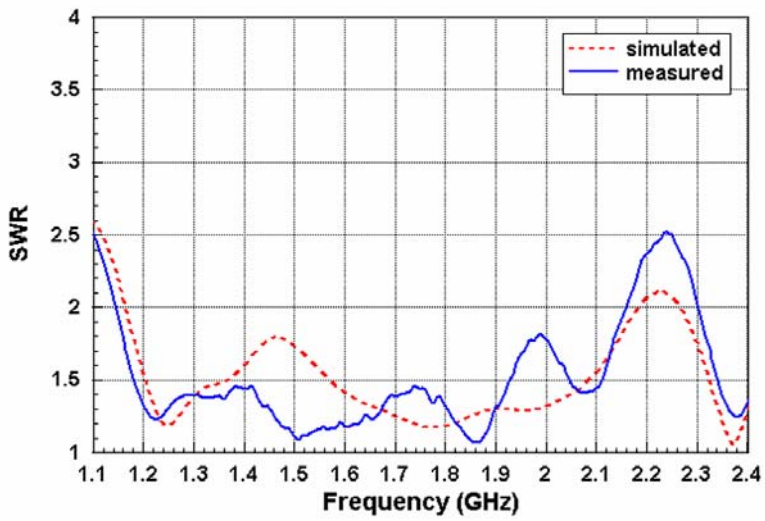

Fig. 40. Simulated and measured SWR for the circularly polarized dual L-probe circular patch antenna utilizing the 90° broadband balun (Type I).

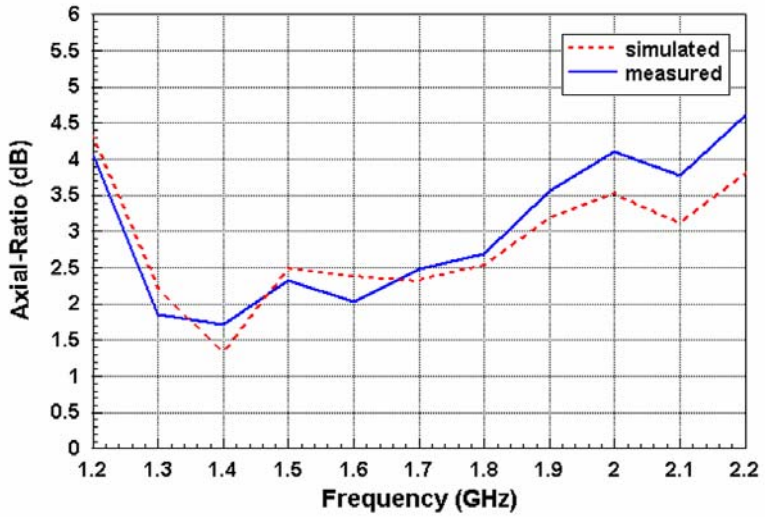

Fig. 41. Simulated and measured axial ratio for the circularly polarized dual L-probe circular patch antenna utilizing the 90° broadband balun (Type I).

Fig. 40 shows the simulated and measured SWR for circularly polarized dual L-probe circular patch antenna utilizing the 90° broadband balun (Type I). The dual L-probe antenna exhibits considerably wide simulated and measured impedance bandwidths (SWR < 2) of 61.5%, from 1.16 to 2.19 GHz, and 61%, from 1.15 to

2.16 GHz, respectively. This is wider than the 42% impedance bandwidth (SWR < 2) attained for the dual L-probe antenna utilizing the 90° hybrid coupler [56].

Fig. 41 shows the simulated and measured axial ratio for the circularly polarized dual L-probe circular patch antenna utilizing the 90° broadband balun (Type I). The dual L-probe antenna exhibits rather wide simulated and measured 3-dB axial-ratio bandwidths of 39%, from 1.26 to 1.87 GHz, and 37.7%, from 1.25 to 1.83 GHz, respectively. This is wider than the 27.23% 3-dB axial ratio bandwidth attained for the dual L-probe antenna utilizing the 90° hybrid coupler [56].

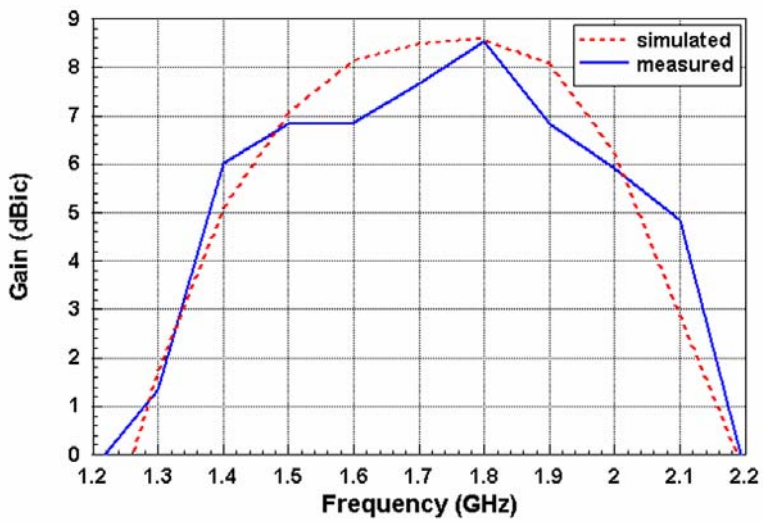

Fig. 42. Simulated and measured gain for the circularly polarized dual L-probe circular patch antenna utilizing the 90° broadband balun (Type I).

Fig. 42 shows the simulated and measured boresight gain for the circularly polarized dual L-probe circular patch antenna utilizing the 90° broadband balun (Type I). The dual L-probe antenna exhibits a simulated 3-dB gain bandwidth (gain > 5.6 dBic) of 34.2%, from 1.43 to 2.02 GHz, with its highest gain of 8.6 dBic at 1.8 GHz, and a measured 3-dB gain bandwidth (gain > 5.53 dBic) of 38.6%, from 1.38 to 2.04 GHz, with its highest gain of 8.53 dBic at 1.8 GHz. The

measured gain is better than 4 dBic across a 43.68% bandwidth, from 1.36 to 2.12 GHz. Combining the measured results in Fig. 40 to 42, the antenna exhibits, in terms of SWR < 2, axial ratio < 3 dB, and gain > 4 dBic, a measured CP bandwidth of 29.47%, from 1.36 to 1.83 GHz. The designated bandwidth of interest will be from 1.3 to 1.8 GHz (32.26%). It is observed that the measured results agree reasonably well with the simulated results.

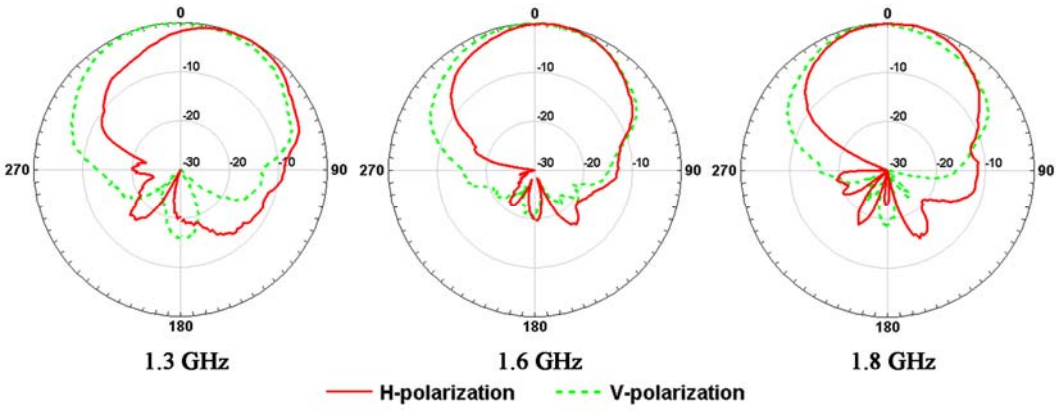

Fig. 43. Measured normalized x-z plane ($\phi = 0^{o}$) radiation patterns for the circularly polarized dual L-probe circular patch antenna utilizing the 90^{o} broadband balun (Type I).

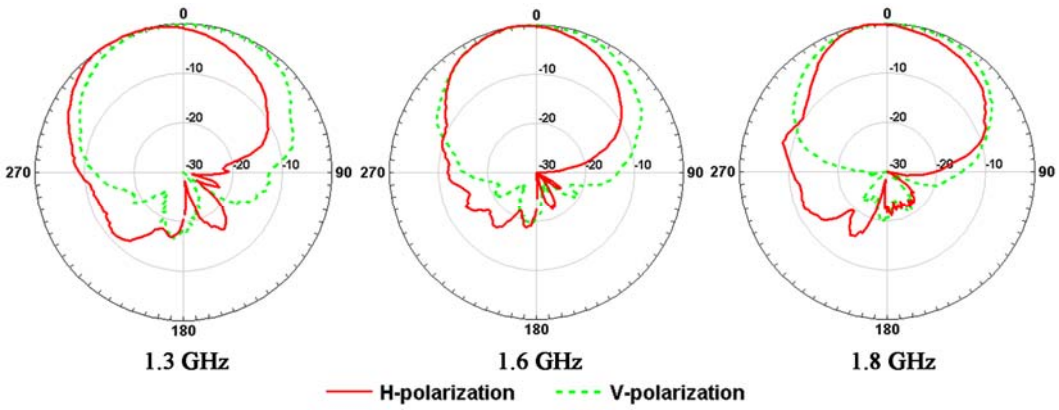

Fig. 44. Measured normalized y-z plane ($\phi = 90^{o}$) radiation patterns for the circularly polarized dual L-probe circular patch antenna utilizing the 90^{o} broadband balun (Type I).

Fig. 43 and 44 show the measured normalized radiation patterns for the circularly polarized dual L-probe circular patch antenna utilizing the 90^o broadband balun (Type I) at the lower frequency edge (1.3 GHz), center frequency (1.6 GHz), and upper frequency edge (1.8 GHz), of the bandwidth of interest, on the x-z ($\phi = 0^o$) and y-z ($\phi = 90^o$) planes, respectively. The measured axial ratio was estimated by taking the ratio between the measured field amplitudes of the H- and V-polarizations. The good agreement between the simulated and measured results for the boresight axial validates the reliability of this approximation. Across this passband, it is observed that on both principle planes, the antenna exhibits generally low axial-ratio at observation angles around its boresight ($\theta = 0^o$). The slight asymmetry observed in the H- and V-polarization patterns can be attributed to the asymmetrical feed orientation of the dual L-probe antenna structure.

3.2.5 Discussions

In this section, the broadband design of a circularly polarized dual L-probe circular patch antenna utilizing the proposed 90^o broadband balun (Type I) has been presented. The broadband balun provides good impedance matching, equal amplitude power splitting and consistent 90^o phase shifting, over a wide band (~57.5%). The use of the proposed broadband balun, in place of the conventional 90^o hybrid coupler, has been shown to provide enhanced impedance and axial ratio bandwidths. The proposed circularly polarized dual L-probe antenna delivers wide measured impedance (SWR < 2), axial ratio (AR < 3 dB), and gain (gain > 4 dBic) bandwidths of 61% (1.15 to 2.16 GHz), 37.7% (1.25 to 1.83 GHz), and 43.68% (1.36 to 2.12 GHz), respectively, for a measured CP operating bandwidth of 29.47%, from 1.36 to 1.83 GHz.

3.3 Broadband Circularly Polarized Quadruple L-Probe Patch Antenna with 90° Broadband Baluns (Type I)

3.3.1 Antenna Design and Geometry

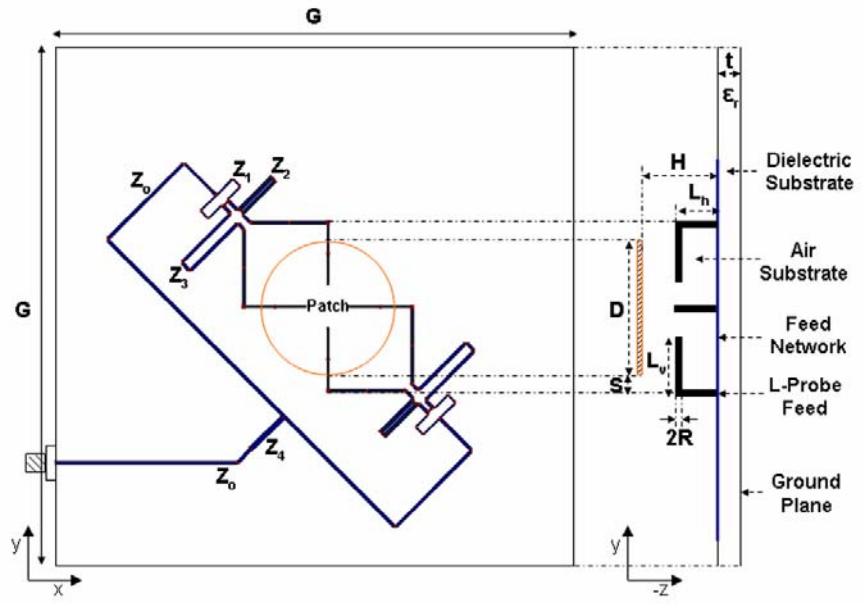

Fig. 45. Geometry of the circularly polarized quadruple L-probe circular patch antenna utilizing the 90° broadband balun (Type I) pair.

The quadruple L-probe circular patch antenna, shown in Fig. 45, is designed for wideband circular polarization operation centered at 1.8 GHz. The four L-probe feeds are orthogonally positioned and supplied equal amplitude power with relative excitation phases of 0°, 90°, 180°, and 270°. This antenna arrangement can be thought of as four sequentially rotated linearly polarized elements collocated in a single patch element. The inherent symmetry in the four point feeding structure allows for the co-polarization in both principle planes to add up, and the cross-circularly polarized components due to higher order modes generation to mutually cancel out. The use of a feed network with wideband impedance matching, equal power splitting and proper phase shifting is required in order to properly control

the amplitude and phase of the linearly polarized field components so as to also reduce the cross-polarization due to multiple reflections and feed phase errors; thus providing the patch antenna with wide impedance and axial ratio bandwidths.

3.3.2 Feed Network Configuration

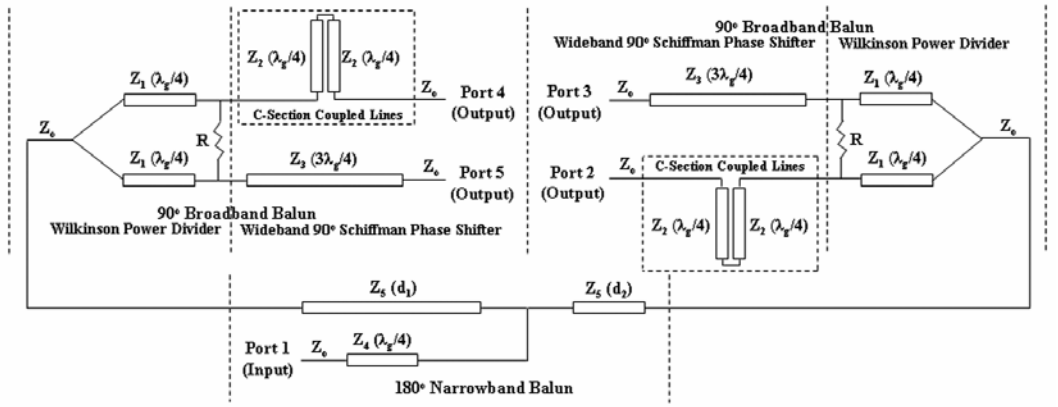

Fig. 46. Schematics of the proposed 90° broadband balun (Type I) pair.

The proposed 90° broadband balun (Type I) pair, shown in Fig. 46, delivers good impedance matching, equal amplitude power splitting and relative excitation phasing of 0°, 90°, 180°, and 270°, over a wide band. The feed network comprises a conventional 180° narrowband balun (Fig. 3) cascaded to a pair of the proposed 90° broadband baluns (Type I) (Fig. 34). To provide the required 180° phase shift between the two 90° broadband baluns (Type I), the lengths of the microstrip branches, d_1 and d_2, must be such that $d_1 - d_2 = \lambda_g / 2$, where λ_g refers to the guide wavelength at a center operating frequency of 1.8 GHz. The characteristic impedances of the microstrip branches are given by $Z_o = 50\ \Omega$, $Z_1 = 70.71\ \Omega$, $Z_2 = 50\ \Omega$, and $Z_3 = 50\ \Omega$, $Z_4 = 35.36\ \Omega$, and $Z_5 = 50\ \Omega$. The use of the 180° broadband balun (Fig. 4) in place of the 180° narrowband balun (Fig. 3) can help maintain the relative excitation phasing of 0°, 90°, 180°, and 270°, over a comparatively wider band. However, simulation shows that this results in worsened impedance

bandwidth, while providing only similar axial ratio and gain bandwidths for the quadruple L-probe antenna in study. This may be attributed to the increased multiple reflections inherent in the more complicated feed network configuration.

3.3.3 Fabrication and Experimental Setup

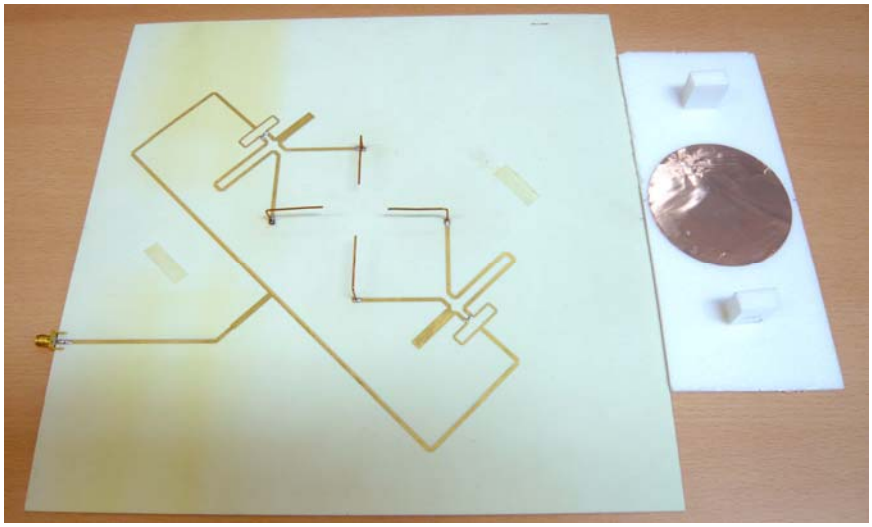

Fig. 47. Prototype of the circularly polarized quadruple L-probe circular patch antenna utilizing the 90^{o} narrowband balun (Type I) pair.

Fig. 47 shows the prototype of the circularly polarized quadruple L-probe circular patch antenna utilizing the 90^{o} broadband balun (Type I) pair. The circular copper patch, of diameter D = 76.5 mm (0.459 λ_o), was positioned at an air substrate height of H = 20 mm (0.12 λ_o) above the feed substrate. The four L-probe feeds, each of diameter 2R = 1 mm, vertical length L_h = 11 mm (0.066 λ_o), and horizontal length L_v = 35 mm (0.21 λ_o), were orthogonally oriented and positioned a distance S = 8.5 mm away from the circumference of the patch, and soldered to the respective output ports of the feed network. The square ground plane is of length G = 300 mm (1.8 λ_o). For comparison, the same antenna and feed network parameters were used for the dual L-probe antenna presented in Section 3.2. The antenna and feed network parameters have actually been optimized for the

quadruple L-probe antenna for a wide impedance bandwidth centering 1.8 GHz. This accounts for the different operating frequency range (downwards shift), observed in Fig. 40 to 42, for the dual L-probe antenna utilizing a single 90^{o} broadband balun (Type I). The impedance measurements were taken using the Agilent E8364B network analyzer, while the far-field radiation measurements were taken using the Hewlett Packard 8510C vector network analyzer and the Orbit-MiDAS far-field measurement system in an anechoic chamber. With a reference linearly polarized standard horn antenna, the comparison method (gain-transfer method) was used to determine the measured gain and the polarization-pattern method was used to estimate the measured axial ratio (See Section 3.2.3).

3.3.4 Impedance and Radiation Performances

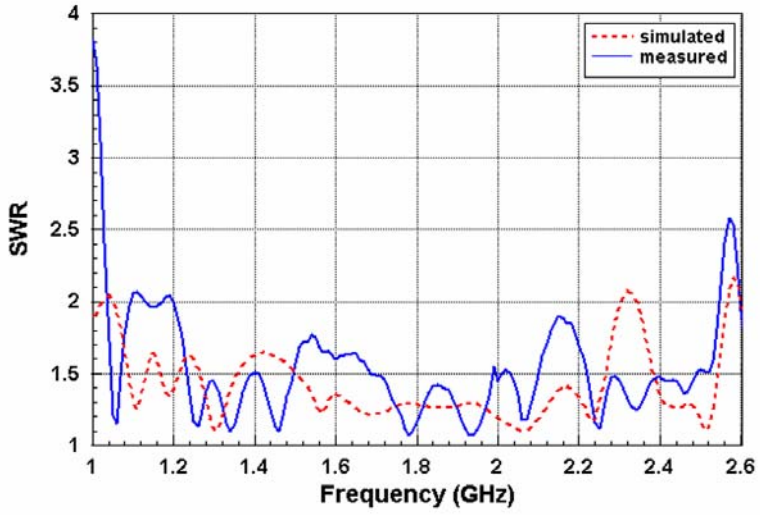

Fig. 48. Simulated and measured SWR for the circularly polarized quadruple L-probe circular patch antenna utilizing the 90^{o} broadband balun (Type I) pair.

Fig. 48 shows the simulated and measured SWR for the circularly polarized quadruple L-probe circular patch antenna utilizing the 90^{o} broadband balun (Type I) pair. The quadruple L-probe antenna exhibits considerably wide simulated and

measured impedance bandwidths (SWR < 2) of 73.8%, from 1.06 to 2.3 GHz and 71.7%, from 1.2 to 2.54 GHz, respectively. This is much wider than the 45% impedance bandwidth attained for the quadruple L-probe antenna utilizing the 90° hybrid coupler pair [56], and comparable to the 79.4% impedance bandwidth attained for the quadruple L-probe antenna utilizing the 90° broadband balun pair (Type II) [57]. The dual L-probe antenna utilizing the 90° broadband balun (Type I), presented in Section 3.2, exhibits a relatively narrower measured impedance bandwidth (SWR < 2) of 61%, from 1.15 to 2.16 GHz.

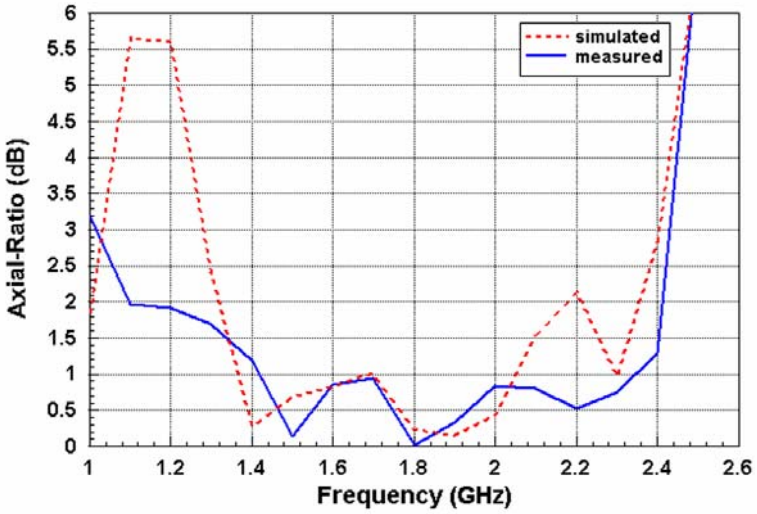

Fig. 49. Simulated and measured axial ratio for the circularly polarized quadruple L-probe circular patch antenna utilizing the 90° broadband balun (Type I) pair.

Fig. 49 shows the simulated and measured axial ratio for the circularly polarized quadruple L-probe circular patch antenna utilizing the 90° broadband balun (Type I) pair. The quadruple L-probe antenna exhibits wide simulated 3-dB and 2-dB axial-ratio bandwidths of 62%, from 1.27 to 2.41 GHz, and 48.8%, from 1.33 to 2.18 GHz, respectively. The measured 3-dB and 2-dB axial ratio bandwidths are 81.6%, from 1.03 to 2.45 GHz, and 77.7%, from 1.07 to 2.43 GHz, respectively. The measured 81.6% 3-dB axial ratio bandwidth is much wider than the 45% 3-

dB axial ratio bandwidth attained for the quadruple L-probe antenna utilizing a 90° hybrid coupler pair [56]. The measured 77.7% 2-dB axial-ratio bandwidth is much wider than the 57% 2-dB axial ratio bandwidth attained for the quadruple L-probe antenna utilizing the 90° broadband balun pair (Type II) [57]. But they have similar 3-dB axial ratio bandwidths of ~81%. The dual L-probe antenna utilizing the 90° broadband balun (Type I), presented in Section 3.2, exhibits a much narrower measured 3-dB axial ratio bandwidth of 37.7%, from 1.25 to 1.83 GHz.

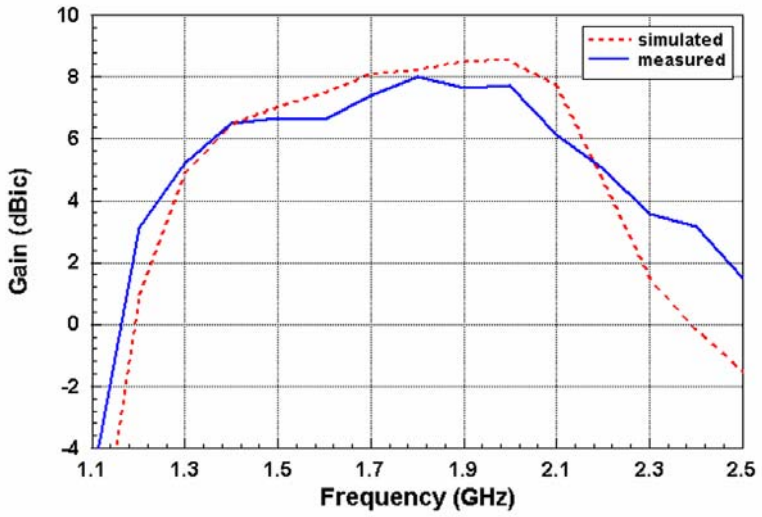

Fig. 50. Simulated and measured gain for the circularly polarized quadruple L-probe circular patch antenna utilizing the 90° broadband balun (Type I) pair.

Fig. 50 shows the simulated and measured boresight gain of the circularly polarized quadruple L-probe antenna utilizing the 90° broadband balun (Type I) pair. The quadruple L-probe antenna exhibits a simulated 3-dB gain bandwidth (gain > 5.6 dBic) of 46.9%, from 1.34 to 2.16 GHz, with its highest gain of 8.6 dBic at 2 GHz, and a measured 3-dB gain bandwidth (gain > 5.1 dBic) of 52.2%, from 1.29 to 2.2 GHz, with its highest gain of 8.1 dBic at 1.8 GHz. The measured gain is better than 4 dBic across a 59.1% bandwidth, from 1.24 to 2.28 GHz. The dual L-probe antenna utilizing the 90° broadband balun (Type I), presented in

Section 3.2, exhibits a relatively narrower measured gain bandwidth (gain > 4 dBic) of 43.68%, from 1.36 to 2.12 GHz. Combining the measured results in Fig. 48 to 50, the antenna exhibits, in terms of SWR < 2, axial ratio < 2 dB, and gain > 4 dBic, a measured CP bandwidth of 59.1%, from 1.24 to 2.28 GHz. The designated bandwidth of interest will be from 1.2 to 2.2 GHz (58.82%). It is observed that the measured results agree rather well with the simulated results.

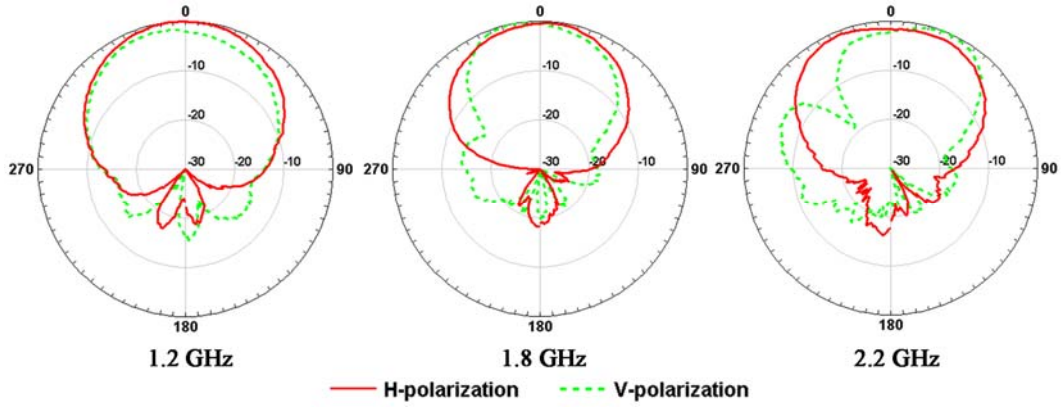

Fig. 51. Measured normalized x-z plane ($\phi = 0^{o}$) radiation patterns for the circularly polarized quadruple L-probe circular patch antenna utilizing the 90^{o} broadband balun (Type I) pair.

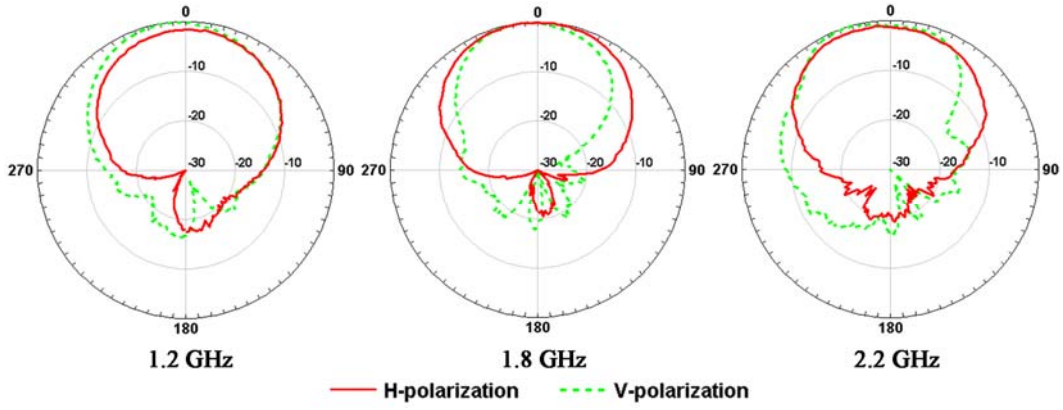

Fig. 52. Measured normalized y-z plane ($\phi = 90^{o}$) radiation patterns for the circularly polarized quadruple L-probe circular patch antenna utilizing the 90^{o} broadband balun (Type I) pair.

Fig. 51 and 52 show the measured normalized radiation patterns for the circularly polarized quadruple L-probe circular patch antenna utilizing the 90^o broadband balun (Type I) pair at the lower frequency edge (1.2 GHz), center frequency (1.8 GHz), and upper frequency edge (2.2 GHz), of the bandwidth of interest, on the x-z ($\phi = 0^o$) and y-z ($\phi = 90^o$) planes, respectively. The measured axial ratio was estimated by taking the ratio between the measured field amplitudes of the H- and V-polarizations. Across this passband, it is observed that on both principle planes, the antenna exhibits generally low angular axial-ratio around its boresight ($\theta = 0^o$) and rather symmetrical H- and V-polarization patterns.

3.3.5 Discussions

In this section, the broadband design of a circularly polarized quadruple L-probe circular patch antenna utilizing the proposed 90^o broadband balun (Type I) pair has been presented. The broadband balun provides good impedance matching, equal amplitude power splitting and consistent 90^o phase shifting, over a wide band (~57.5%). The use of the proposed broadband balun pair, in place of the conventional 90^o hybrid coupler pair, has been shown to provide enhanced impedance and axial ratio bandwidths. The symmetrical four point feeding structure, compared to the two point feeding structure, has also been proven to provide improved impedance, axial ratio and gain bandwidths. The proposed circularly polarized quadruple L-probe antenna delivers wide measured impedance (SWR < 2), axial ratio (AR < 2 dB), and gain (gain > 4 dBic) bandwidths of 71.7% (1.2 to 2.54 GHz), 77.7% (1.07 to 2.43 GHz), and 59.1% (1.24 to 2.28 GHz), respectively, for a measured CP operating bandwidth of 59.1%, from 1.24 to 2.28 GHz. The antenna in study presents a single patch

element solution for multi-frequency, multi-modes wireless communication systems requiring broadband circular polarized coverage encompassing four bands, i.e. GPS1575 (1559-1610 MHz), PCS1800 (1710-1880 MHz), GSM1900 (1850-1990 MHz), and UMTS2000 (1920-2170 MHz).

3.4 Concluding Remarks

The wideband impedance matching, balanced power splitting, and 90^o phase shifting afforded by the 90^o broadband balun (Type I) leads to enhanced impedance bandwidth and the wideband suppression of cross-polarization due to multiple reflections and due to feed phase errors. This cross-polarization suppression shows up in the form of an improved axial ratio bandwidth. Moreover, the balanced and symmetrical four point sequential feed structure, with each feed point supplied wideband equal amplitude power and appropriate phasing, allows for further enhanced impedance bandwidth and the cancellation of the probe leakage radiation and probe coupling, which will in turn lead to suppression of cross-polarization due to higher order modes and due to mutual coupling effects. This cross-polarization suppression shows up in the form of a further improved axial ratio bandwidth.

For the broadband circularly polarized patch antennas presented in Section 3.2 and 3.3, an oral presentation was given in the Dec. 2006 Asia Pacific Microwave Conference (APMC2006) [61], held in Yokohama, Japan, and a full paper has been published in the Feb. 2008 issue of IEEE Transactions on Antennas and Propagation [62].

CHAPTER 4

BROADBAND CIRCULARLY POLARIZED MICROSTRIP ANTENNAS AND ARRAYS

4.1 Research Direction

Circularly polarized microstrip antenna arrays are in great demand for various applications in mobile communications, global positioning systems, and satellite broadcasting. Sequential rotation in circularly polarized microstrip antennas and arrays coupled with an appropriate offset of the feeding phase leads to significant improvements to both the bandwidth and polarization purity. Each element (linearly or circularly polarized) in the subarray is physically rotated with respect to a neighboring element and the phase change generated by the rotation of the given element is offset by an appropriate phase change in the excitation, which is usually created by a line length change in the corporate feed.

The technique of sequential rotation [63], [64], enables errors in the radiated polarization of each element to be cancelled by the adjacent element. The cross-circularly polarized components of the elliptically polarized elements are rejected, as the feeding phase changes are correct for the desired sense of polarization only. This leads to lower axial ratio across a wider bandwidth than that of the individual element. Similarly, reflections from the mismatched elements off resonance add destructively at the corporate feed input terminal. This leads to lower input VSWR across a wider bandwidth than of the individual element. The use of sequentially rotated linearly polarized elements [65], [66], is possible but gives rise to large

diagonal plane grating lobes that severely degrades the gain [66]. To generate circular polarization over the maximum bandwidth, circularly polarized elements with wideband low axial ratio, fed by an isolating power splitter are desired [67]. Analysis of various configurations [68], [69] indicate that the domineering factor determining the performance of most sequentially rotated patch arrays is multiple reflections between the patches and the non-isolating power splitters. For a sequentially rotated 2x2 elements patch array configuration, the cross-polarization improvement factor due to feed phase deviation, multiple reflections, and higher order modes, were all found to be good [69]. The sequential array confers enhanced impedance and axial ratio bandwidths, but the gain bandwidth is still similar to that of a conventional array using the same number of elements [69].

In this chapter, the broadband design of circularly polarized patch antennas and arrays using sequential rotation is presented. The L-probe patch antenna allows for wide impedance bandwidth, and the two-point feed configuration fed by a 90^{o} broadband balun (Type I) has been shown in the previous chapter to deliver improved impedance and axial ratio bandwidths. To achieve even wider impedance and axial ratio bandwidths, each broadband circularly polarized dual L-probe antenna element is sequentially rotated to form a 2x2 patch array configuration, for wideband small impedance mismatch and low axial ratio at each individual element, and fed by a broadband balanced phase shifting feed network, for wideband minimal phase errors. The capacitive-feed technique [70], [71] is also explored as an alternative method for exciting the patch element in bid to extend the axial ratio and gain bandwidths afforded by the asymmetrical dual L-probe feeding structure. The use of a novel 90^{o} broadband balun (Type II) [57]

is proposed. The proposed 90° broadband balun delivers good impedance matching, equal amplitude power splitting and consistent 90° (±5°) phase shifting, across a wide band (~72.5%). In Section 4.2, wideband circular polarization operation is demonstrated for a circularly polarized dual L-probe patch antenna utilizing the proposed 90° broadband balun (Type II). In Section 4.3, wideband circular polarization operation is demonstrated for a circularly polarized dual capacitive-feed L-probe patch antenna utilizing the proposed 90° broadband balun (Type II). In Section 4.4, wideband circular polarization operation is demonstrated for a circularly polarized dual L-probe 2x2 patch array utilizing six of the proposed 90° broadband baluns (Type II).

4.2 Broadband Circularly Polarized Dual L-Probe Patch Antenna with a 90° Broadband Balun (Type II)

4.2.1 Antenna Design and Geometry

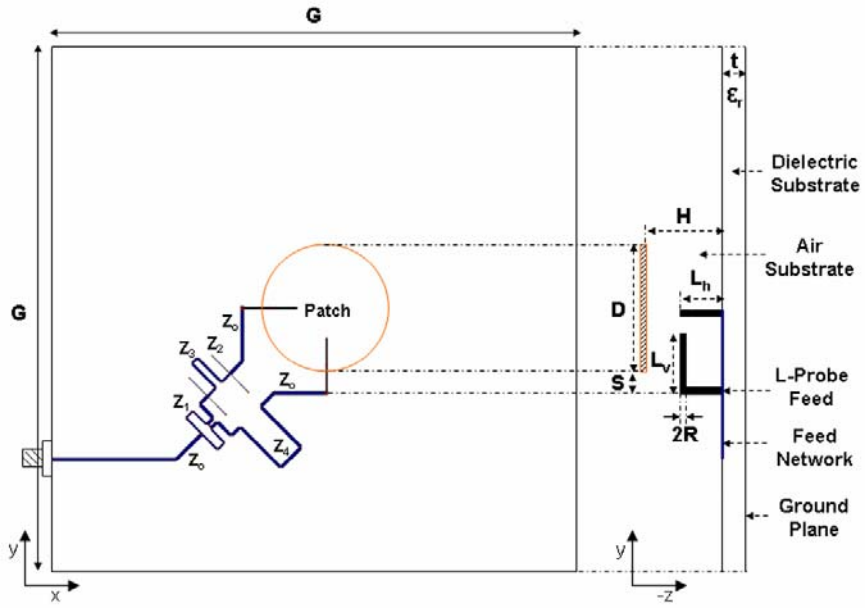

Fig. 53. Geometry of the circularly polarized dual L-probe circular patch antenna utilizing the 90° broadband balun (Type II).

For a single patch element, sequential rotation can be applied to multiple feed points each supplied with equal amplitude power and an appropriate phase offset. The efficacy of the sequential feeding technique in enhancing the axial ratio of the circularly polarized single patch element depends on the number of feed points, and the angular position and phase shift of each feed point. Similar relationships have been shown to hold for patch arrays, whereby sequential rotation is applied to multiple patch elements instead of multiple feed points. The sequential rotation of two and four L-probe feeds for a single circular patch element have been presented in Section 3.2 and 3.3, respectively. Analysis of various sequential feed arrangements for a single circular patch element [68] indicate that the asymmetrical two point feeding structure suffer from mutual coupling effects between the probe feeds, serious axial ratio perturbation due to multiple reflections and higher order modes, and moderate axial ratio perturbation due to feed phase errors. The axial ratio perturbation due to multiple reflections and feed phase errors may be combated with the use of a broadband isolating power divider capable of consistent 90^{o} phase shifting, as demonstrated in Section 3.2. However, the mutual coupling effects and axial ratio perturbation due to higher order modes are better suppressed in a symmetrical four point feeding structure that allows for probe leakage radiation to cancel, leading to reduced probe coupling, and allows for the cross-circularly polarized components to cancel, leading to reduced axial ratio and radiation pattern perturbation. This accounts for the significantly improved impedance and axial ratio bandwidths seen in Section 3.3. The dual L-probe circular patch antenna, shown in Fig. 53, is designed for wideband circular polarization operation. The circular symmetry of the circular patch element gives no azimuthal variation and is well-suited for radiating circular polarized waves.

The two L-probe feeds are orthogonally positioned and supplied equal amplitude power with relative excitation phases of 0^o and 90^o. The use of a 90^o broadband balun (Type II) with wideband impedance matching, equal power splitting and 90^o phase shifting capabilities is studied in order to properly control the amplitude and phase of the linearly polarized field components, so as to reduce the cross-polarization due to multiple reflections and feed phase errors; thus providing the patch antenna with wider impedance and axial ratio bandwidths. This two point feeding structure will be used as one of four wideband circularly polarized elements in the 2x2 sequential-rotated dual L-probe circular patch array presented in Section 4.4. The idea is to design for very wide impedance and axial ratio bandwidths for each circularly polarized elements, so that the sequential array can achieve the widest possible impedance and axial ratio bandwidths. The four point feeding structure was not used, despite its superior circular polarization properties, because the more complicated feeder will prove too complex when cascaded in an array configuration, leading to significant insertion loss that translates to lower radiation efficiency and hence higher gain loss.

4.2.2 Feed Network Configurations

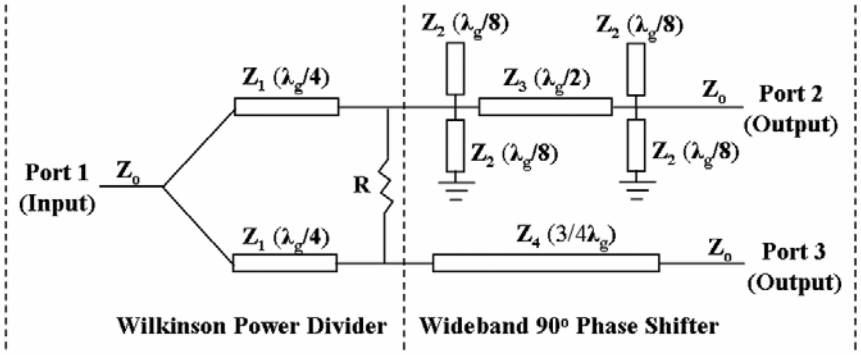

Fig. 54. Schematics of the proposed 90^o broadband balun (Type II).

The proposed 90° broadband balun (Type II), shown in Fig. 54, delivers good impedance matching, balanced power splitting and regular 90° phase shifting, across a wide band. This broadband balun comprises of a 3-dB Wilkinson power divider [39], for wideband impedance matching and balanced power splitting, cascaded with a broadband 180° phase shifter [40], for wideband 90° phase shifting. λ_g refers to the guide wavelength at a center operating frequency. The characteristic impedances of the microstrip branches are given by Z_o = 50 Ω, Z_1 = 70.71 Ω, Z_2 = 125.5 Ω, Z_3 = 62 Ω, and Z_4 = 50 Ω.

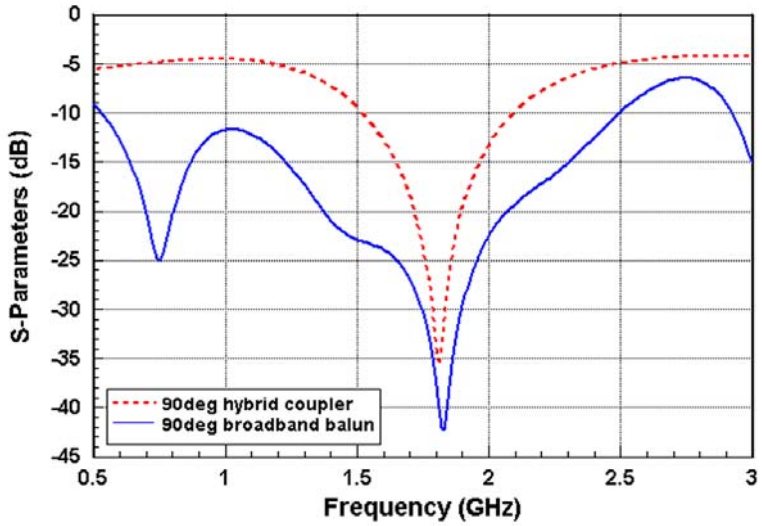

Fig. 55. Simulated input port return loss comparison between the 90° hybrid coupler and 90° broadband balun (Type II).

All simulations presented in this chapter were performed using IE3D. The feed networks were modeled on a Rogers RO4003 laminate of thickness t = 0.8 mm, dielectric constant ε_{r1} = 3.38, and an assumed loss tangent of tan δ = 0.0027. The feed line widths of the 50, 62, 70.71, and 125.5 Ω branches were 1.85, 1.3, 1.02, and 0.25 mm, respectively. For convenient analysis, the input and output ports of the feed networks were all set to 50 Ω.

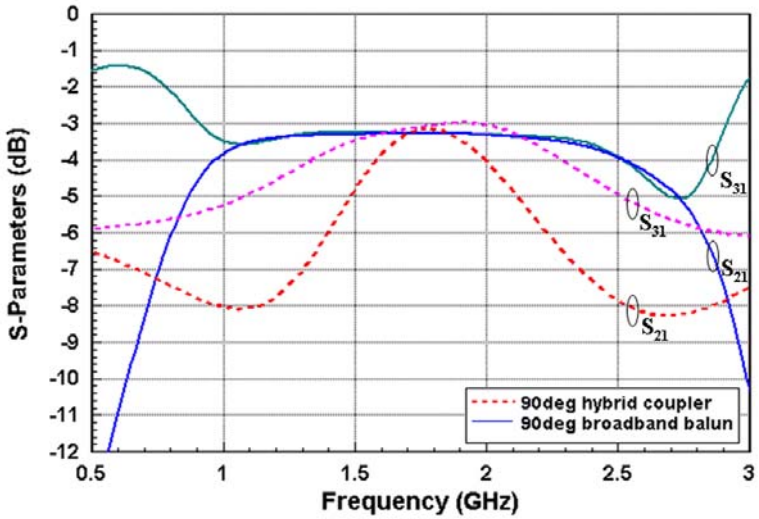

Fig. 56. Simulated output ports amplitude response comparison between the 90° hybrid coupler and 90° broadband balun (Type II).

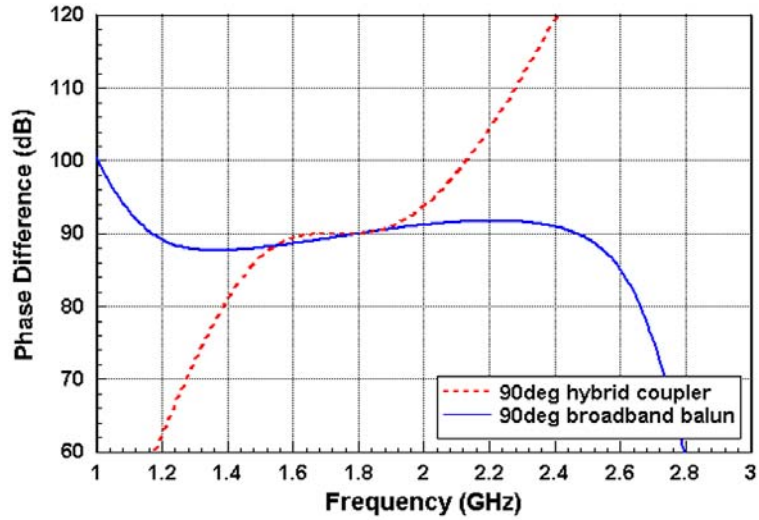

Fig. 57. Simulated output ports phase difference comparison between the 90° hybrid coupler and 90° broadband balun (Type II).

Fig. 55 shows the simulated return loss comparison between the two feeders. The 90° broadband balun (Type II) exhibits a wide impedance bandwidth (S_{11} < -10 dB) of 131.13%, from 0.52 to 2.5 GHz, while the 90° hybrid coupler exhibits a much narrower impedance bandwidth (S_{11} < -10 dB) of 30.9%, from 1.53 to 2.09 GHz. Fig. 56 shows the simulated output ports amplitude response comparison

between the two feeders. The 90^{o} broadband balun (Type II) exhibits balanced output ports power distribution (S_{21} = S_{31} = -3 dB (±0.5 dB)) over a wide band of 72.46%, from 1.1 to 2.35 GHz, while the 90^{o} hybrid coupler exhibits balanced output ports power distribution (S_{21} = S_{31} = -3 dB (±0.5 dB)) over a much narrower band of 14%, from 1.66 to 1.91 GHz. Fig. 57 shows the simulated output ports phase difference comparison between the two feeders. The 90^{o} broadband balun (Type II) exhibits consistent 90^{o} (±5^{o}) output ports phase difference over a considerably wide band of 86.5%, from 1.03 to 2.6 GHz, while the 90^{o} hybrid coupler exhibits consistent 90^{o} (±5^{o}) output ports phase difference over a much narrower band of 32%, from 1.47 to 2.03 GHz.

Combining the simulated results in Fig. 55 to 57, it is observed that the proposed 90^{o} broadband balun (Type II) delivered low input port return loss (S_{11} < -10 dB), balanced output ports power distribution (S_{21} = S_{31} = -3 dB (±0.5 dB)), and consistent 90^{o} (±5^{o}) output ports phase difference, over a significantly wide band of 72.46%, from 1.1 to 2.35 GHz; hence it is termed a “broadband” balun. The conventional 90^{o} hybrid coupler delivered low input port return loss (S11 < -10 dB), balanced output ports power distribution (S_{21} = S_{31} = -3 dB (±0.5 dB)), and consistent 90^{o} (±5^{o}) output ports phase difference over a much narrower band of 14%, from 1.66 to 1.91 GHz; inherently limited by its balanced output port power distribution bandwidth. The 90^{o} broadband balun (Type I), presented in Section 3.2.2, has been shown to deliver a combined bandwidth of 57.5%, from 1.3 to 2.35 GHz. However, its balanced output port distribution (S_{21} = S_{31} = -3 dB (±0.5 dB)) bandwidth of 91.9%, from 0.87 to 2.35 GHz, is relatively wider.

4.2.3 Fabrication and Experimental Setup

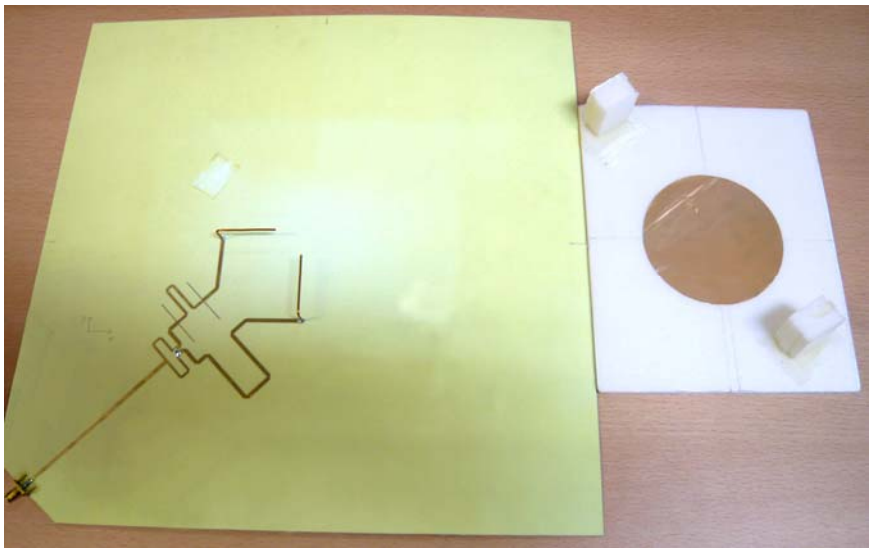

Fig. 58. Prototype of the circularly polarized dual L-probe circular patch antenna utilizing the 90^o broadband balun (Type II).

Fig. 58 shows the prototype of the circularly polarized dual L-probe circular patch antenna utilizing the 90^o broadband balun (Type II). The antenna and feed network parameters were optimized for a wide impedance bandwidth. The circular copper patch, of diameter D = 76.5 mm, was positioned at an air substrate height of H = 20 mm above the feed substrate. The two L-probe feeds, each of diameter 2R = 1 mm, vertical length L_h = 11 mm, and horizontal length L_v = 30.5 mm, were orthogonally oriented and positioned a distance S = 8.5 mm away from the circumference of the patch, and soldered to the respective output ports of the feed network. The square ground plane is of length G = 300 mm. Note that all these antennas parameters are the same as those used for the dual L-probe circular patch antenna utilizing the 90^o broadband balun (Type I) described in Section 3.2.3, save for the horizontal length of the L-probe feed being L_v = 30.5 mm instead of 35 mm. The impedance measurements were taken using the Agilent E8364B network analyzer, while the far-field radiation measurements were taken using the

Hewlett Packard 8510C vector network analyzer and the Orbit-MiDAS far-field measurement system in an anechoic chamber. With a reference linearly polarized standard horn antenna, the comparison method (gain-transfer method) was used to determine the measured gain (See Section 3.2.3) and the rotating-source method was used to determine the measured axial ratio [8], [60].

In the rotating-source method, the linearly polarized reference horn (source) antenna is rotated rapidly and at the same time the direction of observation of the AUT is changed slowly. The rotating source antenna causes the tilt angle of the incident field to rotate at the same rate. Care must be taken to ensure that the time response of the recording system can adequately follow the excursions in the tilt angle. To measure the spinning linear radiation pattern in the x-z and y-z planes, the rate of rotation of the linearly polarized horn (source) antenna is set to 40^{o} per second, while the rate of rotation of the AUT in the elevation plane is set to 1.36^{o} per second. The maxima and minima of the spinning linear radiation pattern (see Fig. 62) correspond to alignment of the source with the major and minor axes of the polarization ellipse, respectively. The axial ratio is determined from the width of the envelope of the spinning linear radiation pattern.

It should be noted that for the polarization-pattern and rotating-source methods, the sense of rotation (LHCP or RHCP) cannot be obtained. The sense of rotation can be separately determined by comparing the outputs of two circularly polarized source antennas which have opposite senses. The use of LHCP and RHCP source antennas, not available in this laboratory, also allows for the determination of the cross-circular polarization levels across the observation angles on and off axis.

4.2.4 Impedance and Radiation Performances

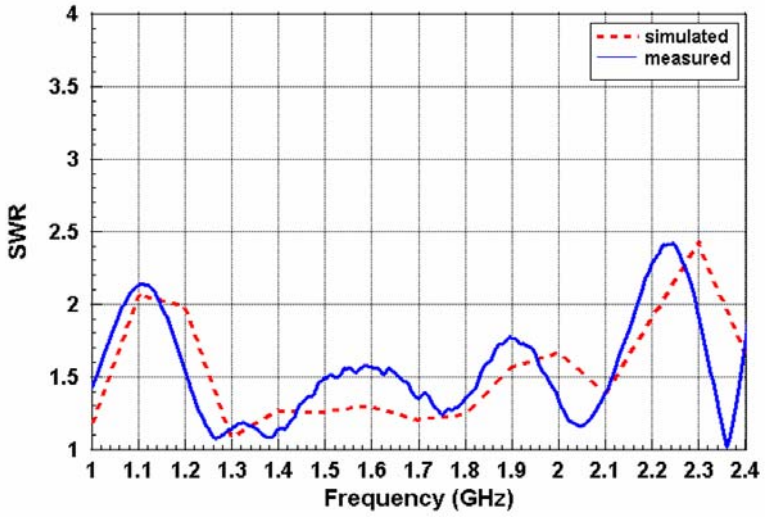

Fig. 59. Simulated and measured SWR for the circularly polarized dual L-probe circular patch antenna utilizing the 90^{o} broadband balun (Type II).

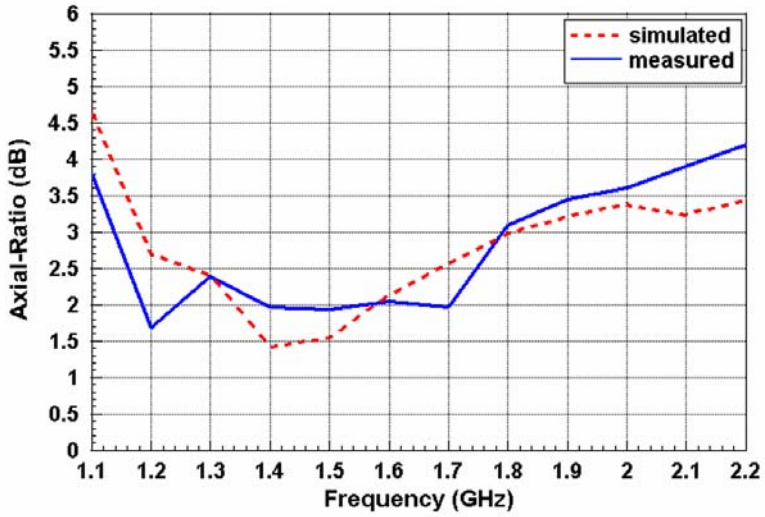

Fig. 60. Simulated and measured axial ratio for the circularly polarized dual L-probe circular patch antenna utilizing the 90^{o} broadband balun (Type II).

Fig. 59 shows the simulated and measured SWR for circularly polarized dual L-probe circular patch antenna utilizing the 90^{o} broadband balun (Type II). The dual L-probe antenna exhibits considerably wide simulated and measured impedance bandwidths (SWR < 2) of 59%, from 1.2 to 2.21 GHz, and 62%, from 1.14 to 2.17 GHz, respectively. This is wider than the 42% impedance bandwidth (SWR < 2)

attained for the dual L-probe antenna utilizing the 90° hybrid coupler [56]. The dual L-probe antenna utilizing the 90° broadband balun (Type I), presented in Section 3.2, exhibits a similar measured impedance bandwidth (SWR < 2) of 61%, from 1.15 to 2.16 GHz.

Fig. 60 shows the simulated and measured axial ratio for the circularly polarized dual L-probe circular patch antenna utilizing the 90° broadband balun (Type II). The dual L-probe antenna exhibits rather wide simulated and measured 3-dB axial-ratio bandwidths of 41.6%, from 1.18 to 1.8 GHz, and 44.37%, from 1.14 to 1.79 GHz, respectively. This is much wider than the 27.23% 3-dB axial ratio bandwidth attained for the dual L-probe antenna utilizing the 90° hybrid coupler [56]. The dual L-probe antenna utilizing the 90° broadband balun (Type I), presented in Section 3.2, exhibits a comparatively narrower measured 3-dB axial ratio bandwidth of 37.7%, from 1.25 to 1.83 GHz. This may be attributed to the relatively narrower operating range of the 90° broadband balun (Type I) balun (~57.5%), compared to that of the 90° broadband balun (Type II) balun (~72.5%).

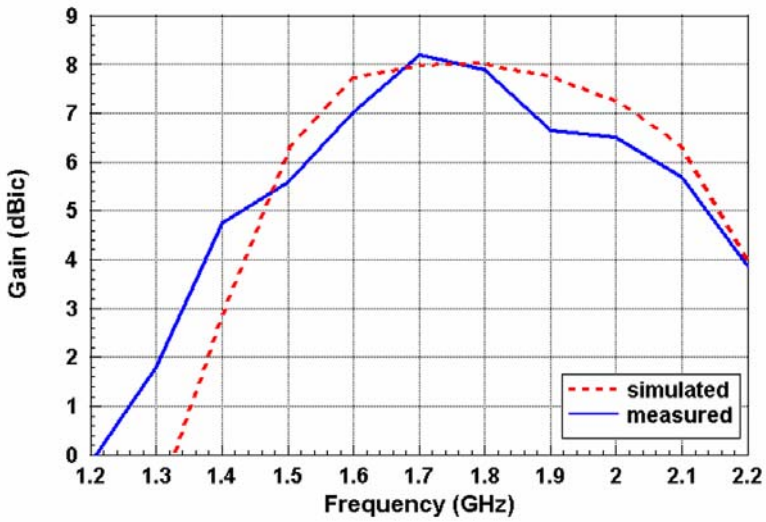

Fig. 61. Simulated and measured gain for the circularly polarized dual L-probe circular patch antenna utilizing the 90° broadband balun (Type II).

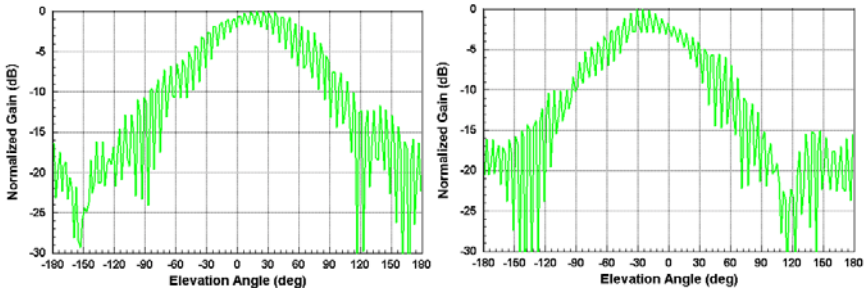

x-z plane y-z plane

(a) 1.2 GHz

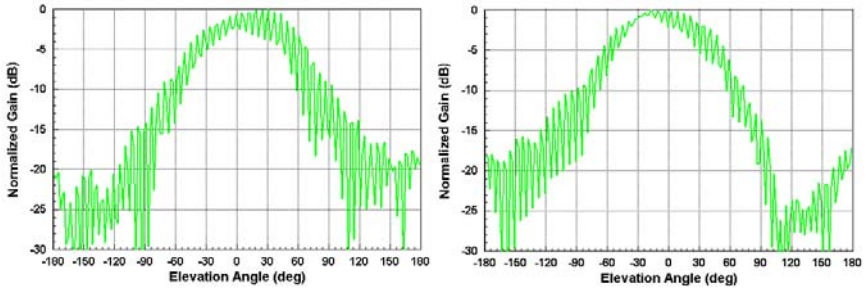

x-z plane y-z plane

(b) 1.5 GHz

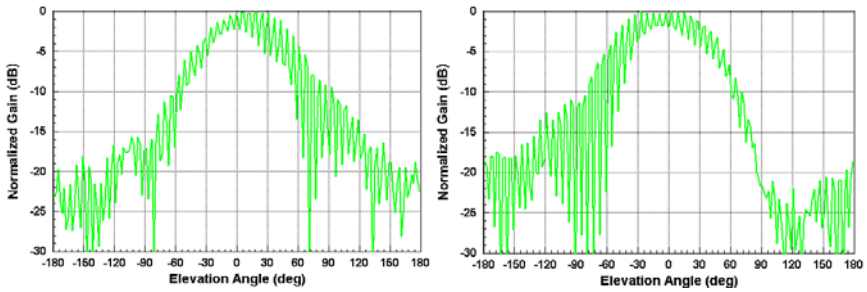

x-z plane y-z plane

(c) 1.7 GHz

Fig. 62. Measured normalized spinning linear radiation patterns for the circularly polarized dual L-probe circular patch antenna utilizing the 90^{o} broadband balun (Type II).

Fig. 61 shows the simulated and measured boresight gain for the circularly polarized dual L-probe circular patch antenna utilizing the 90^{o} broadband balun (Type II). The dual L-probe antenna exhibits a simulated 3-dB gain bandwidth (gain > 5 dBic) of 38.02%, from 1.47 to 2.16 GHz, with its highest gain of 8 dBic at 1.8 GHz, and a measured 3-dB gain bandwidth (gain > 5.2 dBic) of 38.89%, from 1.45 to 2.15 GHz, with its highest gain of 8.2 dBic at 1.7 GHz. The

measured gain is better than 4 dBic across a 45.38% bandwidth, from 1.38 to 2.19 GHz. The dual L-probe antenna utilizing the 90^o broadband balun (Type I), presented in Section 3.2, exhibits a similar measured gain bandwidth (gain > 4 dBic) of 43.68%, from 1.36 to 2.12 GHz. Combining the measured results in Fig. 59 to 61, the antenna exhibits, in terms of SWR < 2, axial ratio < 3 dB, and gain > 4 dBic, a measured CP bandwidth of 25.87%, from 1.38 to 1.79 GHz. The designated bandwidth of interest will be from 1.2 to 1.7 GHz (34.48%). It is observed that the measured results agree rather well with the simulated results.

Fig. 62 shows the measured normalized spinning linear radiation patterns for the circularly polarized dual L-probe circular patch antenna utilizing the 90^o broadband balun (Type II) at the lower frequency edge (1.2 GHz), center frequency (1.5 GHz), and upper frequency edge (1.7 GHz), of the bandwidth of interest, on the x-z ($\phi = 0^o$) and y-z ($\phi = 90^o$) planes, respectively. The measured axial ratio was determined from the width of the envelope of the spinning linear radiation pattern. Across this passband, it is observed that on both principle planes, the antenna exhibits acceptable axial-ratio (AR < 3 dB) across a narrow beamwidth. The slight asymmetry observed in the radiation patterns should be due to the asymmetrical feed orientation of the dual L-probe antenna structure.

4.2.5 Discussions

In this section, the broadband design of a circularly polarized dual L-probe circular patch antenna utilizing the proposed 90^o broadband balun (Type II) has been presented. The broadband balun provides good impedance matching, equal amplitude power splitting and consistent 90^o phase shifting, over a wide band (~72.5%). The use of the proposed broadband balun (Type II), in place of the

conventional 90° hybrid coupler, has been shown to provide enhanced impedance and axial ratio bandwidths. The use of the Type II broadband balun, in place of the Type I broadband balun, has been shown to provide enhanced axial ratio bandwidth but similar impedance and gain bandwidths. The proposed circularly polarized dual L-probe antenna delivers wide measured impedance (SWR < 2), axial ratio (AR < 3 dB), and gain (gain > 4 dBic) bandwidths of 62% (1.14 to 2.17 GHz), 44.37% (1.14 to 1.79 GHz) and 45.38% (1.38 to 2.19 GHz), respectively, for a measured CP operating bandwidth of 25.87%, from 1.38 to 1.79 GHz.

4.3 Broadband Circularly Polarized Dual Capacitive-Feed Patch Antenna with a 90° Broadband Balun (Type II)

4.3.1 Antenna Design and Geometry

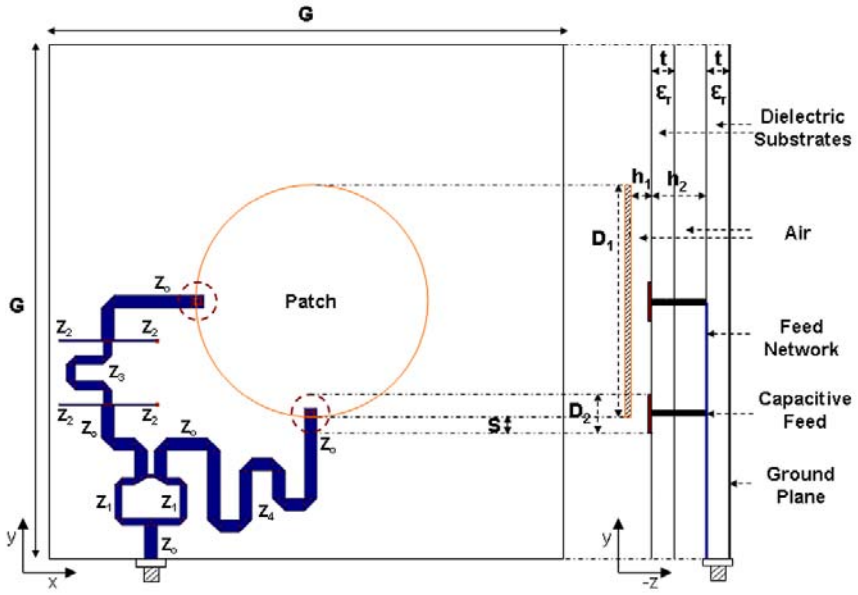

Fig. 63 Geometry of the circularly polarized dual capacitive-feed circular patch antenna utilizing the 90° broadband balun (Type II).

Since the gain profile of a sequential array is similar to that of a conventional array using the same number of elements, the gain bandwidth for a sequential-

rotated 2x2 patch array may not be able to match up to the improved impedance and axial ratio bandwidths. Therefore, the capacitive-feed technique [70], [71] is explored as an alternative method for exciting the patch element in bid to extend the gain bandwidth of the dual L-probe patch antennas presented in Section 3.2 and 4.2. The dual capacitive-feed circular patch antenna, shown in Fig. 63, is designed for wideband circular polarization operation centered at 4.0 GHz. For practical use of its own, the dual capacitive-feed antenna is targeted for a 50% CP bandwidth sufficient to cover the lower UWB band (3.1 to 5.0 GHz). The two capacitive-feeds are orthogonally positioned and supplied equal amplitude power with relative excitation phases of 0^o and 90^o. The use of the 90^o broadband balun (Type II), presented in Section 4.2.2, with wideband impedance matching, equal power splitting and 90^o phase shifting capabilities, is used to control the amplitude and phase of the linearly polarized field components, so as to reduce the cross-polarization due to multiple reflections and feed phase errors; thus providing the patch antenna with wider impedance and axial ratio bandwidths.

4.3.2 Feed Network Configuration

The 90^o broadband balun (Type II), presented in Section 4.2.2, provides more tunable feed line parameters and a wider operating bandwidth of ~72.5% compared to the 90^o broadband balun (Type I). However, one important disadvantage is that the $Z_2 = 125.5\ \Omega$ microstrip branch requires a minimum feed line width of only 0.25 mm on a 0.8 mm thick Rogers RO4003 dielectric substrate. This line width may be too thin and exceed the manufacturing tolerance in some cases. For an optimized set of antenna parameters, the lengths of the various microstrip branches can be further optimized to adjust the impedance and

axial ratio bandwidths to match the gain bandwidth of the antenna in study. The impedance matching is affected mainly by branches Z_1, Z_2 and Z_3, the balanced power splitting is controlled by branches Z_2 and Z_3, while the 90^o phase shifting can be adjusted by tweaking branch Z_4. Here, λ_g refers to the guide wavelength at a center operating frequency of 4.0 GHz.

4.3.3 Fabrication and Experimental Setup

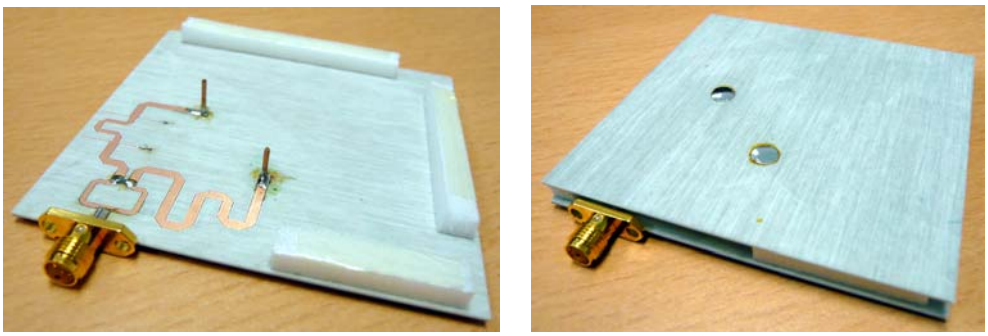

(a) feed network layer (b) capacitive discs layer

(c) patch element layer

Fig. 64. Prototype of the circularly polarized dual capacitive-feed circular patch antenna utilizing the 90^o broadband balun (Type II).

Fig. 64 shows the prototype of the circularly polarized dual capacitive-feed circular patch antenna utilizing the 90^o broadband balun (Type II). The antenna and feed network parameters were optimized for a wide impedance bandwidth centering 4.0 GHz. The circular copper patch, of diameter D_1 = 34 mm (0.453 λ_o), was positioned at an air substrate height of h_1 = 1.5 mm above the capacitive discs

layers. The two capacitive-feeds, each with a probe of diameter 2R = 1 mm and of vertical length h_2 = 4.7 mm, and with a circular disc of diameter D_2 = 5.5 mm, were orthogonally oriented and positioned a distance S = 2.2 mm away from the circumference of the patch, and soldered to the respective output ports of the feed network. The capacitive discs and feed network were respectively printed on separate Rogers RO4003 laminates, each of thickness t = 0.8 mm and dielectric constant ε_r = 3.38. The square ground plane is of length G = 75 mm (1 λ_o). The impedance measurements were taken using the Agilent N5230A network analyzer, while the far-field radiation measurements were taken using the Hewlett Packard 8510C vector network analyzer and the Orbit-MiDAS far-field measurement system in an anechoic chamber. With a reference linearly polarized standard horn antenna, the comparison method (gain-transfer method) was used to determine the measured gain (See Section 3.2.3) and the rotating-source method was used to determine the measured axial ratio (See Section 4.2.3).

4.3.4 Impedance and Radiation Performances

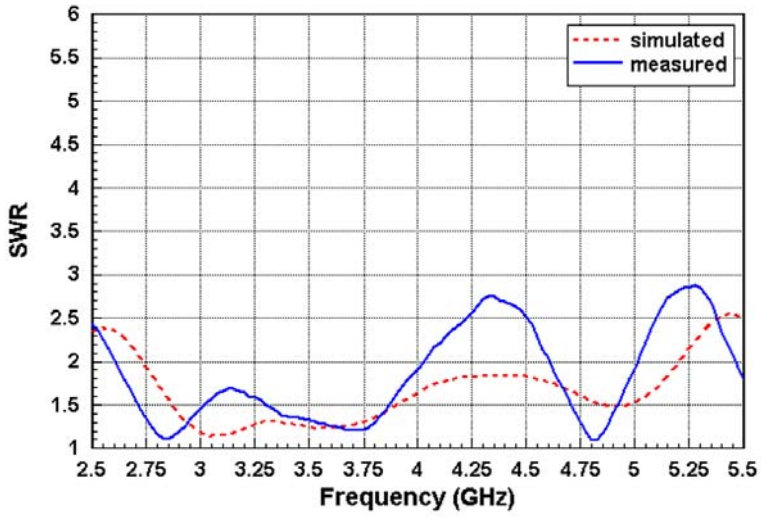

Fig. 65. Simulated and measured SWR for the circularly polarized dual capacitive-feed circular patch antenna utilizing the 90° broadband balun (Type II).

Fig. 65 shows the simulated and measured SWR for circularly polarized dual capacitive-feed circular patch antenna utilizing the 90^{o} broadband balun (Type II). The dual capacitive-feed antenna exhibits wide simulated and measured impedance bandwidths (SWR < 2) of 61.96%, from 2.74 to 5.2 GHz, and 42.77%, from 2.61 to 4.03 GHz, respectively. It is observed that the measured input VSWR has risen sharply between 4.05 to 4.6 GHz, leading to a discrepancy between the simulated and measured SWR results. The dual L-probe antenna utilizing the 90^{o} broadband balun (Type II), presented in Section 4.2, exhibits a much wider measured impedance bandwidth (SWR < 2) of 62%, from 1.14 to 2.17 GHz. The surge in input VSWR should be caused by the increased mutual coupling effects (ie. coupling between the vertical components of the capacitive-feeds) within this frequency range. Probe coupling is not properly cancelled with an asymmetrical two-point feeding structure. The vertical components of the two capacitive-feeds have to be spaced closer together, in terms of open wavelength, compared to that of the vertical components of the two L-probe feeds.

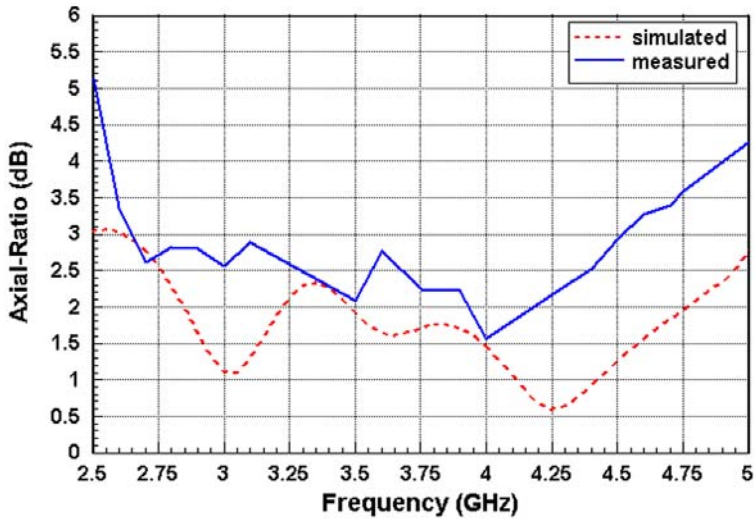

Fig. 66. Simulated and measured axial ratio for the circularly polarized dual capacitive-feed circular patch antenna utilizing the 90^{o} broadband balun (Type II).

Fig. 66 shows the simulated and measured axial ratio for the circularly polarized dual capacitive-feed circular patch antenna utilizing the 90° broadband balun (Type II). The dual capacitive-feed antenna exhibits considerably wide simulated and measured 3-dB axial-ratio bandwidths of > 62.12%, from 2.63 to above 5 GHz, and 52.16%, from 2.65 to 4.52 GHz, respectively. The dual L-probe antenna utilizing the 90° broadband balun (Type II), presented in Section 4.2, exhibits a comparatively narrower measured 3-dB axial ratio bandwidth of 44.37%, from 1.14 to 1.79 GHz. The measured results suggest that, for a given feed network, the capacitive-feed technique is capable of further extending the axial ratio bandwidth afforded by the L-probe proximity feed approach. It should also be noted, however, that for the dual capacitive-feed antenna in study, the impedance matching, balanced power splitting, and 90° phase shifting properties of the 90° broadband balun (Type II) have been carefully optimized in simulation in bid to further increase the 3-dB axial ratio bandwidth to ~50%.

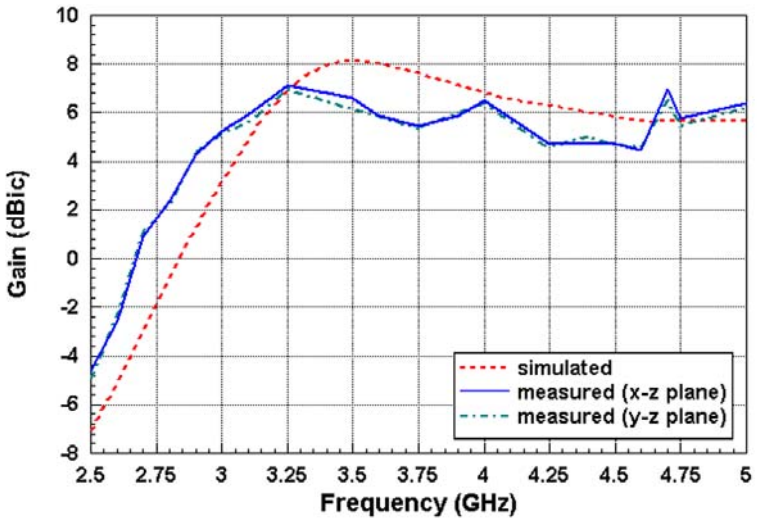

Fig. 67. Simulated and measured gain for the circularly polarized dual capacitive-feed circular patch antenna utilizing the 90° broadband balun (Type II).

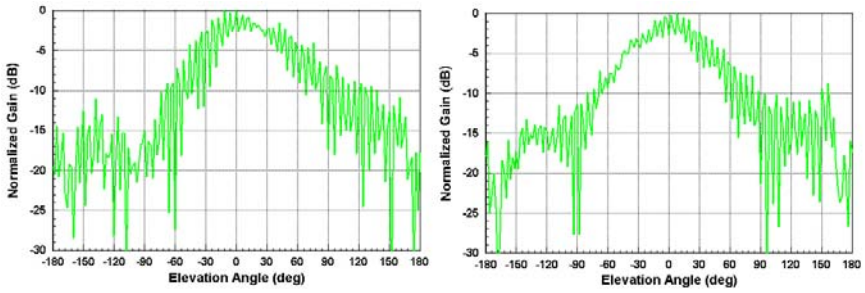

x-z plane y-z plane

(a) 2.7 GHz

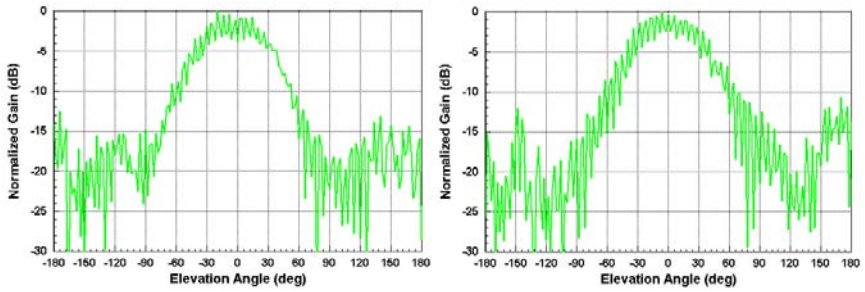

x-z plane y-z plane

(b) 3.75 GHz

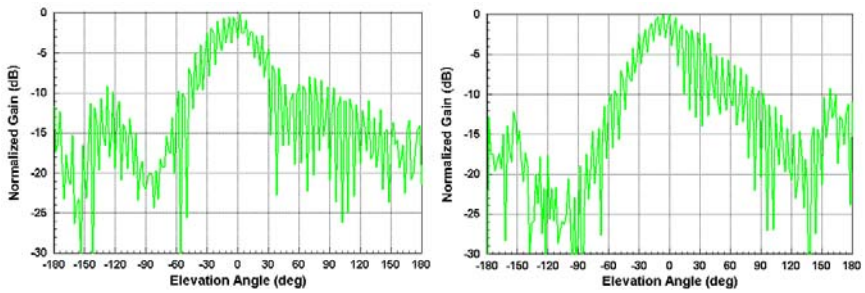

x-z plane y-z plane

(c) 4.5 GHz

Fig. 68. Measured normalized spinning linear radiation patterns for the circularly polarized dual capacitive-feed circular patch antenna utilizing the 90^{o} broadband balun (Type II).

Fig. 67 shows the simulated and measured boresight gain for the circularly polarized dual capacitive-feed circular patch antenna utilizing the 90^{o} broadband balun (Type II). The dual capacitive-feed antenna exhibits a simulated 3-dB gain bandwidth (gain > 5.15 dBic) of > 46.61%, from 3.11 to above 5 GHz, with its highest gain of 8.15 dBic at 3.5 GHz, and a measured 3-dB gain bandwidth (gain > 4 dBic) of > 53.81%, from 2.88 to above 5 GHz, with its highest gain of 7 dBic

at 3.25 GHz. The dual L-probe antenna utilizing the 90^o broadband balun (Type II), presented in Section 4.2, exhibits a comparatively narrower measured gain bandwidth (gain > 4 dBic) of 45.38%, from 1.38 to 2.19 GHz. The measured results suggest that, for a given feed network, the capacitive-feed technique is capable of further extending the gain bandwidth afforded by the L-probe proximity feed approach. Combining the measured results in Fig. 65 to 67, the antenna exhibits, in terms of SWR < 2, axial ratio < 3 dB, and gain > 4 dBic, a measured CP bandwidth of 33.29%, from 2.88 to 4.03 GHz. The designated bandwidth of interest will be from 2.7 to 4.5 GHz (50%). The measured boresight gain profile in the x-z and y-planes are shown to be identical, which suggests that the AUT has been perfectly mounted during the experimental setup to allow for accurate radiation measurements.

Fig. 68 shows the measured normalized spinning linear radiation patterns for the circularly polarized dual capacitive-feed circular patch antenna utilizing the 90^o broadband balun (Type II) at the lower frequency edge (2.7 GHz), center frequency (3.75 GHz), and upper frequency edge (4.5 GHz), of the bandwidth of interest, on the x-z ($\phi = 0^o$) and y-z ($\phi = 90^o$) planes, respectively. The measured axial ratio was determined from the width of the envelope of the spinning linear radiation pattern. Across this passband, it is observed that on both principle planes, the axial-ratio increases sharply off the boresight. This suggests that good circular polarization operation can only take place point-to-point. The slight asymmetry observed in the radiation patterns can be attributed to the asymmetrical feed orientation of the dual L-probe antenna structure.

4.3.5 Discussions

In this section, the broadband design of a circularly polarized dual capacitive-feed circular patch antenna utilizing the proposed 90^o broadband balun (Type II) has been presented. The broadband balun provides good impedance matching, equal amplitude power splitting and consistent 90^o phase shifting, over a wide band (~72.5%). The proposed dual capacitive-feed antenna utilizing the proposed broadband balun (Type II), compared to the dual L-probe antenna utilizing the same broadband balun, has been shown to provide enhanced axial ratio and gain bandwidths (> 50%). However, soldering a coaxial wire perpendicularly onto a capacitive disc is difficult as opposed to simply bending a coaxial wire to form an L-probe feed. Since comparative advantage in terms of measured impedance bandwidth has not been ascertained, the dual L-probe antenna was selected for the sequential array study presented in the following section. The proposed circularly polarized dual capacitive-feed antenna delivers wide measured impedance (SWR < 2), axial ratio (AR < 3 dB), and gain (gain > 4 dBic) bandwidths of 42.77% (2.61 to 4.03 GHz), 52.16% (2.65 to 4.52 GHz), and > 53.81% (2.88 to above 5 GHz), respectively, for a measured CP operating bandwidth of 33.29%, from 2.88 to 4.03 GHz. The gain bandwidth (gain > 4 dBic), dependent on antenna structure and excitation geometry, has been successfully optimized to cover the entire lower UWB band, from 3.1 to 5.0 GHz. The 90^o broadband balun (Type II) can still be further optimized to reduce the input impedance mismatch and feed phase errors across the frequency range of interest, so as to shift the impedance and axial ratio bandwidths to match the design gain bandwidth. This will present a breakthrough compact two point feed patch antenna capable of providing a ~50% CP operation suitable for emerging UWB applications.

4.4 Broadband Circularly Polarized Dual L-Probe Patch Array with 90° Broadband Baluns (Type II)

4.4.1 Antenna Array Configuration

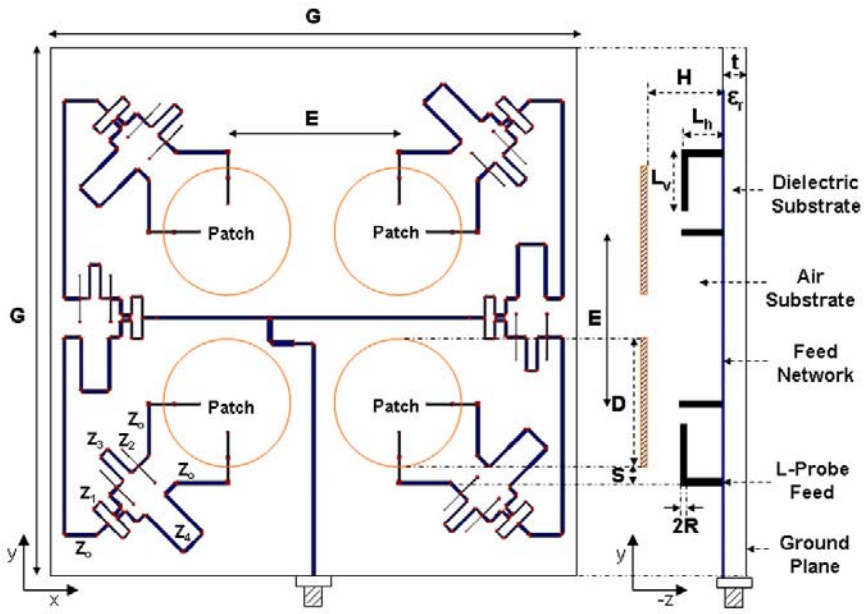

Fig. 69. Geometry of the circularly polarized 2x2 sequential-rotated L-probe circular patch array utilizing six 90° broadband baluns (Type II).

The efficacy of the sequential feeding technique in enhancing the axial ratio of the circularly polarized sequential array depends on the number of elements, and the angular position and phase shift of each element. Analysis of various sequential array configurations [69] indicate that the symmetrical 2x2 elements sequential array is effective in suppressing the cross-circular polarization due to feed phase errors, multiple reflections and, in particular, higher order modes. This holds true for the main beam peak but in some cases, the cross-polarization sidelobes of the sequential array may even be higher than in a conventional array. The 2x2 sequential-rotated dual L-probe circular patch array, shown in Fig. 69, is designed for wideband circular polarization operation centered at 1.8 GHz. The circularly

polarized elements are sequentially rotated and supplied equal amplitude power with relative excitation phases of 0^o, 90^o, 180^o, and 270^o. Each of the four circularly polarized dual L-probe patch elements is fed by a dedicated 90^o broadband balun (Type II). Each dedicated 90^o broadband balun (Type II) provides the two L-probe feeds in each circularly polarized element with impedance matching, equal power splitting and consistent 90^o phase shifting, over a wide band. The four dedicated 90^o broadband baluns (Type II) are in turn connected to the respective output ports of the 90^o broadband balun (Type II) pair described in the next section. The element spacing, E, determines the amount of gain loss. In general, a smaller E can help reduce gain loss but this will be at the expense of higher mutual coupling between the patch elements which implicates both the overall impedance matching and axial ratio.

4.4.2 Feed Network Configuration

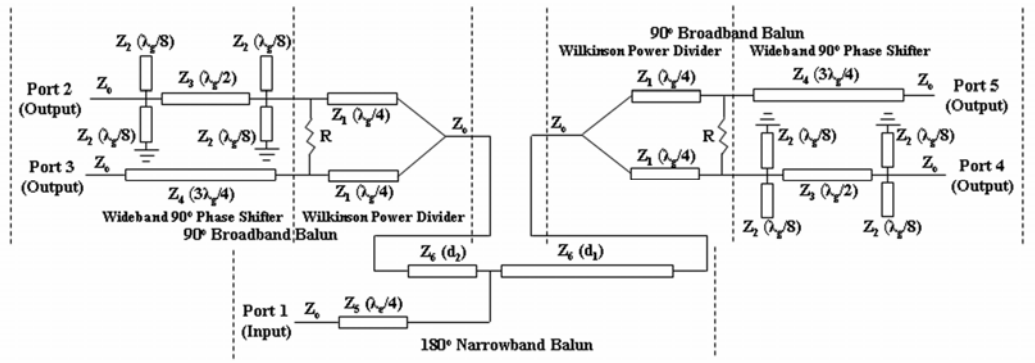

Fig. 70. Schematics of the proposed 90^o broadband balun (Type II) pair.

The proposed 90^o broadband balun (Type II) pair, shown in Fig. 70, delivers good impedance matching, equal amplitude power splitting and relative excitation phasing of 0^o, 90^o, 180^o, and 270^o, over a wide band. The feed network comprises a conventional 180^o narrowband balun (Fig. 3) cascaded to a pair of the proposed 90^o broadband baluns (Type II) (Fig. 54). To provide the required 180^o phase shift

between the two 90° broadband baluns (Type II), the lengths of the microstrip branches, d_1 and d_2, must be such that $d_1 - d_2 = \lambda_g / 2$, where λ_g refers to the guide wavelength at a center operating frequency of 1.8 GHz. The characteristic impedances of the microstrip branches are given by $Z_o = 50\ \Omega$, $Z_1 = 70.71\ \Omega$, $Z_2 = 125.5\ \Omega$, $Z_3 = 62\ \Omega$, and $Z_4 = 50\ \Omega$, $Z_5 = 35.36\ \Omega$, and $Z_6 = 50\ \Omega$.

4.4.3 Fabrication and Experimental Setup

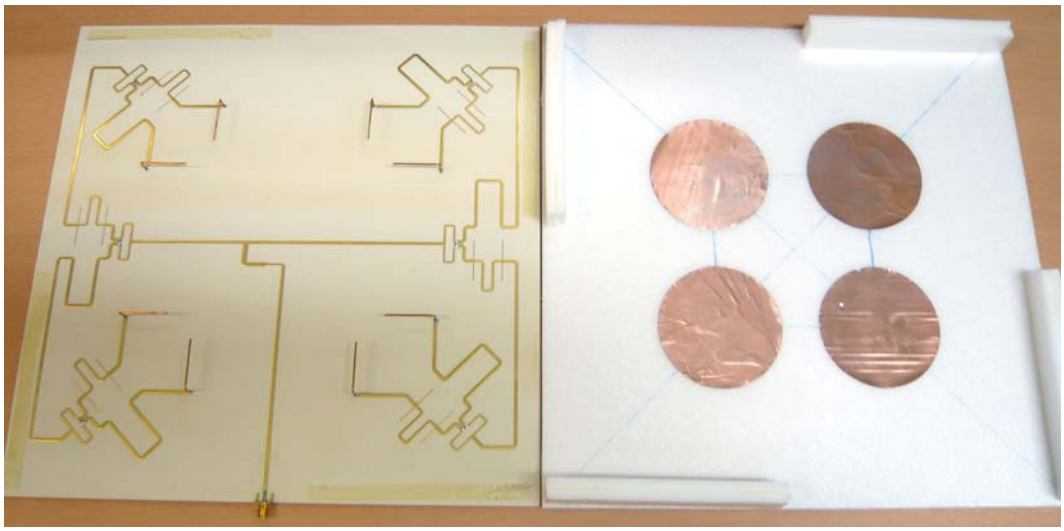

Fig. 71. Prototype of the circularly polarized 2x2 sequential-rotated L-probe circular patch array utilizing six 90° broadband baluns (Type II).

Fig. 71 shows the prototype of the circularly polarized 2x2 sequential-rotated L-probe circular patch array utilizing six 90° broadband baluns (Type II). The antenna and feed network parameters were optimized for a wide impedance bandwidth centering 1.8 GHz. The dual L-probe circular patch antenna utilizing the 90° broadband balun (Type II) described in Section 4.2.3, were used for each of the four circularly polarized elements; maintaining the same antenna parameters. The circular copper patch, of diameter D = 76.5 mm (0.459 λ_o), was positioned at an air substrate height of H = 20 mm (0.12 λ_o) above the feed substrate. The patch element separation was set to E = 100 mm (0.6 λ_o). The two

L-probe feeds, each of diameter 2R = 1 mm, vertical length L_h = 11 mm (0.066 λ_o), and horizontal length L_v = 30.5 mm (0.183 λ_o), were orthogonally oriented and positioned a distance S = 8.5 mm away from the circumference of the patch, and soldered to the respective output ports of the feed network. The square ground plane is of length G = 320 mm (1.92 λ_o). A larger ground plane was used to accommodate the more elaborate feeder footprint. The impedance measurements were taken using the Agilent E8364B network analyzer, while the far-field radiation measurements were taken using the Hewlett Packard 8510C vector network analyzer and the Orbit-MiDAS far-field measurement system in an anechoic chamber. With a reference linearly polarized standard horn antenna, the comparison method (gain-transfer method) was used to determine the measured gain (See Section 3.2.3) and the rotating-source method was used to determine the measured axial ratio (See Section 4.2.3).

4.4.4 Impedance and Radiation Performances

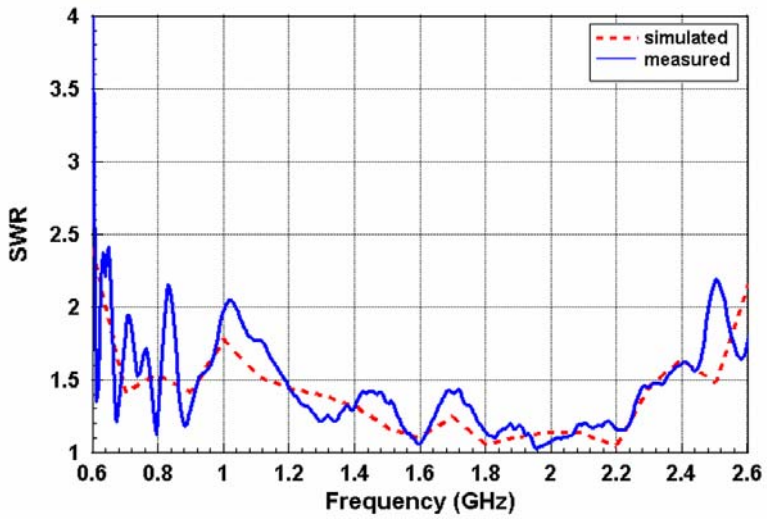

Fig. 72. Simulated and measured SWR for the circularly polarized 2x2 sequential-rotated L-probe circular patch array utilizing six 90° broadband baluns (Type II).

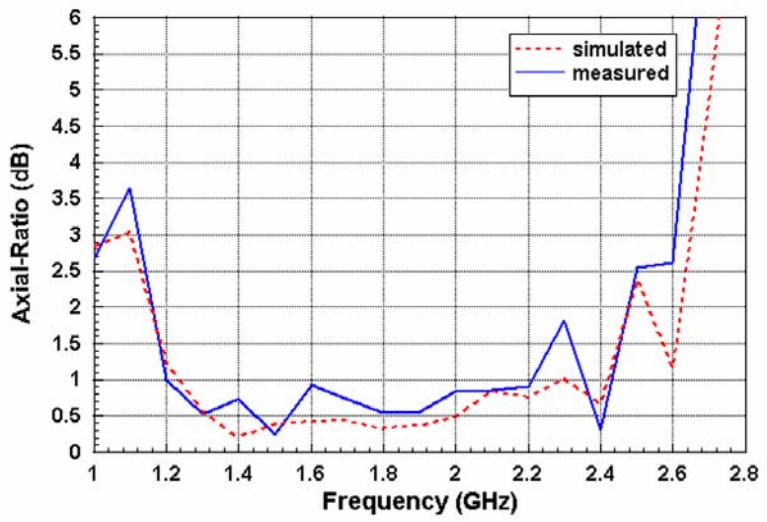

Fig. 73. Simulated and measured axial ratio for the circularly polarized 2x2 sequential-rotated L-probe circular patch array utilizing six 90^{o} broadband baluns (Type II).

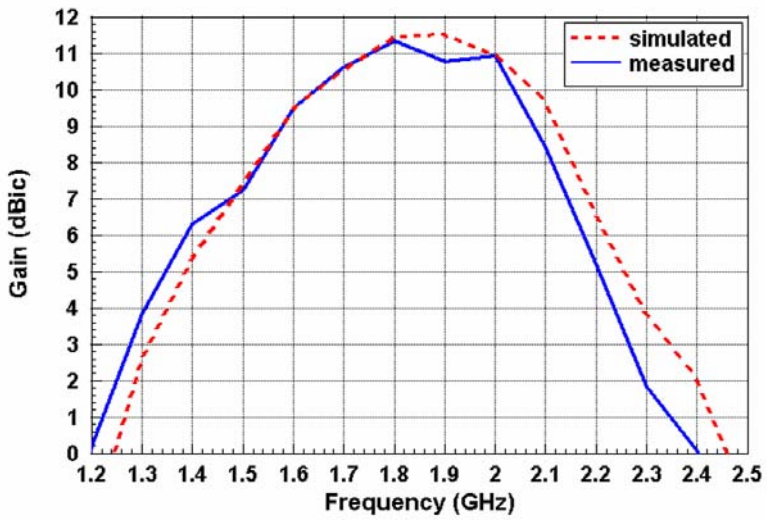

Fig. 74. Simulated and measured gain for the circularly polarized 2x2 sequential-rotated L-probe circular patch array utilizing six 90^{o} broadband baluns (Type II).

Fig. 72 shows the simulated and measured SWR for 2x2 sequential-rotated L-probe circular patch array utilizing six 90^{o} broadband baluns (Type II). The sequential array exhibits considerably wide simulated and measured impedance bandwidths (SWR < 2) of 118.52%, from 0.66 to 2.58 GHz, and 81.36%, from 1.05 to 2.49 GHz, respectively. The dual L-probe antenna utilizing the 90^{o}

broadband balun (Type II), presented in Section 4.2, exhibits a much narrower measured impedance bandwidth (SWR < 2) of 62%, from 1.14 to 2.17 GHz. The measured results suggest that in the sequential array configuration, the reflections from the mismatched elements effectively cancel out in the feeder.

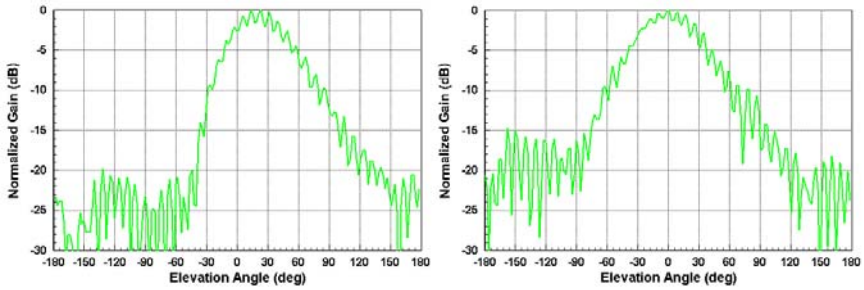

x-z plane y-z plane

(a) 1.2 GHz

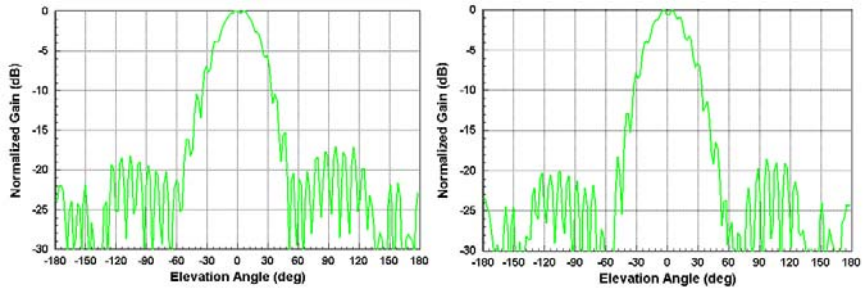

x-z plane y-z plane

(b) 1.8 GHz

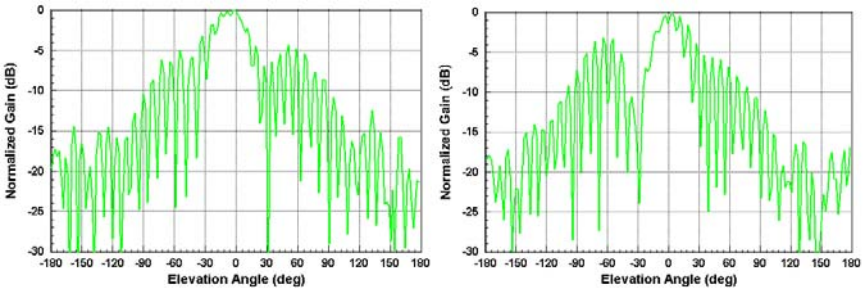

x-z plane y-z plane

(c) 2.2 GHz

Fig. 75. Measured normalized spinning linear radiation patterns for the circularly polarized 2x2 sequential-rotated L-probe circular patch array utilizing six 90^{o} broadband baluns (Type II).

Fig. 73 shows the simulated and measured axial ratio for the circularly polarized 2x2 sequential-rotated L-probe circular patch array utilizing six 90^{o} broadband

baluns (Type II). The sequential array exhibits rather wide simulated 3-dB and 2-dB axial-ratio bandwidths of 82.35%, from 1.1 to 2.64 GHz, and 72.53%, from 1.16 to 2.48 GHz, respectively. The measured 3-dB and 2-dB axial ratio bandwidths are 78.4%, from 1.14 to 2.61 GHz, and 72.53%, from 1.16 to 2.48 GHz, respectively. The dual L-probe antenna utilizing the 90^{o} broadband balun (Type II), presented in Section 3.2, exhibits a much narrower measured 3-dB axial ratio bandwidth of 44.37%, from 1.14 to 1.79 GHz. The measured results suggest that the sequential array configuration has been effective in suppressing the cross-circular polarization components due to feed phase deviation, multiple reflections and higher order modes, hence reducing the related axial ratio perturbation.

Fig. 74 shows the simulated and measured boresight gain for the circularly polarized 2x2 sequential-rotated L-probe circular patch array utilizing six 90^{o} broadband baluns (Type II). The sequential array exhibits a simulated 3-dB gain bandwidth (gain > 8.54 dBic) of 30.89% from 1.56 to 2.13 GHz, with its highest gain of 11.54 dBic at 1.9 GHz, and a measured 3-dB gain bandwidth (gain > 8.35 dBic) of 30.14% from 1.55 to 2.1 GHz, with its highest gain of 11.35 dBic at 1.8 GHz. The measured gain is better than 4 dBic across a 53.11% bandwidth, from 1.3 to 2.24 GHz. The dual L-probe antenna utilizing the 90^{o} broadband balun (Type II), presented in Section 4.2, exhibits a comparatively narrower measured gain bandwidth (gain > 4 dBic) of 45.38%, from 1.38 to 2.19 GHz. Its highest measured gain of 8.2 dBic was observed at 1.7 GHz. The sequential array is deemed to have conferred additional ~3.15 dB gain over its single element counterpart. For a 2x2 array in the absence of any loss (radiation, surface wave, dielectric, ohmic, or connector losses), an additional 6 dB gain is expected. The

discrepancy implies an estimated gain loss of 3 dB accrued mainly to the insertion losses in the feed network. Combining the measured results in Fig. 72 to 74, the antenna exhibits, in terms of SWR < 2, axial ratio < 2 dB, and gain > 4 dBic, a measured CP bandwidth of 53.11%, from 1.3 to 2.24 GHz. The designated bandwidth of interest will be from 1.2 to 2.2 GHz (58.82%). Although increased impedance and axial ratio bandwidths are obtained, the bandwidth over which a specified array gain is maintained is similar to that for a conventional array. The gain bandwidth product is related to array volume which is not changed by sequential rotation. Hence, gain loss remains a significant bandwidth constraint for the sequential array.

It is observed that the measured results agree very well with the simulated results. This is not easy to achieve considering the high degree of accuracy required in soldering and aligning the eight L-probe feeds, and aligning the four patch elements, during the fabrication process. This also ascertains the proper mounting of the AUT during the experimental setup, and confirms the reliability of the rotating-source method in determining the measured axial ratio.

Fig. 75 shows the measured normalized spinning linear radiation patterns for the circularly polarized 2x2 sequential-rotated L-probe circular patch array utilizing six 90^o broadband baluns (Type II) at the lower frequency edge (1.2 GHz), center frequency (1.8 GHz), and upper frequency edge (2.2 GHz), of the bandwidth of interest, on the x-z ($\phi = 0^o$) and y-z ($\phi = 90^o$) planes, respectively. The measured axial ratio was determined from the width of the envelope of the spinning linear radiation pattern. Across this passband, it is observed that on both principle

planes, the sequential array exhibits acceptable axial-ratio (AR < 3 dB) across a narrow beamwidth. In particular, good pattern symmetry and low angular axial ratio around the boresight are observed at the design center frequency of 1.8 GHz, on both principle planes. The circularly polarized dual L-probe antenna utilizing the 90^o broadband balun (Type II), presented in Section 4.2, exhibits in Fig. 62, slightly wider beamwidths across its corresponding bandwidth of interest. This is expected because the 2x2 array configuration will yield higher gain at the expense of narrower beamwidths.

4.4.5 Discussions

In this section, the broadband design of a circularly polarized 2x2 sequential-rotated dual L-probe circular patch array utilizing six proposed 90^o broadband baluns (Type II) has been presented. The broadband balun provides good impedance matching, equal amplitude power splitting and consistent 90^o phase shifting, over a wide band (~72.5%). Each circularly polarized dual L-probe patch element, fed by a dedicated broadband balun, delivers wide measured impedance, axial ratio, and gain bandwidths. The sequential array, composed of four of the circularly polarized dual L-probe patch elements sequentially fed by the proposed broadband balun pair, has been shown to provide enhanced impedance, axial ratio and gain bandwidths over that of each individual element. The proposed circularly polarized sequential array delivers wide measured impedance (SWR < 2), axial ratio (AR < 2 dB), and gain (gain > 4 dBic) bandwidths of 81.36% (1.05 to 2.49 GHz), 72.53% (1.16 to 2.48 GHz), and 53.11% (1.3 to 2.24 GHz), respectively, for a measured CP operating bandwidth of 53.11%, from 1.3 to 2.24 GHz. Although increased impedance and axial ratio bandwidths are obtained, the

bandwidth over which a specified array gain is maintained is similar to that for a conventional array. Hence, gain loss remains a significant bandwidth constraint for the sequential array. The sequential array in study presents a patch array solution for multi-frequency, multi-modes, point-to-point wireless communication systems requiring broadband circular polarized coverage encompassing four bands, i.e. GPS1575 (1559-1610 MHz), PCS1800 (1710-1880 MHz), GSM1900 (1850-1990 MHz), and UMTS2000 (1920-2170 MHz).

4.5 Concluding Remarks

The wideband impedance matching, balanced power splitting, and 90^{o} phasing afforded by the 90^{o} broadband balun (Type II) leads to enhanced impedance bandwidth and the wideband suppression of cross-polarization due to multiple reflections and feed phase errors. This cross-polarization suppression shows up in the form of an improved axial ratio bandwidth. However, the inherent asymmetry of the two point feeding structure implies that the cross-polarization due to higher order modes and mutual coupling effects cannot be properly suppressed. To overcome this, four sets of two point feed patch elements were sequentially rotated to form a balanced and symmetrical 2x2 sequential array, with each element supplied wideband equal amplitude power and appropriate phasing. This allowed for further improved impedance and axial ratio bandwidths.

CHAPTER 5

BROADBAND CIRCULARY POLARIZED DIELECTRIC RESONATOR ANTENNAS

5.1 Research Direction

Dielectric resonator antennas have been widely investigated over the past two decades [72]-[77]. The DRA is essentially a resonant antenna fabricated from a low-loss dielectric material, the resonant frequency of which is predominantly a function of size, shape, and material permittivity. Like the microstrip patch antenna, the DRA shares many attractive features such as low cost, compact size, light weight, and ease of coupling to most transmission lines. More significantly, the DRA avoid the inherent disadvantages of conventional metallic antennas including high conduction loss at millimeter-wave frequencies and low efficiency due to surface wave excitation. Prior studies of the DRA were primarily concentrated on those producing linear polarization [72]-[77].

Circular polarization, compared to linear polarization, allows for greater flexibility in the orientation angle between transmitter and receiver, better mobility and weather penetration, and greater reduction in multipath reflections and other kinds of interference. Consequently, circularly polarized DRA have received more attention in recent years [78]-[87]. Circular polarization is produced when two or more orthogonal linearly polarized modes, of equal amplitude and 90^{o} phase difference, are independently excited. For circular polarization, the DRA may be excited by dual coaxial probe [78], dual conformal strip [79] or with parasitic

strips [80], [81], rotated sequential feed [82], [83], or aperture feed [84]-[86] excited in phase quadrature (90^o). Moreover, a comb-shaped slot loaded cylindrical DRA can also generate circular polarization operation [87]. The dual conformal strip dual-fed approach in [79] has comparatively wider 10-dB return loss and 3-dB axial bandwidths of 13.7% and 20%, respectively.

In this chapter, the broadband design of circularly polarized stripline fed dielectric resonator antennas is presented. To improve the coupling between the microstrip feed line and the DRA, the vertical conformal stripline feed in [88] was adopted. This feed technique has the merits of low back radiation and allows for the DRA to attain a reasonably wide impedance bandwidth. To improve the quality of circular polarization, four vertical conformal striplines were sequentially positioned around the circumference of a cylindrical DRA and supplied balanced power with relative excitation phases of 0^o, 90^o, 180^o, and 270^o as in [56]. The application of a symmetrical four point feeding structure to a cylindrical DRA is new and has not been reported in open literature. The use of a conventional 90^o hybrid coupler pair is proposed. The conventional 90^o hybrid coupler used delivers good impedance matching, equal amplitude power splitting and consistent 90^o ($\pm 5^o$) phase shifting, across a bandwidth of only ~14%. However, this feed network is shown to suffice in extending the impedance and axial ratio bandwidths of the cylindrical DRA. In Section 5.2, wideband circular polarization operation is demonstrated for a circularly polarized dual stripline dielectric resonator antenna utilizing the 90^o hybrid coupler. In Section 5.3, wideband circular polarization operation is demonstrated for a circularly polarized quadruple stripline dielectric resonator antenna utilizing a pair of the 90^o hybrid couplers.

5.2 Broadband Circularly Polarized Dual Stripline Dielectric Resonator Antenna with a 90^o Hybrid Coupler

5.2.1 Antenna Design and Geometry

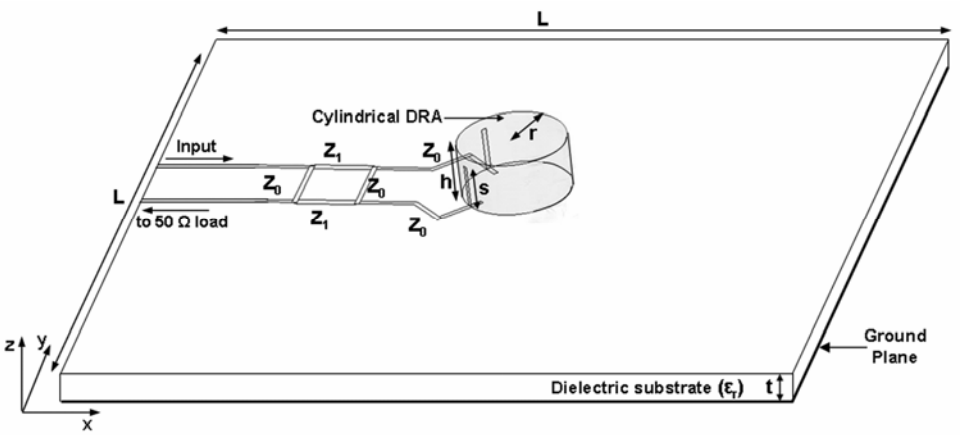

Fig. 76. Geometry of the circularly polarized dual stripline cylindrical dielectric resonator antenna utilizing the 90^o hybrid coupler.

For a single patch element, sequential rotation can be applied to multiple feed points each supplied with equal amplitude power and an appropriate phase offset. It have been demonstrated in Section 3.2 and 4.2 that the axial ratio perturbation due to multiple reflections and feed phase errors may be reduced with the use of a broadband isolating power divider capable of consistent 90^o phase shifting. This two point feeding structure can be conceptually extended to the cylindrical DRA in bid to enhance its impedance and axial bandwidths. The circularly polarized dual stripline cylindrical DRA utilizing the 90^o hybrid coupler, shown in Fig. 76, is designed for wideband circular polarization operation centered at 2.0 GHz. The conformal striplines, which provides improved coupling between the microstrip feed line and the DRA [88], are excited in phase quadrature and displaced orthogonally in space to produce two degenerate TM_{110} mode in phase quadruature. No drilling through the DRA is required. For a given cylindrical

ceramic material of radius r = 20 mm (0.133 λ_o), height h = 20 mm (0.133 λ_o) and relative permittivity ε_r = 9.5, the stripline geometry and positioning, and 90° hybrid coupler feed line parameters are optimized accordingly. This dual stripline cylindrical DRA is used as a comparative benchmark for the quadruple stripline cylindrical DRA presented in the following section.

5.2.2 Feed Network Configuration

The conventional 90° hybrid coupler (Fig. 33), presented in Section 3.2.2, was used in this study. The feed substrate used was a Rogers RO4003 laminate of thickness t = 0.8 mm, dielectric constant ε_r = 3.38, and an assumed loss tangent of tan δ = 0.0027. The feed line widths of the 35.36 and 50 Ω branches were 3.1 and 1.85 mm, respectively. For convenient analysis, the input and output ports of the feed networks were all set to 50 Ω.

5.2.3 Impedance and Radiation Performances

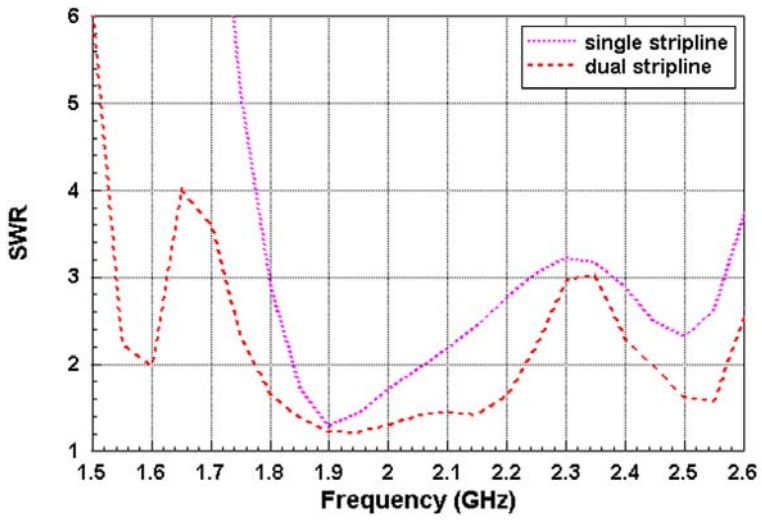

Fig. 77. Simulated SWR comparison between the single stripline cylindrical DRA and the circularly polarized dual stripline cylindrical DRA utilizing the 90° hybrid coupler.

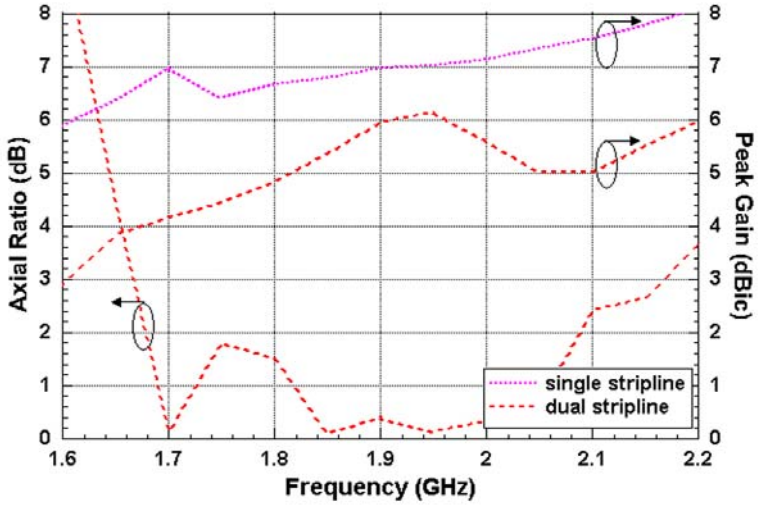

Fig. 78. Simulated axial ratio and gain comparison between the single stripline cylindrical DRA and the circularly polarized dual stripline cylindrical DRA utilizing the 90^{o} hybrid coupler.

All simulations presented in this chapter were performed using Ansoft HFSS, a commercially available 3-D electromagnetic field solver based on the Finite Element Method (FEM). The FEM used in HFSS, compared to the MoM used in IE3D, is a computationally more efficient numerical method for solving finite dielectric structures, as is the case of the DRA studied here.

Fig. 77 shows the simulated SWR comparison between the single stripline cylindrical DRA and the circularly polarized dual stripline cylindrical DRA utilizing the 90^{o} hybrid coupler. The second stripline feed of the dual stripline cylindrical DRA shown in Fig. 76 has been removed, keeping all other antenna parameters. The single stripline feed was excited using a 50 Ω microstrip feed line. The single stripline DRA exhibits a simulated impedance bandwidth (SWR < 2) of 11.28%, from 1.84 to 2.06 GHz. The dual stripline DRA exhibits a relatively wider simulated impedance bandwidth (SWR < 2) of 22.89%, from 1.78 to 2.24 GHz. This simulated input VSWR bandwidth is wider than the measured 13.7%

10-dB return loss bandwidth reported for a similar DRA configuration in [79]. A VSWR of 2 corresponds to a return loss of -9.6 dB.

Fig. 78 shows the simulated axial ratio of the circularly polarized dual stripline cylindrical DRA utilizing the 90^o hybrid coupler and its simulated peak gain comparison with the single stripline DRA. The dual stripline DRA exhibits a simulated 3-dB axial ratio of 26.04%, from 1.67 to 2.17 GHz. This simulated 3-dB axial ratio bandwidth is wider than the measured 20% 3-dB axial ratio bandwidth reported for a similar DRA configuration in [79]. It is observed that the simulator tends to predict wider simulated impedance and axial ratio bandwidths than that measured in [79]. Combining the results in Fig. 77 and 78, the quadruple stripline DRA is found to deliver, in terms of SWR < 2 and axial ratio < 3 dB, a simulated CP bandwidth of 19.75%, from 1.78 to 2.17 GHz. Across this bandwidth, the dual stripline DRA exhibits a peak gain that ranges from 4.7 to 6.2 dBic. The peak gain of the dual stripline DRA is found to be consistently lower than that of the single stripline DRA. Gain loss is accrued to the insertion loss of the 90^o hybrid coupler that diminishes the overall radiation efficiency of the DRA.

5.2.4 Discussions

In this section, the broadband design of a circularly polarized dual stripline cylindrical DRA utilizing the 90^o hybrid coupler has been presented. The 90^o hybrid coupler provides good impedance matching, equal amplitude power splitting and consistent 90^o phase shifting, across a bandwidth of ~14%. The circularly polarized dual stripline DRA delivers simulated impedance (SWR < 2) and axial ratio (AR < 3 dB) bandwidths of 22.89% (1.78 to 2.24 GHz) and

26.04% (1.67 to 2.17 GHz), respectively, for a simulated CP operating bandwidth of 19.75%, from 1.78 to 2.17 GHz.

5.3 Broadband Circularly Polarized Quadruple Stripline Dielectric Resonator Antenna with 90° Hybrid Couplers

5.3.1 Antenna Design and Geometry

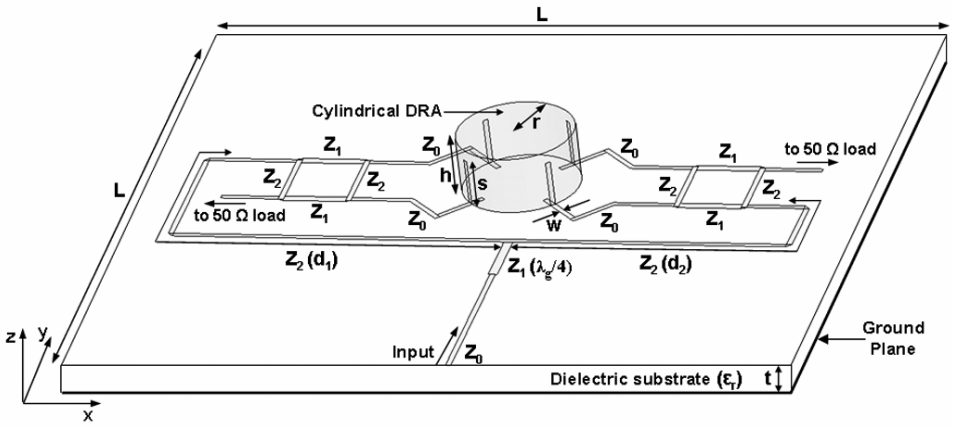

Fig. 79. Geometry of the circularly polarized quadruple stripline cylindrical dielectric resonator antenna utilizing the 90° hybrid coupler pair.

For a two point feed single patch element, the axial ratio perturbation due to multiple reflections and feed phase errors may be combated with the use of a broadband isolating power divider capable of consistent 90° phase shifting. Improved impedance and axial ratio bandwidths have been demonstrated in Section 3.2 and 4.2 for dual L-probe patch elements utilizing broadband feeders. However, for the mutual coupling effects and axial ratio perturbation due to higher order modes to also cancel, a symmetrical four point feeding structure with appropriate feed phasing is necessary. Further improved impedance and axial ratio bandwidths have been demonstrated in Section 3.3 for quadruple L-probe patch elements utilizing broadband feeders. The circularly polarized quadruple stripline

cylindrical DRA utilizing the proposed 90° hybrid coupler pair, shown in Fig. 79, is designed for wideband circular polarization operation centered at 2.0 GHz. The sequentially rotated four point feeding structure for a single patch element is conceptually extended to the cylindrical DRA in bid to further enhance its impedance and axial bandwidths. To achieve dual-fed type circular-polarization, the four orthogonally-orientated vertical strips were supplied equal-amplitude power with relative excitation phases of 0°, 90°, 180°, and 270°.

5.3.2 Feed Network Configuration

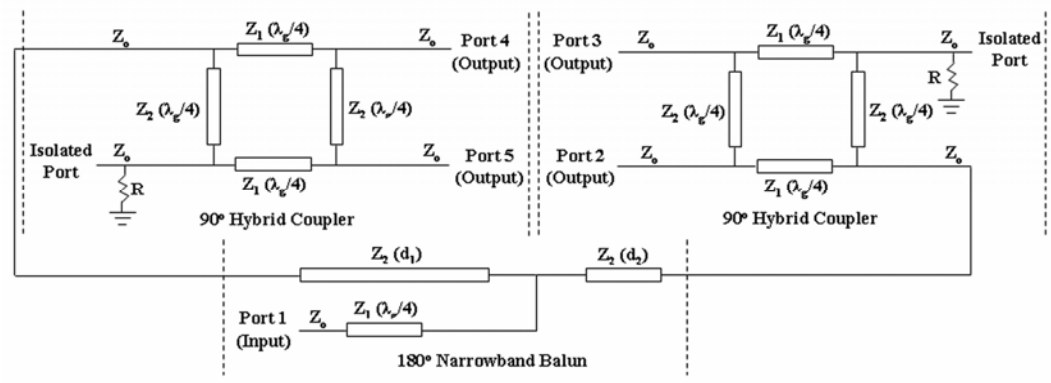

Fig. 80. Schematics of the proposed 90° hybrid coupler pair.

The proposed 90° hybrid coupler pair, shown in Fig. 80, delivers good impedance matching, equal amplitude power splitting and relative excitation phasing of 0°, 90°, 180°, and 270°, over a sufficiently wide band. The feed network comprises a conventional 180° narrowband balun (Fig. 3) cascaded to a pair of 90° hybrid couplers (Fig. 33). To provide the required 180° phase shift between the two 90° hybrid couplers, the lengths of the microstrip branches, d_1 and d_2, must be such that $d_1 - d_2 = \lambda_g / 2$, where λ_g refers to the guide wavelength at a center operating frequency of 2.0 GHz. The characteristic impedances of the microstrip branches

are given by Z_o = 50 Ω, Z_1 = 35.36 Ω, and Z_2 = 50 Ω. The isolated ports were each terminated to a 50 Ω load in the form of a 50 Ω surface mount resistor.

5.3.3 Fabrication and Experimental Setup

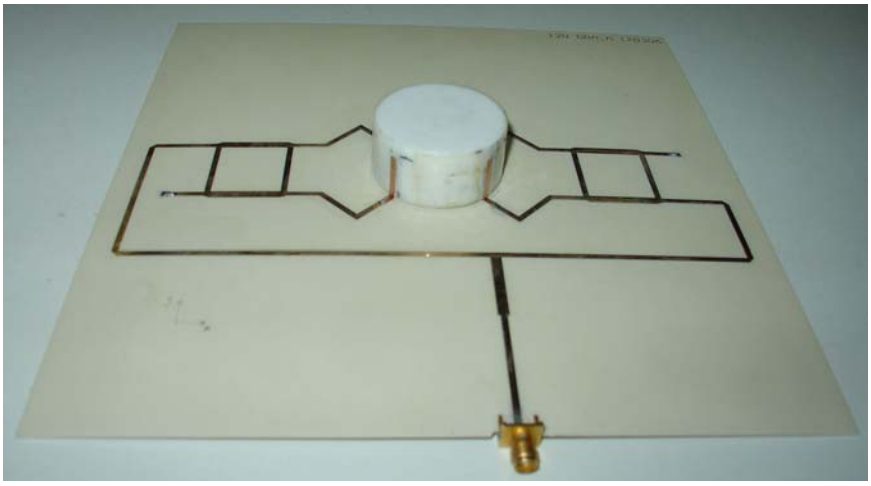

Fig. 81. Prototype of the circularly polarized quadruple stripline cylindrical dielectric resonator antenna utilizing the 90^o hybrid coupler pair.

Fig. 81 shows the prototype of the circularly polarized quadruple stripline cylindrical dielectric resonator antenna utilizing the 90^o hybrid coupler pair. The antenna and feed network parameters were optimized for a wide impedance bandwidth centering 2.0 GHz. The cylindrical DRA, of radius r = 20 mm (0.133 λ_o), height h = 20 mm (0.133 λ_o) and relative permittivity ε_r = 9.5, was positioned at the center of a Rogers RO4003 dielectric substrate of thickness t = 0.8 mm and relative permittivity ε_r = 3.38. The feed network and ground plane were respectively printed on the top and bottom layer of the dielectric substrate. The square ground plane is of length L = 200 mm (1.33 λ_o). The isolated port connects to a 50 Ω surface-mount resistor grounded by a metallic pad with via holes to ground. The four copper tape stripline feeds, of length s = 16 mm (0.107 λ_o) and width w = 1.85 mm, were placed 90^o apart from one another, along the

circumference of the cylindrical DRA. To ensure proper connection, the copper tape stripline ends were soldered onto the respective output ports of the feed network. The impedance measurements were taken using the Agilent E8364B network analyzer, while the far-field radiation measurements were taken using the Hewlett Packard 8510C vector network analyzer and the Orbit-MiDAS far-field measurement system in an anechoic chamber. With a reference linearly polarized standard horn antenna, the comparison method (gain-transfer method) was used to determine the measured gain (See Section 3.2.3) and the rotating-source method was used to determine the measured axial ratio (See Section 4.2.3).

5.3.4 Impedance and Radiation Performances

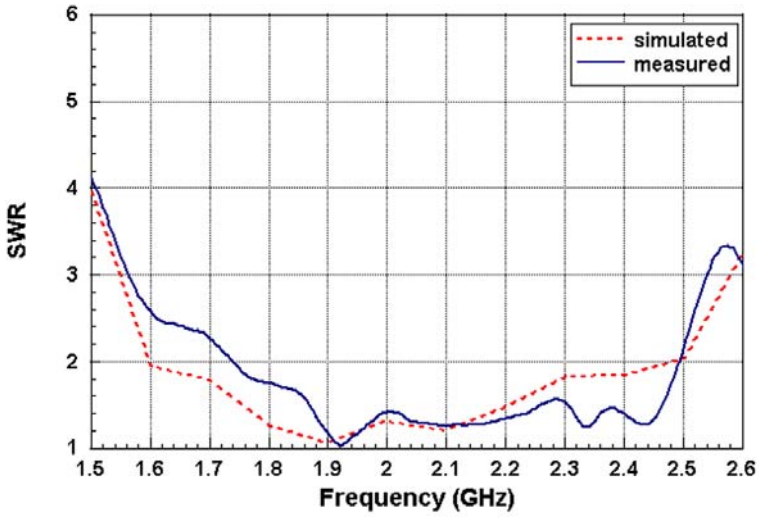

Fig. 82. Simulated and measured SWR for the circularly polarized quadruple stripline cylindrical DRA utilizing the 90^{o} hybrid coupler pair.

Fig. 82 shows the simulated and measured SWR for the circularly polarized quadruple stripline cylindrical DRA utilizing the 90^{o} hybrid coupler pair. The quadruple stripline DRA exhibits simulated and measured impedance bandwidths (SWR < 2) of 43.73%, from 1.59 to 2.48 GHz, and 34.91%, from 1.75 to 2.49

GHz, respectively. In comparison, the single and dual stripline DRA presented in the previous section exhibit much narrower simulated impedance bandwidths (SWR < 2) of 11.28%, from 1.84 to 2.06 GHz, and 22.89%, from 1.78 to 2.24 GHz, respectively. The measured resonant frequency, corresponding to the minimum measured input VSWR, is at 1.92 GHz. In the HFSS simulation, the predicted resonant frequency is 1.88 GHz. The discrepancy between the prediction and measurement may be due to the very thin air gap between the bottom of the dielectric resonator and the ground plane, also described in [89].

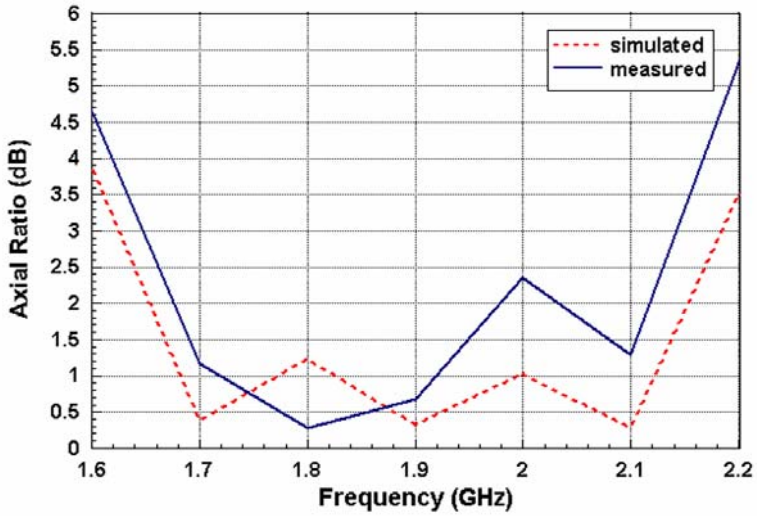

Fig. 83. Simulated and measured axial ratio for the circularly polarized quadruple stripline cylindrical DRA utilizing the 90^{o} hybrid coupler pair.

Fig. 83 shows the simulated and measured axial ratio for the circularly polarized quadruple stripline cylindrical DRA utilizing the 90^{o} hybrid coupler pair. The quadruple stripline DRA exhibits simulated and measured 3-dB axial-ratio bandwidths of 28.9%, from 1.63 to 2.18 GHz, and 25.9%, from 1.65 to 2.14 GHz, respectively. In comparison, the dual stripline DRA presented in the previous section exhibits a slightly narrower simulated 3-dB axial ratio of 26.04%, from 1.67 to 2.17 GHz. At 1.8 GHz, a minimum measured boresight axial ratio of 0.3

dB is seen. It is observed that the simulator tends to predict wider simulated impedance and axial ratio bandwidths than that measured. Combining the results in Fig. 82 and 83, the quadruple stripline DRA is found to deliver, in terms of SWR < 2 and axial ratio < 3 dB, simulated and measured CP bandwidths of 28.9%, from 1.63 to 2.18 GHz, and 20.1%, from 1.75 to 2.14 GHz, respectively. The designated bandwidth of interest will be from 1.75 to 2.1 GHz (18.18%).

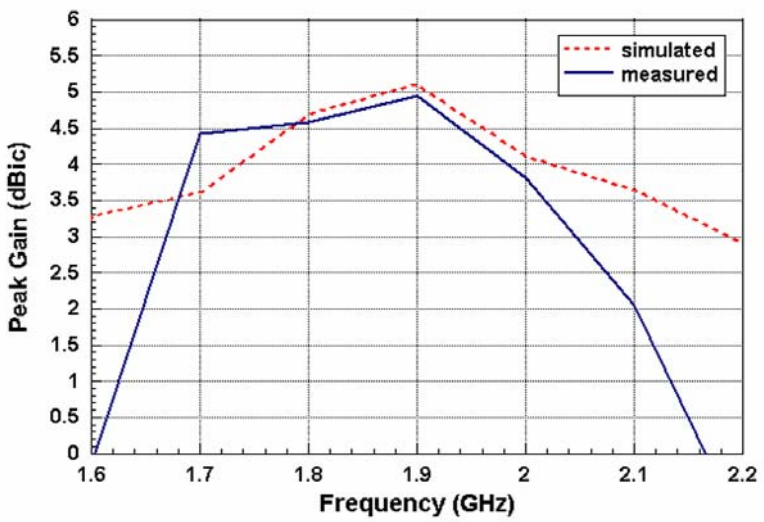

Fig. 84. Simulated and measured peak gain for the circularly polarized quadruple stripline cylindrical DRA utilizing the 90^{o} hybrid coupler pair.

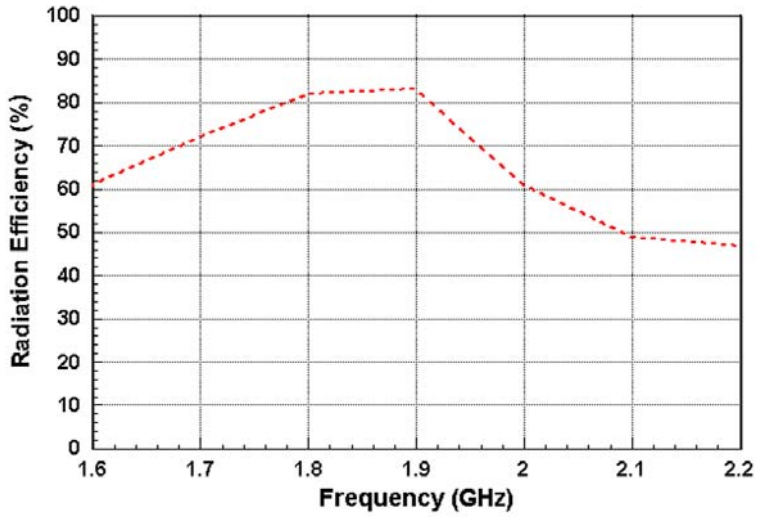

Fig. 85. Simulated radiation efficiency for the circularly polarized quadruple stripline cylindrical DRA utilizing the 90^{o} hybrid coupler pair.

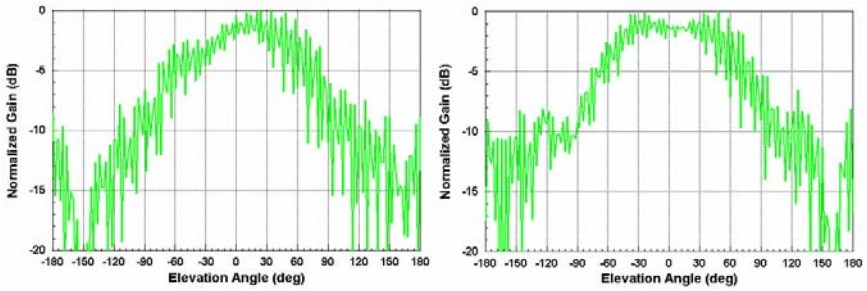

x-z plane y-z plane

(a) 1.75 GHz

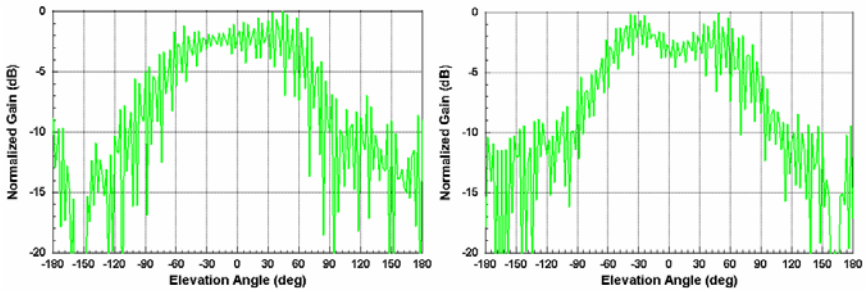

x-z plane y-z plane

(b) 1.9 GHz

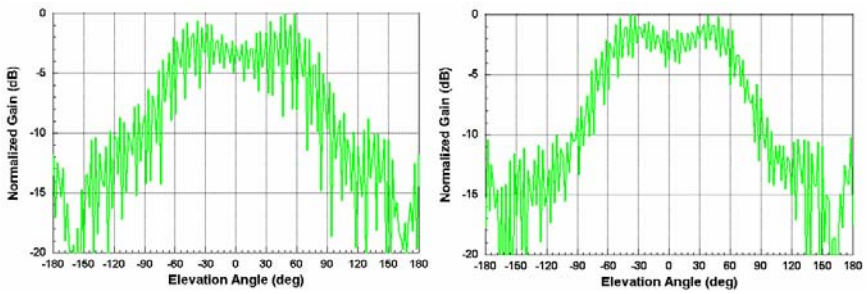

x-z plane y-z plane

(c) 2.1 GHz

Fig. 86. Measured normalized spinning linear radiation patterns for the circularly polarized quadruple stripline cylindrical dielectric resonator antenna utilizing the 90^{o} hybrid coupler pair.

Fig. 84 shows the simulated and measured peak gain for the circularly polarized quadruple stripline cylindrical DRA utilizing the 90^{o} hybrid coupler pair. The quadruple stripline DRA exhibits a measured 3-dB gain bandwidth (gain > 1.95 dBic) of 24%, from 1.65 to 2.1 GHz, with its highest gain of 4.95 dBic at 1.9 GHz. The peak gain of the quadruple stripline DRA is found to be consistently lower than that of the dual stripline DRA, across the bandwidth of interest. Gain

loss is accrued to the insertion loss of the 90^o hybrid coupler pair that diminishes the overall radiation efficiency of the DRA.

Fig. 85 shows the simulated radiation efficiency for the circularly polarized quadruple stripline cylindrical DRA utilizing the 90^o hybrid coupler pair. It is seen that the radiation efficiency ranges from 50% to 80%, within the measured CP operating bandwidth, from 1.75 to 2.14 GHz. The verification of the simulated radiation efficiency from HFSS has been carried out in [90]. It should be noted that the reliability of the radiation efficiency data extracted from the HFSS-based simulation results is very much dependent on the settings of the radiation air-box.

Fig. 86 shows the measured normalized spinning linear radiation patterns for the circularly polarized quadruple stripline cylindrical DRA utilizing the 90^o hybrid coupler pair at the lower frequency edge (1.75 GHz), center frequency (1.9 GHz), and upper frequency edge (2.1 GHz), of the bandwidth of interest, on the x-z ($\phi = 0^o$) and y-z ($\phi = 90^o$) planes, respectively. On both principle planes, symmetry is observed and the axial-ratio is found to be less than 3 dB across a 60^o beamwidth. The ripples in the envelope of the measured radiation patterns can be attributed to the diffracted fields from the edges of the finite ground plane [91]. The slight dip of the radiation patterns at the boresight can be explained by the dependence on the ground plane size [92].

5.3.5 Discussions

In this section, the broadband design of a circularly polarized quadruple stripline cylindrical DRA utilizing the proposed 90^o hybrid coupler pair has been presented.

The 90^o hybrid coupler provides good impedance matching, equal amplitude power splitting and consistent 90^o phase shifting, across a bandwidth of ~14%. The proposed circularly polarized quadruple stripline DRA delivers measured impedance (SWR < 2) and axial ratio (AR < 3 dB) bandwidths of 34.91% (1.75 to 2.49 GHz) and 25.9% (1.65 to 2.14 GHz), respectively, for a measured CP operating bandwidth of 20.1%, from 1.75 to 2.14 GHz. The simulated CP operating bandwidth of 28.9%, from 1.63 to 2.18 GHz, is much wider than that of the dual stripline DRA presented in the previous section. The DRA in study lends itself to mobile base station applications requiring broadband circular polarized coverage encompassing three bands, i.e. PCS1800 (1710-1880 MHz), GSM1900 (1850-1990 MHz), and UMTS2000 (1920-2170 MHz).

5.4 Concluding Remarks

The balanced and symmetrical four point sequential feed structure demonstrated in the previous chapters have been successfully extended to the cylindrical DRA. The impedance and axial ratio bandwidths are improved over the two point sequential feed structure. This, however, was achieved at the expense of higher insertion loss due to the more complex feed network; resulting in the diminished gain and radiation efficiency of a DRA intended for low losses.

For the broadband circularly polarized cylindrical dielectric resonator antenna presented in Section 5.3, an oral presentation was given in the Nov. 2006 IEICE International Symposium on Antennas and Propagation (ISAP2006) [93], held in Singapore, and a full paper was published in the Jul. 2007 issue of IEEE Transactions on Antennas and Propagation [94].

CHAPTER 6

CONCLUSION

6.1 Summary of Important Results

Table 2 Simulated Return Loss, Output Ports Power Distribution and Output Ports Phase Difference for Various Feed Networks

Source	**Feed Network**	**S_{11} < -10 dB**	**$\|S_{21}\|$ = $\|S_{31}\|$ = -3 dB (±0.5 dB)**	**$\|S_{21}\|$ = $\|S_{31}\|$ = -3 dB (±1 dB)**	**$\angle S_{21} - \angle S_{31}$ = 90^o ($\pm 5^o$)**	**$\angle S_{21} - \angle S_{31}$ = 180^o ($\pm 5^o$)**	**Common BW**
Sect 2.2	180^o narrowband balun	188.8%	-	114.2%	-	4.53%	4.53%
Sect 2.2	180^o broadband balun	67.57%	-	60.79%	-	55.72%	52.58%
Sect 3.2	90^o hybrid coupler	30.9%	14%	-	32%	-	14%
Sect 3.2	90^o broadband balun (Type I)	187.6%	91.9%	-	66.7%	-	57.5%
Sect 4.2	90^o broadband balun (Type II)	131.1%	72.46%	-	86.5%	-	72.46%

Table 3 Measured SWR, Cross-Polarization Levels, Input Port Isolation and Gain for Single and Dual Linearly Polarized Square Patch Antennas Utilizing Various Feed Configurations within Bandwidth of Interest (1.7 to 2.2 GHz)

Source	**Feed Structure**	**Feed Network**	**SWR**	**X-Pol**	**S_{21}**	**Gain**
Sect 2.2	Dual L-probe	180^o narrowband balun	< 1.5	< -8.3 dB	-	> 6.49 dBi
Sect 2.2	Dual L-probe	180^o broadband balun	< 1.5	< -22.1 dB	-	> 6.16 dBi
Sect 2.3	Quadruple L-probe	2 x 180^o broadband balun	< 1.8	< -15 dB	< -33 dB	> 6 dBi

Table 4 Measured SWR, Axial Ratio and Gain Bandwidths for Circularly Polarized Circular Patch Antennas Utilizing Various Feed Configurations

Source	Feed Structure	Feed Network	SWR < 2	AR < 3 dB	Gain > 4 dBic	Common BW
[56]	Dual L-probe	90° hybrid coupler	42%	27.23%	-	-
[56]	Quadruple L-probe	2 x 90° hybrid coupler	45%	45%	-	-
Sect 3.2	Dual L-probe	90° broadband balun (Type I)	61%	37.7%	43.68%	29.47%
Sect 3.3	Quadruple L-probe	2 x 90° broadband balun (Type I)	71.7%	81.6%	59.1%	59.1%
Sect 4.2	Dual L-probe	90° broadband balun (Type II)	62%	44.37%	45.38%	25.87%
[57]	Quadruple L-probe	2 x 90° broadband balun (Type II)	79.4%	82%	54.44%	54.44%
Sect 4.3	Dual Cap-Feed	90° broadband balun (Type II)	42.77%	52.16%	>53.81%	33.29%
Sect 4.4	Dual L-probe 2x2 array	6 x 90° broadband balun (Type II)	81.36%	78.4 %	53.11%	53.11%

6.2 Suggestions for Future Works

The study on broadband polarization control for dual linearly polarized patch antennas can be extended to dual circularly polarized patch antennas. This is no easy task as preliminary simulations show that the isolation for dual circular polarization, both for the same sense and for the opposite sense, is worse than the isolation for dual linear polarization by ~10 dB. Dual circularly polarized patch antenna are useful for RFID readers requiring switchable transmit and receive circular polarization operation to read the passive linearly polarized tags.

Three types of broadband baluns have been proposed in this thesis. For various sequential feed configurations, the broadband baluns have been shown to confer the antenna improved impedance and polarization (or axial ratio) bandwidths. This, however, was at the expense of a more complicated feed circuitry and a larger footprint. A more simplified and compact design for the feed network is

desired so that it can provide more even lower installation cost, and be practically simple enough to repeat in array configurations. The various feed networks can also be studied for different antenna ground plane size.

Further work can be dedicated to improving the performance of the sequential array presented in Section 4.4. The array can be studied for various element spacing, to find the optimum configuration for minimal gain loss. Also, a more optimal broadband feed network, comprising a different cascade of broadband baluns, can be developed to further improve the array impedance and radiation performances and minimize insertion losses. For better overall gain bandwidth, antennas with higher gain and flatter gain profile can be used for each element.

6.3 Concluding Remarks

The broadband design of dual and circularly polarized microstrip antennas demands precise wideband control of individual orthogonal radiated polarizations. In this thesis, it has been ascertained that the polarization performance of a dual or circularly polarized antenna can be enhanced within a broad impedance bandwidth with the proper design of its excitation geometry. The two and four point sequential feed structure, compared to a single feed point structure, have been shown to yield wider impedance and polarization (or axial ratio) bandwidths. The proposed broadband balanced feed networks each supplies impedance matching, balanced power splitting, and appropriate phasing, to each feed point, throughout a wide bandwidth. The use of a relatively broadband balun has been shown to significantly extend the allowable impedance, polarization and isolation

bandwidths of the dual linearly polarized antenna, and the allowable impedance and axial ratio bandwidths of the circularly polarized antenna.

In Chapter 2, the use of a 180^o broadband balun is proposed and has been shown, in simulation, to deliver low input port return loss (S_{11} < -10 dB), balanced output ports power distribution ($S_{21} = S_{31}$ = -3 dB (±1.0 dB)), and consistent 180^o ($\pm 5^o$) output ports phase difference over a wide bandwidth of 52.58%, The conventional 180^o broadband balun has been shown, in simulation, to afford only a 4.53% bandwidth, inherently limited by its narrowband 180^o ($\pm 5^o$) phase shifting capability. Wideband cross-polarization suppression has been demonstrated for a linearly polarized two point L-probe fed square patch element utilizing the proposed 180^o broadband balun. This antenna has been found, in measurement, to deliver good impedance matching (SWR < 2), high gain (> 6 dBi), symmetrical E- and H-plane co-polarization patterns, and consistently low E- and H-plane cross-polarizations levels (< -21 dB), across the across a wide bandwidth of ~30%. Wideband cross-polarization suppression and input port decoupling has demonstrated for a dual linearly polarized four point L-probe fed square patch element utilizing a pair of the proposed 180^o broadband balun. This antenna has been found, in measurement, to deliver good impedance matching (SWR < 2), improved input port isolation (> 33 dB), high gain (> 6 dBi), symmetrical E- and H-plane co-polarization patterns, and consistently low E- and H-plane cross-polarizations levels (< -15 dB), over a wide bandwidth of ~25%.

In Chapter 3, the use of a 90^o broadband balun (Type I) is proposed and has been shown, in simulation, to deliver low input port return loss (S_{11} < -10 dB), balanced

output ports power distribution (S_{21} = S_{31} = -3 dB (±0.5 dB)), and consistent 90^o (±5^o) output ports phase difference, over a wide bandwidth of 57.5%. The conventional 90^o hybrid coupler has been shown, in simulation, to afford only a 14% bandwidth, inherently limited by its narrowband balanced output ports power distribution (S_{21} = S_{31} = -3 dB (±0.5 dB)). Wideband circular polarization operation has been demonstrated for a two point L-probe fed circular patch element utilizing the proposed 90^o broadband balun (Type I). This antenna has been found, in measurement, to deliver good impedance matching (SWR < 2), sufficiently low axial ratio (AR < 3 dB), and sufficiently high gain (gain > 4 dBic), over a wide bandwidth of 29.47%. Improved wideband circular polarization operation has been demonstrated for a four point L-probe fed circular patch element utilizing a pair of the proposed 90^o broadband balun (Type I). This antenna, has been found, in measurement, to deliver good impedance matching (SWR < 2), sufficiently low axial ratio (AR < 2 dB), and sufficiently high gain (gain > 4 dBic), over a wide bandwidth of 59.1%.

In Chapter 4, the use of a 90^o broadband balun (Type II) is proposed and has been shown, in simulation, to deliver low input port return loss (S_{11} < -10 dB), balanced output ports power distribution (S_{21} = S_{31} = -3 dB (±0.5 dB)), and consistent 90^o (±5^o) output ports phase difference, over a wide bandwidth of 72.46%. Wideband circular polarization operation has been demonstrated for a two point L-probe fed circular patch element utilizing the proposed 90^o broadband balun (Type II). This antenna has been found, in measurement, to deliver good impedance matching (SWR < 2), sufficiently low axial ratio (AR < 3 dB), and sufficiently low gain (gain > 4 dBic), over a wide bandwidth of 25.87%. Improved wideband circular

polarization operation has demonstrated for a two point capacitive-fed circular patch element utilizing a pair of the proposed 90^{o} broadband balun (Type II). This antenna has been found, in measurement, to deliver good impedance matching (SWR < 2), sufficiently low axial ratio (AR < 3 dB), and sufficiently high gain (gain > 4 dBic), over a wide bandwidth of 33.29%. Further improved wideband circular polarization operation has been demonstrated for a sequential patch array composed of four sets of two point L-probe fed circular patch elements utilizing six of the proposed 90^{o} broadband balun (Type II). This 2x2 element antenna array has been shown, in measurement, to deliver good impedance matching (SWR < 2), lower axial ratio (AR < 2 dB), and sufficiently high gain (gain > 4 dBic), over a wide bandwidth of 53.11%.

In Chapter 5, the use of a conventional 90^{o} hybrid coupler is proposed for a cylindrical dielectric resonator antenna. Wideband circular polarization operation has been demonstrated for a two point stripline feed cylindrical dielectric resonator antenna utilizing the conventional 90^{o} hybrid coupler. Improved wideband circular polarization operation has been demonstrated for a four point stripline fed cylindrical dielectric resonator antenna utilizing a pair of the conventional 90^{o} hybrid coupler. This antenna has been found, in measurement, to deliver good impedance matching (SWR < 2) and sufficiently low axial ratio (AR < 3 dB), over a wide bandwidth of 20.1%.

The excitation geometry has direct implications on the wideband control of individual orthogonal radiated polarizations necessary for the broadband design of dual and circularly polarized antennas. It has been ascertained that a two point

feeding structure affords wider impedance and polarization bandwidths compared to a single point feeding structure. It has also been confirmed that a four point feeding structure affords significantly wider impedance and polarization bandwidths compared to a two point feeding structure. Performance comparisons of the various antenna structures adopting the proposed and conventional feed networks have been given. The proposed use of the broadband baluns presented in this thesis can be conceptually extended to other antenna structures, and the results reported should be of relevance and interest to the microwave community.

REFERENCES

[1] J. D. Kraus, "Antennas since Hertz and Marconi," *IEEE Trans. Antennas Propag.*, vol. AP-33, no. 2, pp. 131-137, Feb. 1985.

[2] C. A. Balanis, "Antenna theory: a review," *Proceedings of the IEEE*, vol. 80, no. 1, Jan. 1992, pp. 7-23.

[3] D. M. Pozar, "Microstrip antennas," *Proceedings of the IEEE*, vol. 80, no. 1, Jan. 1992, pp. 79-91.

[4] C. A. Balanis, "Microstrip antennas" *in* "Antenna Theory: Analysis and Design," 2nd Ed., New York: John Wiley & Sons, 1997, pp. 722-784.

[5] D. M. Pozar, "A review of bandwidth enhancement techniques for microstrip antennas," in *Microstrip Antennas: The Analysis and Design of Microstrip Antennas and Arrays*, New York: IEEE Press, 1995, pp. 157-166.

[6] Z. N. Chen and M. Y. W. Chia, *Broadband Planar Antennas: Design and Applications*, New York: John Wiley & Sons, 2006.

[7] "IEEE standard definitions of terms for antennas," IEEE Std 145-1993, Mar. 18, 1993.

[8] "IEEE standard test procedures for antennas", IEEE Std 149-1979, Aug. 8, 1980, pp. 61-85.

[9] P. S. Hall, "Review of techniques for dual and circularly polarised microstrip antennas," in *Microstrip Antennas: The Analysis and Design of Microstrip Antennas and Arrays*, New York: IEEE Press, 1995, pp. 107-116.

[10] A. C. Ludwig, "The definition of cross polarization," *IEEE Trans. Antennas Propag.*, vol. 21, no. 1, Jan. 1973, pp. 116-119.

[11] M. L. Oberhart, Y. T. Lo, and R. Q. H. Lee, "New simple feed network for an array module of four microstrip elements," Electron. Lett., vol. 23, no. 9, Apr. 1987, pp. 436-437.

[12] D. H. Schaubert, D. M. Pozar, and A. Adrian, "Effect of microstrip antenna substrate thickness and permittivity: Comparison of theories and experiment," *IEEE Trans. Antennas Propag.*, vol. 37, no. 6, Jun. 1989, pp. 677-682.

[13] E. Chang, S. A. Long, and W. F. Richards, "Experimental investigation of electrically thick rectangular microstrip antennas," *IEEE Trans. Antennas Propag.,* vol. 34, no. 6, Jun. 1986, pp. 767-772.

[14] P. S. Hall, "Probe compensation in thick microstrip patches," *Electron. Lett.*, vol. 23, no. 11, May. 1987, pp. 606-607.

[15] T. Huynh and K. F. Lee, "Single-layer single-patch wideband microstrip antenna," *Electron. Lett.,* vol. 31, no. 16, Aug. 1995, pp. 1310-1312.

[16] K. M. Luk, C. L. Mak, Y. L. Chow, and K. F. Lee, "Broadband microstrip patch antenna," *Electron. Lett.*, vol. 34, no. 15, Jul. 1998, pp. 1442-1443.

[17] C. L. Mak, K. M. Luk, K. F. Lee, and Y. L. Chow, "Experimental study of microstrip patch antenna with an L-shaped probe," *IEEE Trans. Antennas Propag.*, vol. 48, no. 5, May. 2000, pp. 777-783.

[18] Y. X. Guo, C. L. Mak, K. M. Luk, K. F. Lee, "Analysis and design of L-probe proximity fed-patch antennas," *IEEE Trans. Antennas Propag.*, vol. 49, no. 2, Feb. 2001, pp. 145-149.

[19] H. Wong, K. L. Lau, K. M. Luk, "Design of dual-polarized L-probe patch antenna arrays with high isolation," *IEEE Trans. Antennas Propag.*, vol. 52, no. 1, Jan. 2004, pp. 45-52.

[20] A. Petosa, A. Ittipiboon, and N. Gagnon, "Suppression of unwanted probe radiation in wideband probe-fed microstrip patches," *Electron. Lett.*, vol. 35, no. 5, Mar. 1999, pp. 355-357.

[21] K. Levis, A. Ittipiboon, and A. Petosa, "Probe radiation cancellation in wideband probe-fed microstrip arrays," *Electron. Lett.*, vol. 36, no. 7, Mar. 2000, pp. 606-607.

[22] Z. N. Chen and M. Y. W. Chia, "Broad-band suspended probe-fed plate antenna with low cross-polarization levels," *IEEE Trans. Antennas Propag.*, vol. 51, no. 2, Feb. 2003, pp. 345-346.

[23] Z. N. Chen and M. Y. W. Chia, "Center-fed microstrip patch antenna," *IEEE Trans. Antennas Propag.*, vol. 51, no. 3, Mar. 2003, pp. 483-487.

[24] Z. N. Chen and M. Y. W. Chia, "A novel center-fed suspended plate antenna," *IEEE Trans. Antennas Propag.*, vol. 51, no. 6, Jun. 2003, pp. 1407-1410.

[25] Z. N. Chen and M. Y. W. Chia, "Experimental study on radiation performance of probe-fed suspended plate antennas," *IEEE Trans. Antennas Propag.*, vol. 51, no. 8, Aug. 2003, pp. 1964-1971.

[26] P. Li, H. W. Lai, K. M. Luk, and K. L. Lau, "A wideband patch antenna with cross-polarization suppression," *IEEE Antennas Wireless Propag. Lett.*, vol. 3, no. 1, Jan. 2004, pp. 211-214.

[27] A. Adrian and D. H. Schaubert, "Dual aperture-coupled microstrip antenna for dual or circular polarization," *Electron. Lett.*, vol. 23, Nov. 1987, pp. 1226-1228.

[28] C. H. Tsao, Y. M. Hwang, F. Kilburg, and F. Dietrich, "Aperture-coupled patch antennas with wide-bandwidth and dual-polarization capabilities," in

Proc. IEEE Antennas and Propagation Symp. Dig., Syracuse, NY, Jun. 1988, pp. 936-939.

[29] M. Edimo, A. Sharaiha, and C. Terret, "Optimized feeding of dual polarized broadband aperture-coupled printed antenna," *Electron. Lett.*, vol. 28, no. 19, Sept. 1992, pp. 1785-1787.

[30] L. Habib, G. Kossiavas, and A. Papiernik, "Cross-shaped patch with etched bars for dual polarization," *Electron. Lett.*, vol. 29, no. 10, May. 1993, pp. 916-918.

[31] M. Yamazaki, E. T. Rahardjo, and M. Haneishi, "Construction of a slot-coupled planar antenna for dual polarization," *Electron. Lett.*, vol. 30, no. 22, Oct. 1994, pp. 1814-1815.

[32] P. Brachat and J. M. Baracco, "Dual–polarization slot-coupled printed antennas fed by stripline," *IEEE Trans. Antennas Propog.*, vol. 43, no. 7, Jul. 1995, pp. 738-742.

[33] S. Gao, L. W. Li, P. Gardner and P. S. Hall, "Wideband dual-polarized microstrip patch antenna, *Electron. Lett*., vol. 37, Sept. 2001, pp. 1213-1214.

[34] K. L. Wong, H. C. Tung, and T. W. Chiou, "Broadband Dual-polarized aperture-coupled patch antennas with modified H-shaped coupling slots," *IEEE Trans. Antennas Propag.*, vol. 50, no. 2, Feb. 2002, pp. 188-191.

[35] Y. X. Guo, K. M. Luk, and K. F. Lee, "Broadband Dual Polarization Patch element for cellular-phone base stations," *IEEE Trans. Antennas Propag.*, vol. 50, no. 2, Feb. 2002, pp. 251-253.

[36] K. L. Wong and T. W. Chiou, "Broad-band dual-polarized patch antennas fed by capacitively coupled feed and slot-coupled feed," *IEEE Trans. Antennas Propag.*, vol. 50, no. 3, Mar. 2002, pp. 346-351.

[37] Z. Y. Zhang, Y. X. Guo, L. C. Ong, and M. Y. W. Chia, "A new wideband planar balun on a single-layer PCB," *IEEE Microw. Wireless Comp. Lett.*, vol. 15, no. 6, Jun. 2005, pp. 416-418.

[38] T. Huynh and K. F. Lee, "Cross polarization characteristics of rectangular patch antennas," in *Proc. IEEE Antennas Propag. Symp. Dig.*, vol. 2, Jun. 1988, pp. 708-711.

[39] E. Wilkinson, "An N-way hybrid power divider," *IEEE Trans. Microw. Theory Tech.*, vol. 8, no. 1, Jan. 1960, pp. 116-118.

[40] S. Y. Eom and H. K. Park, "New switched-network phase shifter with broadband characteristics," *Microw. Opt. Technol. Lett.*, vol. 38, no. 4, Aug. 2003, pp. 255-257.

[41] Y. X. Guo, **K. W. Khoo**, L. C. Ong, and K. M. Luk, "Wideband low cross-polarization patch antenna using a broadband balun," *Radio Sci.*, vol. 42, no. 5, Oct. 2007, RS5008.

[42] **K. W. Khoo**, Y. X. Guo, and L. C. Ong, "Wideband dual-polarized patch antenna," in *Proc. 10th IEEE Int. Conf. on Communication Systems, ICCS2006*, Singapore, Oct. 2006.

[43] Y. X. Guo, **K. W. Khoo**, and L. C. Ong, "Wideband dual-polarized patch antenna with broadband baluns," *IEEE Trans. Antennas Propag.*, vol. 55, no. 1, Jan. 2007, pp. 78-83.

[44] H. Iwasaki, "A circularly polarized small-size microstrip antenna with a cross slot," *IEEE Trans. Antennas Propag.*, vol. 44, no. 10, Oct. 1996, pp. 1399-1401.

[45] W. K. Lo., J. L. Hu, C. H. Chan, and K. M. Luk, "L-shaped probe-feed circularly polarized microstrip patch antenna with a cross slot," *Microw. Opt. Technol. Lett.*, vol. 25, no. 4, May. 2000, pp. 251-253.

[46] J. S. Row, "The design of a square-ring slot antenna for circular polarization," *IEEE Trans Antennas and Propag.*, vol. 53, no. 6, Jun. 2005, pp. 1967-1972.

[47] F. S. Chang, K. L. Wong, and T. W. Chiou, "Low-cost broadband circularly polarized patch antenna," *IEEE Trans. Antennas Propag.*, vol. 51, no. 10, Oct. 2003, pp. 3006-3009.

[48] K. L. Chung and A. S. Mohan, "A systematic design method to obtain broadband characteristics for singly-fed electromagnetically coupled patch antennas for circularly polarization," *IEEE Trans. Antennas Propag.*, vol. 51, no. 12, Dec. 2003, pp. 3239-3248.

[49] S. D. Targonski and D. M. Pozar, "Design of wideband circularly polarized aperture-coupled microstrip antennas," *IEEE Trans. Antennas Propag.*, vol. 41, no. 2, Feb. 1993, pp. 214-220.

[50] D. M. Pozar and S. M. Duffy, "A dual-band circularly polarized aperture-coupled stacked microstrip antenna for global positioning satellite," *IEEE Trans. Antennas Propag.*, vol. 45, no. 11, Nov. 1997, pp. 1618-1625.

[51] K. L. Wong and T. W. Chiou, "Single-patch broadband circularly-polarized microstrip antennas," in *IEEE Antennas Propag. Soc. Int. Symp. Dig.*, vol. 2, Jul. 2000, pp.984-987.

[52] K. L. Lau and K. M. Luk, "A novel wide-band circularly polarized patch antenna based on L-probe and aperture-coupling techniques," *IEEE Trans. Antennas Propag.*, vol. 53, no. 1, Jan. 2005, pp. 577-580.

[53] P. H. Rao, V. F. Fusco, and R. Cahill, "Wide-band linear and circularly polarized patch antenna using a printed stepped T-feed," *IEEE Trans. Antennas Propag.*, vol. 50, no. 3, Mar. 2002, pp. 356-361.

[54] J. Q. Howell, "Microstrip antennas," *IEEE Trans. Antennas Propag.*, vol. 23, no. 1, Jan. 1975, pp. 90-93.

[55] X. M. Qing, "Broadband aperture-coupled circularly polarized microstrip antenna fed by a three-stub hybrid coupler," *Microw. Opt. Technol. Lett.*, vol. 40, no. 1, Jan. 2004, pp. 38-41.

[56] W. K. Lo, C. H. Chan, and K. M. Luk, "Bandwidth enhancement of circularly polarized microstrip patch antenna using multiple L-shaped probe feeds," *Microw. Opt. Technol. Lett.*, vol. 42, no. 4, Aug. 2004, pp. 263-265.

[57] L. Bian, Y. X. Guo, L. C. Ong, and X. Q. Shi, "Wideband circularly-polarized patch antenna," *IEEE Trans. Antennas Propag.*, vol. 54, no. 9, Sept. 2006, pp. 2682-2686.

[58] D. M. Pozar, "Power dividers and directional couplers" in *Microwave Engineering*, 2nd ed., New York: John Wiley & Sons, 1998, pp. 379-383.

[59] Y. X. Guo, Z. Y. Zhang, and L. C. Ong, "Improved wideband Schiffman phase shifter," *IEEE Trans. Microw. Theory Tech.*, vol. 54, no.3, Mar. 2006, pp. 1196-1200.

[60] J. D. Kraus and R. J. Marhefka, "Measurement of different antenna parameters" in *Antennas for All Applications*, 3rd ed., New York: McGraw-Hill, 2003, pp. 379-383.

[61] Y. X. Guo, **K. W. Khoo**, and L. C. Ong, "Ultra-wideband circularly polarized patch antenna," in *Proc. Asia Pacific Microw. Conf., APMC2006*, Yokohama, Japan, Dec. 2006, pp. 1644-1646.

[62] Y. X. Guo, **K. W. Khoo**, and L. C. Ong, "Wideband circularly polarized patch antenna using broadband baluns", *IEEE Trans. Antennas Propag.*, vol. 56, no. 2, Feb. 2008, pp. 319-326.

[63] T. Teshirogi, M. Tanaka, and W. Chujo, "Wideband circularly polarized array antenna with sequential rotations and phase shift of elements," in *Proc. Int. Symp. on Antennas Propag.*, *ISAP1985*, 1985, pp. 117-120.

[64] M. Haneishi, "Circularly polarised SHF planar array composed of microstrip pairs elements," in *Proc. Int. Symp. on Antennas Propag.*, *ISAP1985*, 1985, pp. 125-128.

[65] J. Huang, "A technique for an array to generate circular polarization with linearly polarized elements," *IEEE Trans. Antennas & Propag.,* vol. 34*,* no. 9, Sept. 1989, pp. 1113-1124.

[66] P. S. Hall, J. Huang, E. Rammos, and A. Roederer, "Gain of circularly polarised arrays composed of linearly polarised elements," *Electron. Lett.*, vol. 25, no. 2, Jan. 1989, pp. 124-125.

[67] M. S. Smith and P. S. Hall, "Analysis of radiation pattern effects in sequentially rotated arrays," *IEE Proc.*, vol. 141, no. 4, Aug. 1994, pp. 313-320.

[68] P. S. Hall, J. S. Dahele, and J. R. James, "Design principles of sequentially fed wide bandwidth, circularly polarised microstrip antennas," *IEE Proc.*, vol. 136, pt. H, no. 5, Oct. 1989, pp. 381-389.

[69] P. S. Hall, "Application of sequential feeding to wide bandwidth circularly polarised microstrip patch array," *IEE Proc.*, vol. 136, pt. H, no. 5, Oct. 1989, pp. 390-398.

[70] K. L. Wong and T. W. Chiou, "Single patch broadband circularly polarized microstrip antennas," in *Proc. IEEE Antennas Propag. Soc. Int. Symp.*, 2000, vol. 2, pp. 984-987.

[71] G. A. E. Vandenbosch and A. R. Van de Capelle, “Study of the capacitively fed microstrip antenna element,” *IEEE Trans. Antennas & Propag.,* vol. 42, no. 12, Dec. 1994, pp. 1648-1652.

[72] S. A. Long, M. W. McAllister, and L. C. Shen, “The resonant cylindrical dielectric cavity antenna,” *IEEE Trans. Antennas Propag.*, vol. 31, no. 3, May. 1983, pp. 406–412.

[73] A. Petosa, A. Ittipiboon, Y. M. M. Antar, and D. Roscoe, “Recent advances in dielectric resonator antenna technology,” *IEEE Antennas Propag. Mag.*, vol. 40, no. 3, Jun. 1998, pp. 35–48.

[74] G. P. Junker, A. A. Kishk, and A. W. Glisson, “Input impedance of dielectric resonator antennas excited by a coaxial probe,” *IEEE Trans. Antennas Propag.*, vol. 42, no. 7, Jul. 1994, pp. 960–966.

[75] R. A. Kranenbrug and S. A. Long, “Microstrip transmission line excitation of dielectric resonator antennas,” *Electron. Lett.*, vol. 24, no. 18, Sept. 1988, pp. 1156–1157.

[76] J. T. H. St. Martin, Y. M. M. Antar, A. A. Kishk, A. Ittipiboon, and M. Cuhaci, “Dielectric resonator antenna using aperture coupling,” *Electron. Lett.*, vol. 26, no. 24, Dec. 1990, pp. 2015–2016.

[77] R. A. Kranenbrug, S. A. Long, and J. T. Williams, “Coplanar waveguide excitation of dielectric resonator antennas,” *IEEE Trans. Antennas Propag.*, vol. 39, no. 1, Jan. 1991, pp. 119–122.

[78] G. Drossos, Z. Wu, and L. E. Davis, “Circular polarized cylindrical dielectric resonator antenna,” *Electron. Lett.*, vol. 32, no. 4, Feb. 1996, pp. 281–283.

[79] K. W. Leung, W. C. Wong, K. M. Luk, and E. K. N. Yung, "Circular-polarized dielectric resonator antenna excited by dual conformal strips," *Electron. Lett.*, vol. 36, no. 6, Mar. 2000, pp. 484–486.

[80] R. T. Long, R. J. Dorris, S. A. Long, M. A. Khayat, and J. T. Williams, "Use of parasitic strip to produce circular polarization and increased bandwidth for cylindrical dielectric resonator antenna," *Electron. Lett.*, vol. 37, no.7, Mar. 2001, pp. 406–408.

[81] K.W. Leung and H.K. Ng, "Theory and experiment of circularly polarized dielectric resonator antenna with a parasitic patch," *IEEE Trans. Antennas Propag.*, vol. 51, no. 3, Mar. 2003, pp. 405–412.

[82] M. Haneishi and H. Takazawa, "Broadband circularly polarized planar array composed of a pair of dielectric resonator antennas," *Electron. Lett.*, vol. 21, no. 10, May. 1985, pp. 437–438.

[83] A. A. Kishk, "Application of rotated sequential feeding for circular polarization bandwidth enhancement of planar arrays with single-fed DRA elements," in *Proc. IEEE Antennas and Propag. Soc. Symp.*, vol. 4, Jun. 2003, pp. 664–667.

[84] M. B. Oliver, Y. M. M. Antar, R. K. Mongia, and A. Ittipiboon, "Circularly polarized rectangular dielectric resonator antenna," *Electron. Lett.*, vol. 31, Mar. 1995, pp. 418–419.

[85] K. P. Esselle, "Circularly polarized higher-order rectangular dielectric resonator antenna," *Electron. Lett.*, vol. 32, Feb. 1996, pp. 150–151.

[86] R. Chair, S. L. S. Yang, A. A. Kishk, K. F. Lee, and K. M. Luk, "Aperture fed wideband circularly polarized rectangular stair shaped dielectric resonator antenna," *IEEE Trans. Antennas Propag.*, vol. 54, no. 4, Apr. 2006, pp. 1350–1352.

[87] L. C. Y. Chu, D. Guha, and Y. M. M. Antar, "Comb-shaped circularly polarised dielectric resonator antenna," *Electron. Lett.*, vol. 42, no. 14, Jul. 2006, pp. 785–787.

[88] K. M. Luk, M. T. Lee, K. W. Leung, and E. K. N. Yeung, "Technique for improving coupling between microstripline and dielectric resonator antenna," *Electron. Lett.*, vol. 35, Mar. 1999, pp. 357–358.

[89] G. P. Junker, A. A. Kishk, A. W. Glisson, and D. Kajfez, "Effect of fabrication imperfections for ground-plane-backed dielectric resonator antennas," *IEEE Antennas Propag. Mag.*, vol. 37, no.1, Feb. 1995, pp. 40–47.

[90] D. Guha and Y. M. M. Antar, "New half-hemispherical dielectric resonator antenna for broadband monopole-type radiation," *IEEE Trans. Antennas Propag.*, vol. 54, no. 12, Dec. 2006, pp. 3621–3628.

[91] R. K. Mongia, A. Ittipiboon, M. Cuhaci, and D. Roscoe, "Circularly polarized dielectric resonator antenna," *Electron. Lett.*, vol. 30, no. 17, Aug. 1994, pp. 1361–1362.

[92] Y. X. Guo, K. M. Luk, and K. F. Lee, "L-probe fed thick-substrate patch antenna mounted on a finite ground plane," *IEEE Trans. Antennas Propag.*, vol. 51, no. 8, Aug. 2003, pp. 1955–1963.

[93] **K. W. Khoo**, Y. X. Guo, and L. C. Ong, "Broadband circularly-polarized cylindrical dielectric resonator antenna," in *Proc. IEICE Int. Symp. on Antennas and Propag., ISAP2006*, Singapore, Nov. 2006.

[94] **K. W. Khoo**, Y. X. Guo, and L. C. Ong, "Wideband circularly-polarized dielectric resonator antenna," *IEEE Trans. Antennas Propag.*, vol. 55, no. 7, Jul. 2007, pp. 1929-1932.

LIST OF PUBLICATIONS

[1] Y. X. Guo, **K. W. Khoo**, and L. C. Ong, "Wideband dual-polarized patch antenna with broadband baluns," *IEEE Trans. Antennas Propag.*, vol. 55, no. 1, Jan. 2007, pp. 78-83.

[2] **K. W. Khoo**, Y. X. Guo, and L. C. Ong, "Wideband circularly-polarized dielectric resonator antenna," *IEEE Trans. Antennas Propag.*, vol. 55, no. 7, Jul. 2007, pp. 1929-1932.

[3] Y. X. Guo, **K. W. Khoo**, L. C. Ong, and K. M. Luk, "Wideband low cross-polarization patch antenna using a broadband balun," *Radio Sci.*, vol. 42, no. 5, Oct. 2007, RS5008.

[4] Y. X. Guo, **K. W. Khoo**, and L. C. Ong, "Wideband circularly-polarized patch antenna using broadband baluns", *IEEE Trans. Antennas Propag.*, vol. 56, no. 2, Feb. 2008, pp. 319-326.

[5] **K. W. Khoo**, Y. X. Guo, and L. C. Ong, "Wideband dual-polarized patch antenna," in *Proc. 10th IEEE Int. Conf. on Communication Systems, ICCS2006*, Singapore, Oct. 2006.

[6] **K. W. Khoo**, Y. X. Guo, and L. C. Ong, "Broadband circularly-polarized cylindrical dielectric resonator antenna," in *Proc. IEICE Int. Symp. on Antennas and Propag., ISAP2006*, Singapore, Nov. 2006.

[7] Y. X. Guo, **K. W. Khoo**, and L. C. Ong, "Ultra-wideband circularly polarized patch antenna," in *Proc. Asia Pacific Microw. Conf., APMC2006*, Yokohama, Japan, Dec. 2006, pp.1644-1646.